Monolithic fiber/foam-structured catalysts
beyond honeycombs and micro-channels

Zhao, Guofeng; Moulijn, Jacob A.; Kapteijn, Frederik; Dautzenberg, Frits M.; Xu, Bin; Lu, Yong

Citation (APA)
Zhao, G., Moulijn, J. A., Kapteijn, F., Dautzenberg, F. M., Xu, B., & Lu, Y. (2023). Monolithic fiber/foam-structured catalysts: beyond honeycombs and micro-channels. *Catalysis Reviews - Science and Engineering*, *66 (2024)*(5), 1870-1950. https://doi.org/10.1080/01614940.2023.2240661

Important note
To cite this publication, please use the final published version (if applicable).
Please check the document version above.

Taylor & Francis
Taylor & Francis Group

REVIEW ARTICLE

Monolithic fiber/foam-structured catalysts: beyond honeycombs and micro-channels

Guofeng Zhao[a], Jacob A. Moulijn[b], Frederik Kapteijn[b], Frits M. Dautzenberg[c], Bin Xu[d], and Yong Lu [a,e]

[a]School of Chemistry and Molecular Engineering, East China Normal University, Shanghai, China; [b]Chemical Engineering Department, Delft University of Technology, Delft, Netherlands; [c]Serenix Corporation, Fort Collins, USA; [d]ECO Zhuo Xin Energy-Saving Technology (Shanghai) Company Limited, Shanghai, China; [e]Institute of ECO-Chongming, Shanghai, China

ABSTRACT

Heterogeneous catalysis plays a pivotal role in the current chemical and energy vectors production. Notably, to fully utilize the intrinsic activity and selectivity of a catalyst, the chemical reactor has to be designed and operated optimally to achieve enhanced heat/mass transfer, well-defined contact time of reactants, uniform flow pattern, and high permeability. Structured catalysts are a promising strategy to overcome the major drawbacks encountered in the traditional packed-bed reactor technology due to the improved hydrodynamics in combination with enhanced heat/mass transfer. Newly emerged fiber/foam-substrates, with an entirely open 3D network structure, bring distinct advantages over the honeycomb and micro-channel contacting methods, including free radial diffusion, eddy-mixing driven heat/mass transfer, large area-to-volume ratio, and high contacting efficiency. However, how to place the nanocatalysts onto the fiber/foam-substrates is a challenging problem because the commercial washcoating method has great limitations such as the nonuniformity and easy exfoliation of coatings. This review discusses the newly developed non-dip-coating methods for the fiber/foam-structured catalysts and their promising applications in the strongly exo-/endo-thermic and/or high throughput reaction processes.

1. Introduction

Heterogeneous catalysis is the heart for reducing CO_2 emissions, addressing energy challenges, making chemicals production green and sustainable, and decreasing environmental burdens, which influence many aspects of our daily life profoundly.[1] It is of course a nano-scaled surface/interface intrinsically dependent process, but far more than this, it is also essentially constrained by the hydrodynamic and heat/mass-transferring behavior in a macro-scaled

CONTACT Guofeng Zhao ✉ gfzhao@chem.ecnu.edu.cn 🖂 State Key Laboratory of Molecular & Process Engineering, Shanghai Key Laboratory of Green Chemistry and Chemical Processes, School of Chemistry and Molecular Engineering, East China Normal University, Shanghai, China; Yong Lu ✉ ylu@chem.ecnu.edu.cn 🖂 State Key Laboratory of Molecular & Process Engineering, Shanghai Key Laboratory of Green Chemistry and Chemical Processes, School of Chemistry and Molecular Engineering, East China Normal University, Shanghai, China

catalyst bed.[2] These constraints emerging in reaction engineering not only greatly reduce the process efficiency but also deteriorate the catalyst activity/ selectivity and even stability.

Process intensification (PI), an inviting avenue to the safe, compact, and energy-efficient processes, is attracting ever-increasing attentions from both catalysis and engineering fields.[3–7] In July 2016, the "European Cluster on Catalysis" published the "Science and Technology Roadmap on Catalysis for Europe," in which the synthetic multi-catalyst/multi-reactor (such as the micro-reactor and integrated modular catalytic systems in a plug-and-play fashion) was pushed forward as a priority to address the catalysis complexity.[7] Structured catalysts are considered as one type of design strategy for PI in terms of optimizing the hydrodynamic behavior in catalyst bed, enhancing the interphase (gas/solid and gas/liquid/solid) heat/mass transfer in the local-scale catalyst body as well as the global heat transfer at reactor scale, while maintaining the limited pressure drop within catalyst bed at high throughput operation. Therefore, the development and use of structured catalysts are taken as one of the priorities for the PI.[2–9] Specifically, the structured catalysts consist of ceramic (e.g., Al_2O_3, cordierite, and SiC) or metal (e.g., stainless steel, Ni, Al, and Cu) substrates (pre-shaped in the form of a single continuous structure with stable geometry, e.g., honeycomb), and catalytic layers adhered to these substrates. Clearly, this manner can achieve a "macro-micro-nano" organization of the catalytic materials onto the substrate surfaces through adhesion or chemical bonding between them, for instance.[10,11] The current researches and applications of structured catalysts are mainly focused on the regular-void-pattern monolithic honeycombs and micro-channels, which are catalytically functionalized by the washcoating techniques. The honeycomb structured catalysts achieve a high catalytic efficiency and a low pressure drop during high throughput operations and have been widely used in catalytic combustion, catalytic purification of automobile exhaust, denitration of flue gas, and even the anthraquinone hydrogenation.[12] The micro-channel ones have been applied in some processes such as the Fischer-Tropsch synthesis[13] and gas-phase "propylene-peroxide" epoxidation,[14] aiming to seek a solution for their strong reaction heat effect. Comprehensive reviews and books on the honeycomb and micro-channel structured catalysts have been published in the last two decades.[2, 8, 9, 15–22] However, on the one hand, the honeycomb and micro-channel structured catalysts suffer from radial transfer restriction and channel blocking, and on the other hand, the washcoating technique based on the "bottom (fine catalyst particles)-up (substrate washcoating)" strategy costs highly and is not easy to be implemented.

In the last decades, the irregular-void-pattern monoliths such as fibers and foams have continuously appeared and attracted wide attentions.[23–25] Besides having high porosity as typically for the regular-void-pattern

honeycombs and micro-channels, the fiber/foam substrates not only have irregular three-dimensional (3D) network, open structure, and high area-to-volume ratio but also exhibit additional advantages in elimination of radial diffusion limitation, eddy-mixing intensification of heat/mass-transfer, and convenience of large-scale preparation. Moreover, the metal (or SiC) fibers/foams also have high thermal conductivity and unique form factor that can provide a great flexibility in the geometric appearance when filling up the reactors.[3] These features offer a new technical approach to solve the problems for very fast and heat/mass-transfer-restricted reactions and to meet the special requirements of the high throughput operations but with a low pressure drop such as for the environmental catalysis.[26–28] Examples of these reactions include the methane synthesis from coal/biomass, methanol to propylene, dimethyl oxalate hydrogenation to ethylene glycol, VOCs/CH_4 catalytic combustion, O_3 decomposition, methane reformation to syngas, and gas-phase selective oxidation of alcohols. However, there are significant challenges in the catalytic functionalization of such fiber/foam substrates. Through the washcoating method, the catalytic layer from several to tens of microns can be coated onto substrates but with a limited weight content (usually <20%). Especially for the metal fiber/foam substrates, there exist some other severe problems: the coefficient differences in thermal expansion between the catalytic layer and metal substrates, easily causing the coating cracking and spalling; the irregular angular of fiber/foam skeleton, causing the stress effect and concomitant coating uniformity.[7,29] Hence, developing novel methods to efficiently and cost-effectively impart catalytic function to the metal fibers and foams is particularly desirable.

In the last decade, a concept of "*in situ* catalytic functionalization" was raised, and a great progress has been made to establish various non-dip-coating methods. The fiber/foam-structured catalysts can be tailored via controlling reactions to grow nano-composites onto the fiber/foam substrate surfaces in multilevels from nano-, micro-, meso- to macro-scales in one-step. The non-dip-coating methods include spray deposition, electrophoretic deposition, galvanic replacement deposition, wet chemical etching, solvothermal treatment, cross-linking molecules assisted self-organization, and direct growth of catalytic compounds. These methods can overcome the washcoating limitations to a great extent, opening an opportunity to extend structured catalysts from the regular-void-pattern honeycombs and micro-channels to the irregular-void-pattern fibers and foams. Moreover, the distinctive integrated "top-down" strategies can be established to achieve an effective coupling of "flow and heat/mass transfer in reactor" (top) with "catalysis on surface and interface" (down). The contents of this review are as follows: brief introduction of features and applications of the regular-void-pattern honeycomb and micro-channel catalysts; enhancement of heat/mass transfer; non-dip-coating methods for the fiber/foam-substrate functionalization; applications of the fiber/foam-structured catalysts in typical exo-/endo-thermic and/or

high-throughput reaction processes; conclusions and future of the fiber/foam-structured catalysts.

## 2. Regular-void-pattern honeycomb and micro-channel catalysts

It has been widely recognized that a heterogeneous catalyst can efficiently work only when its chemical compositions are well organized from "nano" to "macro" scales (i.e., from the nanostructure of the catalyst surface/interface up to the macro-geometry of the catalyst body).[1–3] Conventional practical catalysts are usually shaped into millimetric granules or pellets, but some frustrating problems emerge such as mass/heat transfer limitations and non-regular flow pattern; moreover, these millimetric catalysts are chaotically filled into fixed-bed reactors, resulting in a high pressure drop when reactants pass through the bed.[9] Contrarily, the structured catalysts are qualified to overcome these problems due to their enhanced heat/mass transfer in combination with the improved hydrodynamics and low pressure drop.[2,30] Configuration of thin catalytic layers coated onto monolithic substrates is a common type of structured catalysts (Figure 1).[2] The substrates are made of ceramic or metal
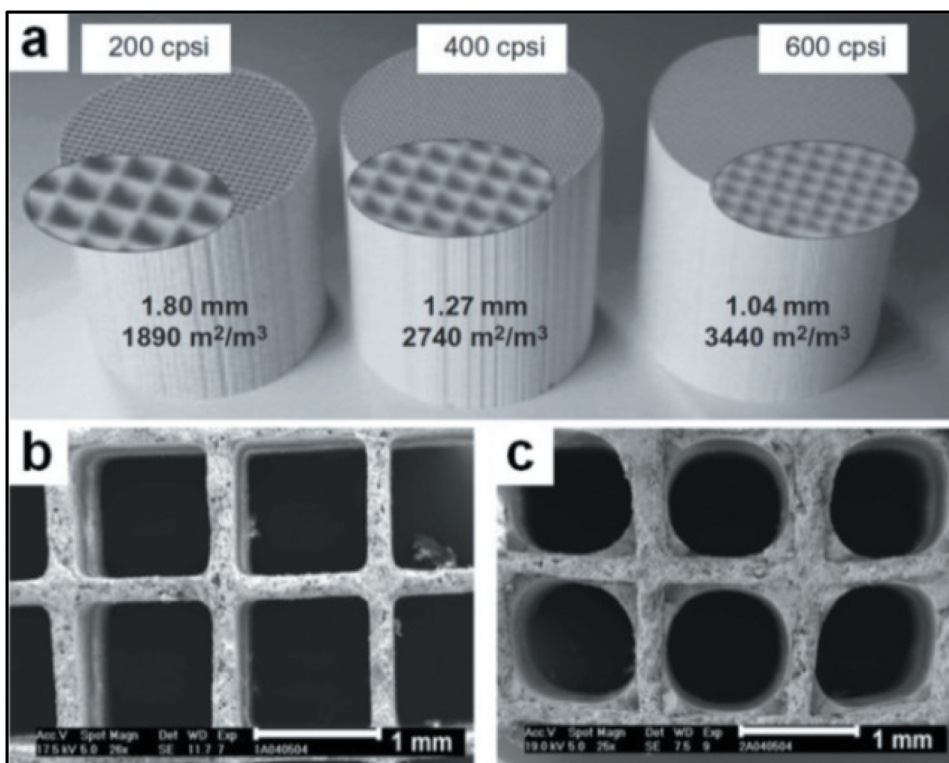
Figure 1. Typical configuration of thin catalytic layers coated onto the "backbone" of monoliths (taking honeycombs as examples here). (a) Typical honeycombs with different numbers of cells per square inch; the numbers below are the geometric surface areas ($m^2_{geometric}/m^3_{reactor}$). Scanning electron microscope (SEM) images of a monolith: before (b) and after (c) coating an α-Al_2O_3 layer (Reprinted with permission from ref.[2] Copyright 2006 by Taylor & Francis Group).

with channels running through them, while the catalytic layer is washcoated in a 10–100 μm thickness onto the channel walls. Clearly, the high void fraction of such structured catalysts allows a low pressure drop at high throughput operations, while the short gas diffusion distance in the thin catalytic layer improves the mass transfer.[10,31]

Over the past several decades, the regular-void-pattern structured catalysts have found many industrial and environmental applications, where the pressure drop is greatly smaller by two to three orders of magnitude than in the conventional particulate-catalyst-fixed-bed reactors.[2] The first practical applications of the regular-void-pattern structured catalysts are based on honeycombs for the decolorization of nitric acid tail gas, car exhaust emission control, and NO_x removal from power station emission.[2,32] After these successful applications, the honeycombs (with square or triangular channels in parallel of 0.5–4 mm diameter) have become the standard substrates for structured catalysts in most environmental applications. The arranged catalysts (Figure 2a) are identified as
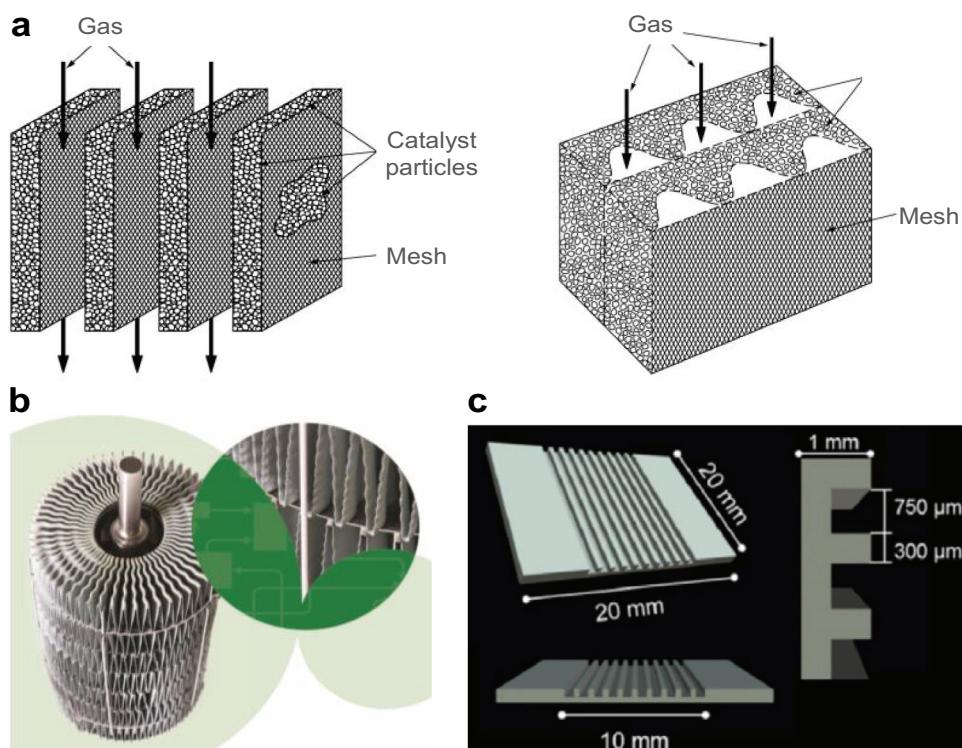
Figure 2. (A) Schematic illustration of arranged catalysts. (b) Optical photograph of "fan" shaped metal foil for the CH_4-steam reformer (Reprinted with permission from ref.[33] Copyright 2006 Elsevier). (c) Schematic illustration of micro-channel catalysts (Reprinted with permission from ref.[13] Copyright 2006 Elsevier).

another common type of the regular-void-pattern catalysts, due to the good heat exchange between the reaction zone of arranged catalysts and their surroundings. Recently, a distinctive "fan" shaped metal foil (Figure 2b) has been manipulated to combine the heat transfer properties, reactive surface area, and pressure drop characteristics, which is available within the tubular steam reformers.[33] Moreover, the micro-channel catalysts (Figure 2c) are industrially presented for the gas-phase propene epoxidation with H_2O_2 and the Fischer-Tropsch synthesis.[13] Besides above commercial applications and pilot-scale demonstrations, these structured catalysts also exhibit great potentials and are successfully studied in the following applications at developmental stage[2]: methanation, hydrogen cyanide production, alkane to oxygenate, and oxidative dehydrogenation.

The regular-void-pattern catalysts have also drawn great attention for three-phase reactions. The main advantages are the same as in the above two-phase cases: short diffusion distance inside the thin catalytic layer and low pressure drop within the catalyst bed, resulting in a high catalyst utilization and improved selectivity. Selective hydrogenation, oxidative wastewater treatment, and biochemical processes seem to be the first areas, in which the structured catalysts will find promising applications. One process of H_2O_2 production using alkyl-anthraquinone has reached full scale with several plants in operation (such as EKA AKZO/Nobel).[34] Catalytic wet air oxidation (Nippon Shokubai process) has also reached the level in large scale.[35] In particular, catalytic distillation is another interesting process that offers ample scope for the structured catalyst abilities.[36] This process comprises a gas–liquid reaction over the structured catalysts with counter current gas–liquid flows and removal of products, which is very favorable for the kinetically and thermodynamically limited reactions. In addition, the flooding of a reactor is a considerable limitation for the counter current catalytic distillation processes in conventional fixed-bed reactors, but will not occur to that extent in cases using structured catalysts.

However, uniform distribution of the catalytic components on substrates is not easily achievable, and weak adhesion of the catalytic components is a problem because leaching occurs for reactions in solvents or with great temperature changes.[29] Moreover, the thin catalytic layer leads to a low active-component loading, which is not important for the diffusion-limited reactions but a clear disadvantage for the kinetically limited ones. Furthermore, the other critical disadvantages of using ceramic substrates are their low heat transfer, poor temperature management in the endo-/exo-thermic reactions, and the lack of radial mixing for fast reactions.[2,37,38]

## 3. Irregular-void-pattern fiber/foam-structured catalysts: enhanced heat/mass transfer

3.1. Fiber/foam-structured catalysts

The monolithic fiber/foam substrates have high porosity, irregular 3D network, open structure, and high area/volume ratio; moreover, the metal fibers/foams also have high thermal conductivity and unique form factor.[3] These features permit the low pressure drop, high mass/heat transfer, and high radial mixing efficiency (Figure 3a).[26–28, 41] The fiber substrates are of large variety, and their properties are in dependence of the chosen materials (such as ceramic, metal, or glass) and manufacturing process. Two basic kinds of fibers are applied: unordered sintered metal fiber-sheets, which are industrially used for filter applications, and ordered knitted or woven fiber-meshes. A review of the metal-fiber catalysts was given by Matatov-Meytal and Sheintuch,[42] and these catalysts applied to several typical reactions at early stage have been summarized therein. Foams are 3D-cellular substrates with entirely open interconnected networks (Figure 3a). Although they do not have regular channels like the honeycombs, they still possess typical features of the structured catalysts (such as high voidage and improved mass transfer); moreover, the open structure of foams leads to a great turbulence (to increase convective heat transport[24]), and the continuous skeleton of foams enhances the heat conduction. The properties and catalytic applications of foams at early stage have been reviewed.[43]

3.2. Enhanced mass transfer in fiber/foam-structured catalysts

A large number of catalytic processes, especially those displaying very fast reaction kinetics, are limited by the mass transfer of reactants in catalyst as well as the high pressure drop during high throughput operations. The catalytic combustion of volatile organic compounds (VOCs) is an important application scenario, because this process must run at a high flow rate (caused by high VOCs dilution by air) and is in a diffusional regime. The ceramic monoliths (such as the typical honeycomb burners) have been adopted.[2] However, an apparent disadvantage of honeycomb burners is the forbidden mass transfer among their parallel channels.

As clearly shown in Figure 3, the fiber/foam-structured catalysts have irregular 3D network, high void fraction, high area-to-volume ratio, and entirely open structure. Specifically, the cylinders in microfibrous monoliths are arrayed in the form of different alignments (Figure 3b)[39]; the open-cell foams are 3D cellular materials made of interconnected struts (Figure 3c), forming a continuous network that encloses the cavities (cells).[40] The flow paths through the fiber/foam-structured catalysts are tortuous, and the flow is thus segmented ceaselessly by the fiber/foam
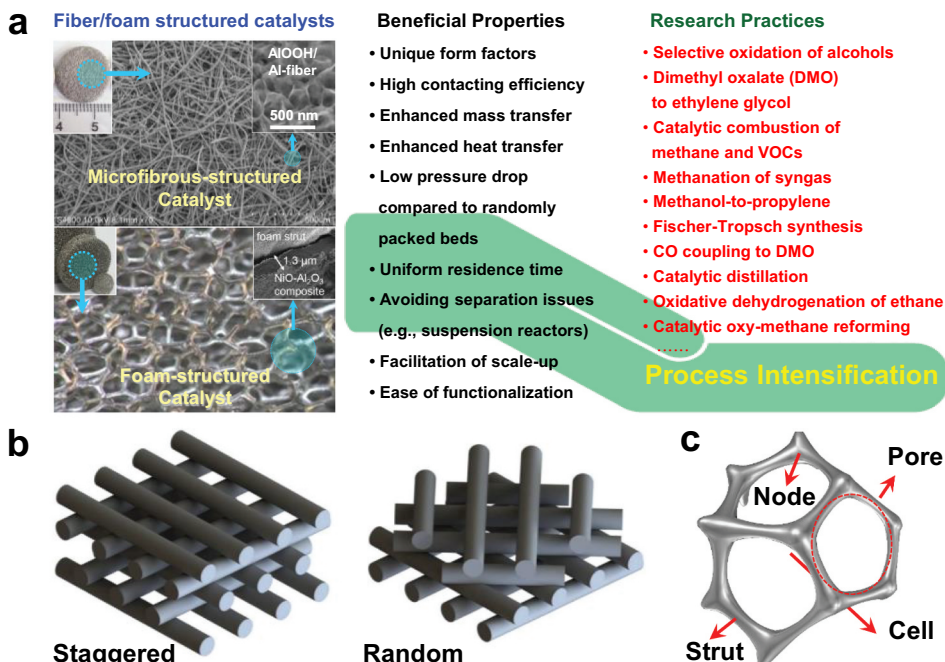
Figure 3. (A) Fiber/foam-structured catalysts engineered from nano- to macro-scales: beneficial properties and research practices (Reprinted with permission from ref.[3] Copyright 2016 Elsevier). (b) Differently arranged fibers (Reprinted with permission from ref.[39] Copyright 2017 Elsevier). (c) Schematic illustration of network of foam (Reprinted with permission from ref.[40] Copyright 2019 Elsevier).

struts, and the as-segmented flows are mixed ceaselessly, which could intensify the heat/mass transfer. Taking the selective catalytic reduction of nitrogen oxides with ammonia (NH_3-SCR) as an example, the advantages of enhanced mass transfer and its promotion effect on reaction rate in the reactor filled with a FeCrAl-foam catalyst (30 pores per inch) are clearly visible over the reactor filled with particulate catalysts (grain size of 2 mm).[44] This contributes to a great enhancement of the infinite rate constant (A_0, pre-exponential factor): 3.3×10^4 s^{-1} for the FeCrAl-foam catalyst vs. 1.2×10^4 s^{-1} for the particulate catalyst. Moreover, high voidage of the fiber/foam-structured catalysts results in a low pressure drop especially for the high throughput reaction processes.[41] Mass transfer in the fiber/foam-structured catalysts is multiply affected, not only by the operation conditions (pressure and temperature) and fluid properties (composition, viscosity, etc.) but also by the size/shape of void space and curvature of flow paths. However, the researches on these aspects are far less than on the honeycomb catalysts, and the mass transfer in the fiber/foam-structured catalysts is mainly studied on the "gas–solid" system.

Several correlations describing the mass transfer in different fiber-based catalysts have been published,[45] but so far there is no correlation to well predict the mass transfer over a wide range of conditions. Reichelt et al.[39] developed a correlation to describe the mass transfer in packed beds of spheres, which is derived on the basis of existing theoretical and semi-empirical correlations. The resulting correlation is applicable with good accuracy for a wide range of Reynolds numbers (Re), Schmidt numbers (Sc), and bed void fraction (ε_B). Moreover, this correlation can be applied to the fiber-based catalysts but leads to a problem of choosing a proper characteristic length. The two potential characteristic lengths are the hydraulic diameter (d_h; $d_h = 4\varepsilon_B/S_v$) and Sauter diameter (d_s; $d_s = 1.5d_h(1-\varepsilon_B)/\varepsilon_B$).[39] Notably, S_V (surface-to-volume ratio) is the proportion of the void fraction (ε_B) and hydraulic diameter (d_h) and is a determining factor in the gas–solid heat/mass transfer. For the fiber substrates, their disordered structure creates a complex path, assuming that the base elements are infinitely long cylindrical fibers. The S_v is given as: $S_v = 4(1-\varepsilon)/d_f$ (d_f is fiber diameter, equal to d_h)[46–48] The results in ref. [42] indicate that d_s is a proper choice, allowing the calculation of mass transfer in both the packed beds and fiber-based catalysts by a single correlation. With d_s as the characteristic length, a generalized form of the mass transfer correlation is obtained to be applicable to the fiber-based catalysts. Notably, this correlation can be transferred to d_h as characteristic length by applying the equation ($d_h = 4\varepsilon_B/S_v$). The accuracy and applicability of this correlation to both fiber-based and packed beds is not affected by choosing between these two options.

For the foam substrates, assessment of gas–solid mass transfer is still debated in literature, but evaluable findings could be obtained in several aspects. The geometrical models assume that the foams consist of repeating unit cells (such as cubic,[49] dodecahedral,[47] and tetrakaidecahedral[48]); and the latter polyhedron, also called a Kelvin cell, is deemed to characterize the foam geometry best.[50] Moreover, the identification of characteristic length is a key issue, because it is an important parameter to be adopted in a series of correlations, such as Sherwood numbers. Originally, the equivalent channel diameter is assumed to be the pore size,[24] but later, the mean pore diameter is defined as the size of internal pore window and strut diameter.[51] For metal foams, Giani et al.[25] stated that the average strut diameter ($d_{s,av}$) is a more representative characteristic length when considering the flow path in foam structure, and they developed a correlation based on the analogy with convective heat transfer in bundles of tubes. This approach is further refined by combining the experimental tests on CO oxidation with the computational fluid dynamic simulations (CFD), developing a correlation based on the combination of asymptotic contributions with creeping and turbulent flow, respectively.[52]

3.3. Enhanced heat transfer in fiber/foam-structured catalysts

Because of the low thermal conductivity of particulate catalyst bed, the heat transfer imposes a size limitation (i.e., a maximum reactor tube diameter of <100 mm) on industrially typical multi-tubular packed-bed reactors for highly exothermic (e.g., selective oxidation reactions) and endothermic (e.g., CH_4 steam reforming) reactions. For example, the Fischer-Tropsch synthesis has a reaction heat of −165 kJ/mol of CH_2,[53] leading to an adiabatic temperature rise of 1600 °C.[54,55] The calculations showed that the radial heat transfer in a gas–solid fixed-bed reactor can be enhanced by one order of magnitude when replacing the randomly packed catalyst pellets with the monolithic catalysts that have a high thermal conductivity.[56] This enhancement is due to the change of dominant heat transfer in the tube from convection to conduction,[56] resulting in a reduced risk of runaway, less catalyst deactivation, better selectivity, and the potential for novel design of an industrial reactor with increased throughput and/or enlarged tube diameter.[57]

The metal fiber/foam-structured catalysts are interesting as they have not only a high degree of interconnectivity that can promote radial mixing but also improved heat transfer that is originated from the continuous metal channels or bridges for heat conduction.[58] For instance, the Cu-fiber[59] or Ni-foam[60] packed bed offers much greater radial effective thermal conductivity than that of the particulate-catalyst bed. The thermal conductivities of catalysts can be experimentally determined by measuring the heating curve in a transient test (Figure 4a).[61] In this test, the tube was filled with stagnant N_2 at ambient pressure, and the apparatus was dipped into a water bath of constant temperature. The transient temperature was recorded until it approached the water bath temperature. The Euler implicit method and Newton-Raphson search algorithms were used to extract the effective thermal conductivity from the temperature-time profiles.[58] High heat transfer of the fiber/foam catalysts can be demonstrated by taking the improved Nusselt number (a critical parameter to characterize the effective heat transfer coefficient for catalyst) as an example. Richardson et al. experimentally measured and theoretically calculated the Nusselt numbers at 800 °C for a ceramic foam (30 pores per inch) and spheres (0.5 mm).[24] The foam has a Nusselt number fourfold higher than that of the spheres, with a two- to fivefold increase in the radial heat transfer coefficient.

Despite the improved heat transfer of the fiber/foam-structured catalysts, no a priori model exists to accurately predict their effective thermal conductivities. Some theoretical and empirical models have been proposed to predict the thermal conductivities of the fibrous materials with stagnant gas or low gas flow rate, including series model,[62] parallel model,[62] Dul'new's model,[63] and Mantle's model.[64] The series and parallel models represent lower and upper limits for the conductivity of composite materials, respectively. The
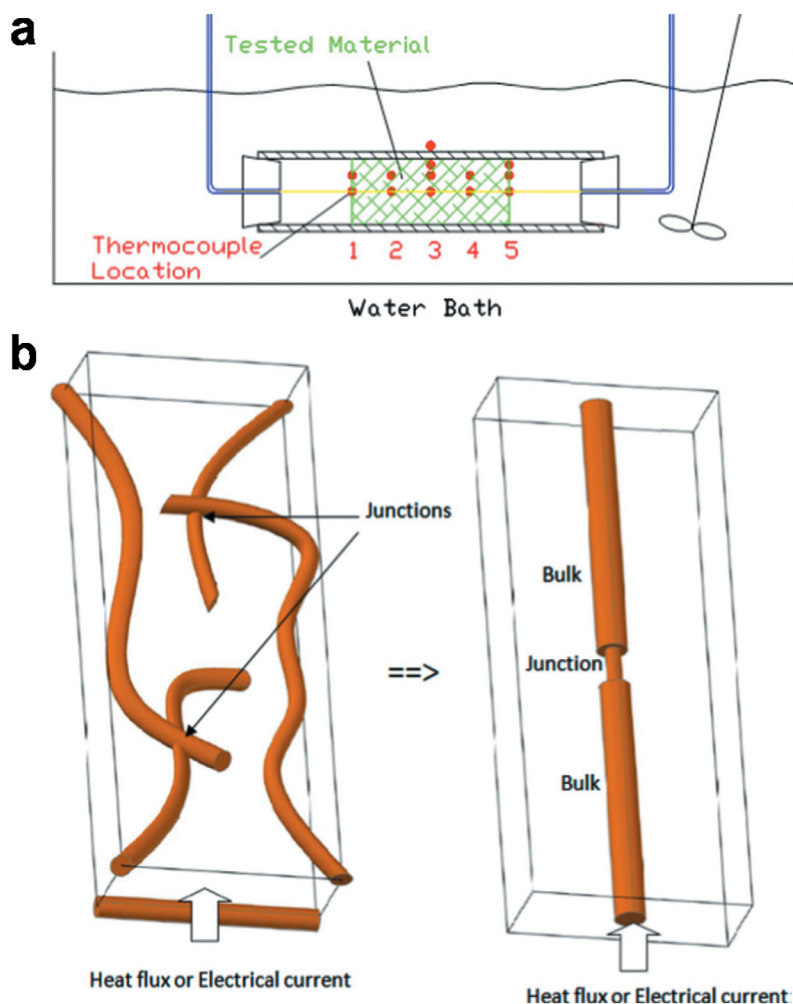
Figure 4. (A) Apparatus for thermal conductivity measurement. (b) Idealized model of the fiber junction factor (Reprinted with permission from ref.[61] Copyright 2013 Elsevier).

Dul'new's model assumes that the fibers are infinitely long cylinders and the model parameters are regressed from unsintered fibrous materials. The effective thermal conductivity of the sintered fibers cannot be fitted well by the Dul'new's model as the unsintered fiber length of 3 mm is too small to meet the assumption of the infinite fiber length. The Mantle's model derives an empirical equation that compensates for the effects of porosity and aspect ratio (length/diameter) of the sintered metal fibers, but the connection quality between fibers is much more crucial to the thermal conductivity of fibers with an aspect ratio of >50. Therefore, a model that considers the connection quality between fibers is required and may offer a good correlation between the prediction and experimental data. The connection quality in sintered microfibers can be represented by the junction factor, and a practical model

(Figure 4b) taking the junction factor of fibers into account is developed to predict the effective thermal conductivity of fibers.[62–64]

The struts in foam are believed to be the predominant backbone contribution to the high thermal conductivity and require an accurate foundation with respect to the physical properties and junction factor between struts. For the foam materials, theoretical assessment of the gas–solid heat transfer is still open to debate in literature, but the junction factor is easily determined by measuring the material's electrical resistance. Appropriate electrical measurements provide a facile method to determine the thermal conductivity of foams (as well as fiber monoliths).[61] The efforts to optimize the fiber/foam preparation procedures can be guided by the junction factor. Especially for the sintered microfibers, the effects of the sintering temperature and sintering time were studied, showing that the junction factor and effective thermal conductivity can be improved by increasing the sintering temperature and prolonging the sintering time.

4. Non-dip-coating catalytic functionalization of fiber/foam substrates

Generally, the fiber/foam substrates are not qualified directly as desired catalytic supports or catalysts, mainly because their surface areas are too low for the catalytic components to be highly dispersed. To process them into suitable monolithic catalysts, the effective and efficient catalytic functionalization is particularly desirable. Traditionally, a layer of high-surface-area support, such as Al_2O_3, must be deposited onto the fiber/foam surface by the washcoating technique. Unfortunately, this technique for the fiber/foam substrates suffers from the weak adherence to layers,[65] pore blocking,[46] and high cost. In recent years, some non-dip-coating techniques have been developed for effectively and efficiently imparting catalytic function to the fiber/foam substrates, especially for the metal ones, including spray deposition, electrophoretic deposition, galvanic replacement deposition, chemical etching, *in-situ* growth of zeolites, endogenous growth of $AlOOH/Al_2O_3$, *in-situ* growth of layered double hydroxides, and cross-linking molecules assisted self-organization. Hence, this section is to summarize these novel methods reported in the last decade.

4.1. Spray deposition method

Ahlström-Silversand and Odenbrand developed a novel spray deposition technique to fabricate a wire mesh catalyst.[66,67] By plasma-spraying an Al_2O_3-polyamide mixture onto a FeCrAl-wire mesh using a plasma spray equipment (Figure 5) followed by burning off the polyamide,[66] a thin Al_2O_3 layer with a well-defined macro-porosity but a low surface area (<1 m²/g) is created. By treating the as-obtained material then with an Al_2O_3-sol, the surface area
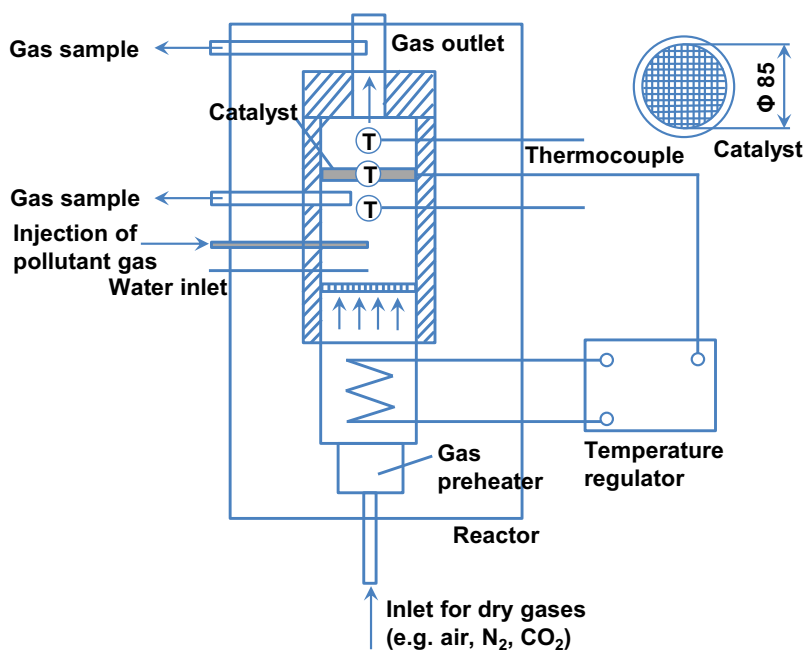
Figure 5. Experimental set up for plasma spray (Reprinted with permission from ref.[66] Copyright 1997 Elsevier).
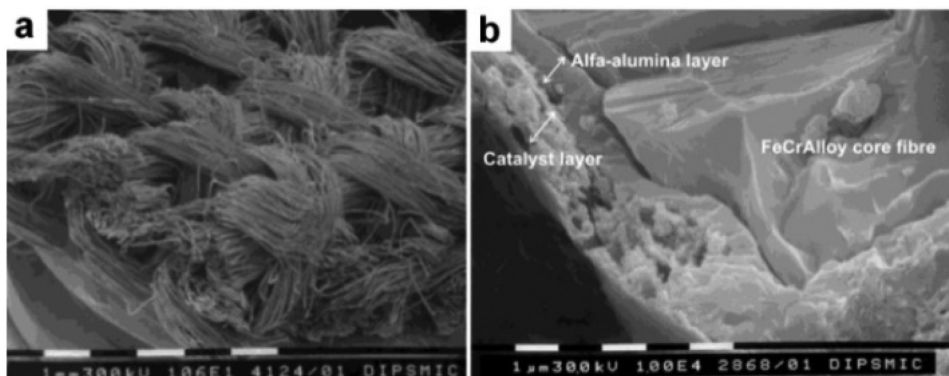
Figure 6. (A) Optical photograph of FeCrAl-fiber. (b) SEM image of the $LaMnO_3 \cdot MgO/FeCrAl$-fiber prepared by spray pyrolysis (Reprinted with permission from ref.[70] Copyright 2004 American Chemical Society).

can be increased by a factor of 50 or more. The Al_2O_3 layer can be catalytically activated with PdPt or V_2O_5-CuO, for instance, through an impregnation step.

Meille et al. presented a one-step spray coating strategy to adhere to a porous γ-Al_2O_3 layer onto substrates,[68] with a large surface area (about 200 $m^2 \, g^{-1}$) and a controlled thickness (1–200 μm) of as-deposited layer. Prior to the spray coating, a standard suspension needs to be prepared, and in order

to obtain a homogeneous Al_2O_3 layer, the Al_2O_3 particles must be strongly anchored on the thoroughly cleaned substrates. The investigation showed that the expected thickness of layer is dependent on the pre-treatment of substrate, concentration of Al_2O_3, and pH of suspension.

Specchia et al.[69,70] reported a spray pyrolysis method to prepare a new catalytic FeCrAl-fiber-mat burner for the natural gas combustion in domestic applications according to an accurate micro-structural design. The typical preparation of such catalyst consists of three optimized steps: (i) optimal pre-oxidation of a FeCrAl-fiber-mat at 1200 °C so as to favor the growth of α-Al_2O_3 layer, (ii) deposition via the spray-pyrolysis of a previously developed perovskite catalyst ($LaMnO_3 \cdot 2ZrO_2$ or $LaMnO_3 \cdot MgO$, Figure 6), and (iii) calcination at 900 °C for the stabilization and complete crystallization of the catalytic phases. Notably, the spray deposition cycle can be repeated several times to get a desired catalyst loading.[71] After extensive aging under practical operating conditions (repeated on-off cycles and prolonged durations under high-temperature radiating conditions), the burner exhibits a limited loss in catalytic performance.

4.2. Electrophoretic deposition method

Based on the deposition of particles of colloid suspension on the surface of an electrode under an electric field, Vorob'eva and Kustov first applied the electrophoretic deposition (EPD) to prepare monolithic-fiber-mesh catalysts.[72] The Al_2O_3-sol was initially prepared by the hydrolysis of aluminum isopropoxide. A monolithic-fiber-mesh made of 50 μm stainless steel fiber was used for the EPD operation, and in order to improve the adhesion, the fiber surface was cleaned by electrochemical method. To deposit Al_2O_3, the pieces of fiber-mesh were placed into the sol solution as a cathode, and a direct current was passed (Figure 7a). After drying and calcining, the EPD-coated sample could be obtained with an Al_2O_3 layer tunable from 1 to 15 μm.

This EPD technique was later employed to deposit Al_2O_3 on wire-mesh substrates by Quan et al.,[73–75] and the detailed procedures were described in ref. [73]. Typically, the wire-mesh-sheet made of 0.20 mm stainless-steel wire, with a size of hole opening approximately 0.95 cm, was etched with 0.1 M HCl and subsequently washed with distilled water in order to remove grease. The Al_2O_3 suspension was prepared, and an as-cleaned wire-mesh-sheet was placed into the suspension as cathode with a stainless-steel plate as anode whose area was larger than the cathode. The experiments were performed at room temperature, and a coating with a deposited thickness of about 50 μm was obtained within 10 min. The sample was dried and then calcined to achieve a well-adhered Al_2O_3 layer (Figure 7b,c). Nitrate of Ce, La, Cu, Al, or Ba was loaded on as-formed Al_2O_3 layer by the impregnation method followed by calcination (Figure 7d),[73] and it was also found that the layer
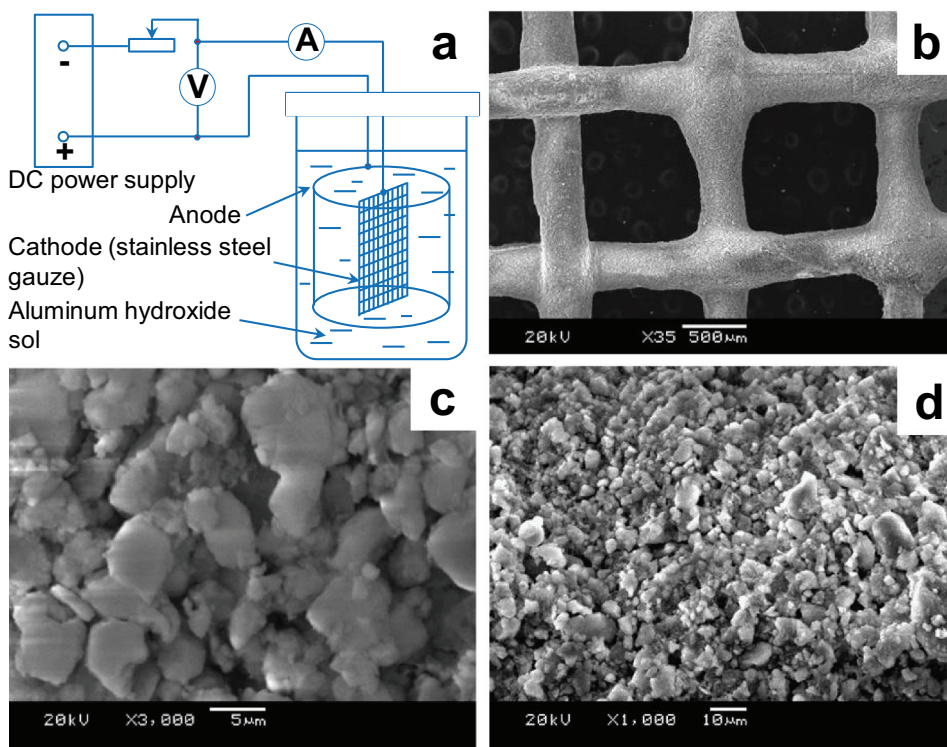
Figure 7. (A) Apparatus for coating Al_2O_3 on stainless steel gauze by EPD (Reprinted with permission from ref.[72] Copyright 2000 Elsevier). (b,c) SEM micrographs of Al_2O_3 coating by EPD. (d) SEM micrograph of coating impregnated with lanthanum nitrate (Reprinted with permission from ref.[73] Copyright 2006 Elsevier).

has an excellent vibration-resistant ability. Subsequently, they successfully deposited Al_2O_3 layer onto the wire-mesh-honeycomb (WMH) substrates and further prepared a series of WMH-structured catalysts by the same methods. Moreover, the WMH substrates could also be coated with metal (Al, Ti) powders by the EPD method, and the resulting metal layers were subsequently oxidized to be transformed into their oxide layers.[41,76]

4.3. Galvanic replacement deposition method

The galvanic replacement reaction can spontaneously take place between the metal ions with higher potentials and the metal substrates with lower ones. For example, Au nanoparticles (NPs) can be firmly deposited onto a Ni-microfiber (8 μm diameter) surface by immersing the Ni-microfiber into a $HAuCl_4$ aqueous solution, because of the large potential difference between Ni^0/Ni^{2+} (−0.23 V) and Au^0/Au^{3+} (1.69 V)[77]; the Au NPs can also be galvanically deposited onto a Cu-microfiber in the same way,[78] owing to the great potential difference between Cu^0/Cu^+
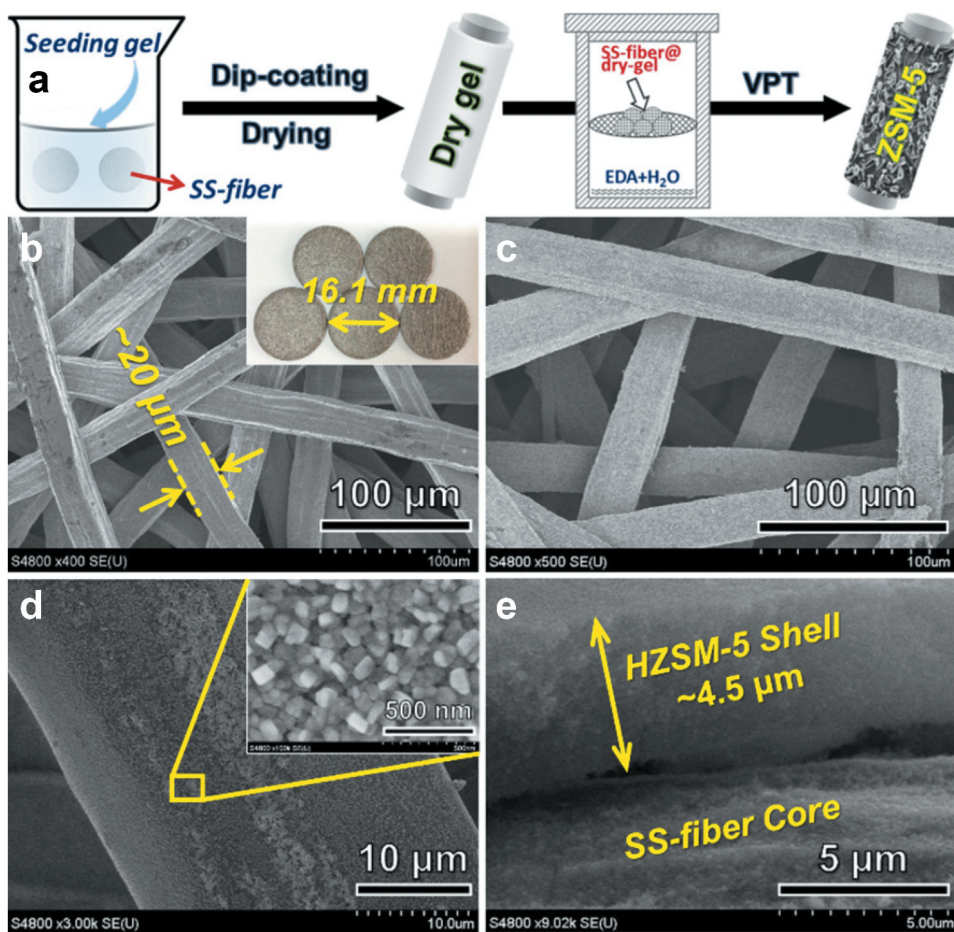
Figure 8. (A) Schematic illustration for the top-down fabrication strategy of coupling dip-coating with seed-assisted VPT method. (B) Photograph and SEM images of the SS-fiber substrate. (C-E) SEM images of the representative HZSM-5/SS-fiber catalyst with 23.0 wt% HZSM-5, showing the monolithic and surface structures (Reprinted with permission from ref.[83] Copyright 2018 Elsevier).

(0.19 V) and Au^0/Au^{3+} (1.69 V). Analogously, the galvanic deposition of Ag NPs on a Ni-microfiber surface can proceed automatically, of which the driving force comes from the large difference in potentials between Ni^0/Ni^{2+} (−0.23 V) and Ag^0/Ag^+ (0.8 V).[79] Moreover, the big potential difference between Ni^0/Ni^{2+} (−0.23 V) and Pd^0/Pd^{2+} (0.95 V) allowed us to galvanically deposit Pd NPs on a Ni-foam surface to form a Pd/Ni-foam catalyst.[80] Based on this approach, a series of fiber/foam-structured catalysts were fabricated from nano- to macro-scales in one step for the exo-/endothermic and/or high throughput reactions.

4.4. Chemical etching method

The precious metal NPs (such as Ag, Au, and Pd) can be effectively deposited onto some fiber/foam substrates via the galvanic reaction, but the base metals with low potentials (such as Ni, Fe, Cu, Co, Mn, and Zn) cannot be deposited through this way. Therefore, a chemical etching method was developed to functionalize the metal fibers and foams. For example, the monolithic Ni-foam tablets (such as 100 pores per inch, 2 mm thickness, equal diameter to reactor inner one) were directly immersed into a chemical etching solution (e.g., 1.0 mM sodium dodecyl sulfate ($C_{12}H_{25}OSO_3Na$), 0.2 M acetic acid (CH_3COOH), and 0.3 M aluminum nitrate ($Al(NO_3)_3$)) at desired temperature for some time.[60] The as-etched tablets were washed with distilled water for several times, dried overnight, and calcined in air. Finally, a nanocomposite layer of NiO-Al_2O_3 could be generated and deposited onto the Ni-foam firmly and homogeneously. By simply adding cerium nitrate ($Ce(NO_3)_3$) to the above etching solution, a uniform catalytic layer consisting of NiO-CeO_2-Al_2O_3 nanocomposites of a 3 μm thickness can also be efficiently *in situ* formed onto the Ni-foam surface, by directly immersing a Ni-foam into the etching solution followed by calcination.[81] Several binary nanocomposites of Ni-MO_x (M = Al, Zr, or Y) can be loaded onto the Ni-foam via such one-step wet chemical etching method.[82] What to be more noted is that the monolithic structure and high heat/mass transfer of Ni-foam were well retained after etching, which offers high quality for the strongly exo-/endothermic and/or high throughput reactions, such as the methanation of CO and/or CO_2, catalytic oxy-methane reforming, dry reforming of methane, and catalytic combustion.

4.5. Solvothermal method

4.5.1. In-situ growth of ZSM-5 zeolite via hydrothermal synthesis

One microfibrous-structured ZSM-5 catalyst was obtained by direct growth of zeolite crystals onto a 3D porous network of 316 L stainless steel microfibers (SS-fiber).[10] Typically, the circular chips of SS-fiber substrate were seeded by ZSM-5 using the dip-coating method. Then, such seeded chips were placed into a Teflon-lined steel autoclave filled with a synthesis gel, followed by hydrothermal treatment. As-made ZSM-5/SS-fiber samples were directly calcined in air at 550 °C for 5 h to remove the organic template and then converted into their H-form via the ion-exchange and calcination at 550 °C for 5 h.

To improve the ZSM-5 synthesis efficiency and reduce the synthesis cost, Ding et al. attempted to synthesize ZSM-5/SS-fiber (Figure 8) by the high-efficiency vapor-phase transport (VPT) method.[83] Typical VPT procedures for the ZSM-5/SS-fiber preparation were as follows: circular chips

of SS-fiber were dipped into a synthesis sol containing silicalite-1 seeds (which was prepared according to the reported method[84]) and dried at 100 °C to evaporate water. By repeating the dip-coating and drying operations, the content of dry gel coated on the SS-fiber could be accurately controlled in the range of 20–25 wt%. Subsequently, the circular chips of dry-gel/SS-fiber and ethylenediamine solution were transferred into a Teflon-lined stainless-steel autoclave, in which the circular chips were physically separated from the solution by a stainless steel mesh. The crystallization was carried out at 180 °C for 120 h. After that, as-obtained products were dried at 100 °C, and then calcined at 550 °C for 5 h in air to remove the template.

In order to achieve a hierarchical porous structure in the ZSM-5 layer grown on SS-fiber, caramel was introduced into the synthesis system as a pore-forming agent.[85] Typically, circular chips of SS-fiber substrate were seeded with silicalite-1 (MFI-type)[84] by the dip-coating method. As-seeded chips and synthesis sol were sealed into a Teflon-lined stainless-steel autoclave and crystallized at 180 °C for 48 h. As-synthesized meso-ZSM-5/SS-fibers were rinsed thoroughly with water, dried at 100 °C overnight, and calcined in air at 550 °C for 5 h.

Furthermore, a monolithic hollow-B-ZSM-5/SS-fiber catalyst was tailored through the seed (silicalite-1)-assisted dry-gel VPT method and subsequent alkali-leaching treatment.[86] First, the parent silicalite-1@B-ZSM-5/SS-fiber catalyst was obtained by direct growth of silicalite-1@B-ZSM-5 on a SS-fiber via the seed (silicalite-1)-assisted VPT method (detailed preparation in ref. [86]). Subsequently, the silicalite-1 core in the silicalite-1@B-ZSM-5 was leached out by alkali treatment in a mild Na_2CO_3 media at 60 °C for 6 h, leading to a great enhancement of mesoporosity development because of the abundant hollow structures left behind. After washing with deionized water thoroughly, the hollow-B-ZSM-5/SS-fiber was converted into its H-form via the ion-exchange and calcination at 550 °C for 5 h.

4.5.2. Endogenous growth of boehmite and/or alumina via steam-only oxidation

The Al_2O_3 is a widely used support for the heterogeneous catalysts due to its large surface area and high hydrothermal stability. Macroscopically engineering of Al_2O_3 honeycombs and open-cell foams still remains challenging owing to their poor mechanical strength, and the Al_2O_3 deposition on ceramic and metal materials by dip-coating techniques suffers from nonuniformity and exfoliation of coatings.[2] Recently, a promising route has been developed to achieve endogenous growth of AlOOH nanosheets (ns-AlOOH, which can be converted into γ-Al_2O_3 and/or α-Al_2O_3) via a steam-only oxidation method (based on the reaction: $2Al + 4H_2O = 2AlOOH + 3H_2$) on various Al substrates, such as the microfibers, foams, tubes, and foils.[87,88]

4.5.3. Hydrothermal growth of layered double hydroxides

The layered double hydroxides (LDHs) are a family of naturally occurring or synthetic hydrotalcite-like materials, presenting the $[Mg(OH)_2]$ brucite-like layered structure. The divalent metal cations (such as Mg^{2+}, Ni^{2+}, Zn^{2+}, Cu^{2+}, and Mn^{2+}) can be substituted with trivalent ones (such as Al^{3+}, Fe^{3+}, or Cr^{3+}) within their brucite-like layers to give a positively charged layer, and the positive charge is balanced by a wide variety of anions (such as CO_3^{2-}, SO_4^{2-}, NO_3^-, Cl^-, or OH^-) within their interlayer domain. Therefore, LDHs are represented by a common formula $[M^{2+}_{1-x}M^{3+}_x(OH)_2](A^{n-})_{x/n}\cdot mH_2O$.[89] It is expectable to obtain a metal oxide composite by designing a suitable LDHs-precursor with needed catalytically active metal cations and subsequently calcining in a controlled manner. As-made oxide composites are characteristic of large surface area, high thermal stability, and homogeneous distribution, thus attracting ever-growing interests in catalysis.[90–92]

In order to process these LDHs-derived oxides into qualified catalysts, Zhang et al. first reported a method, by which the LDHs can be fabricated on a porous anodic alumina/aluminum (PAO/Al) substrate via an *in-situ* crystallization technique.[93] Typically, the $Ni(NO_3)_2$ and NH_4NO_3 were dissolved in deionized water, and the solution pH was adjusted to 6.5 by adding 1% aqueous ammonia solution; then, the PAO/Al substrates were placed vertically in the above solution inside a Teflon-lined stainless steel autoclave, which was placed in a water bath at 75 °C for 36 h. After the completion of LDHs growth, the samples were taken out of the autoclave, rinsed with ethanol, and dried at room temperature, and the NiAl-LDH/PAO/Al product was obtained. Subsequently, Wei et al.[94] fabricated a monolithic Cu-Co catalyst via the growth of CuCoAl-LDHs onto a monolithic Al substrate followed by a calcination-reduction treatment (Figure 9). This catalyst exhibits a potential application as a highly effective catalyst for the NH_3BH_3 decomposition to produce hydrogen. It was verified that the high dispersion of Cu-Co species plays a key role in greatly enhancing the activity of this catalyst.

4.5.4. Endogenous growth via hydrothermal treatment

Some fibers and foams, such as Ni-fiber/-foam and Cu-fiber/-foam, have high chemical activity, which can be utilized to endogenously grow the catalytic layers (such as Ni- and Cu-containing layers) onto their parent fibers/foam surfaces. In a typical synthesis of a Ni-foam-structured Ni-based catalyst, the Ni-foam was first cleaned with a HCl aqueous solution in an ultrasonic bath for several minutes, thoroughly washed using deionized water and absolute ethanol, and dried at 100 °C for 12 h; the NH_4Cl and metal nitrates (such as $Mn(NO_3)_2$) were dissolved in distilled water under stirring; the Ni-foam was immersed into the above solution and was hydrothermally treated inside a Teflon-lined stainless steel autoclave at required temperature for some time; as-treated Ni-foam was washed several
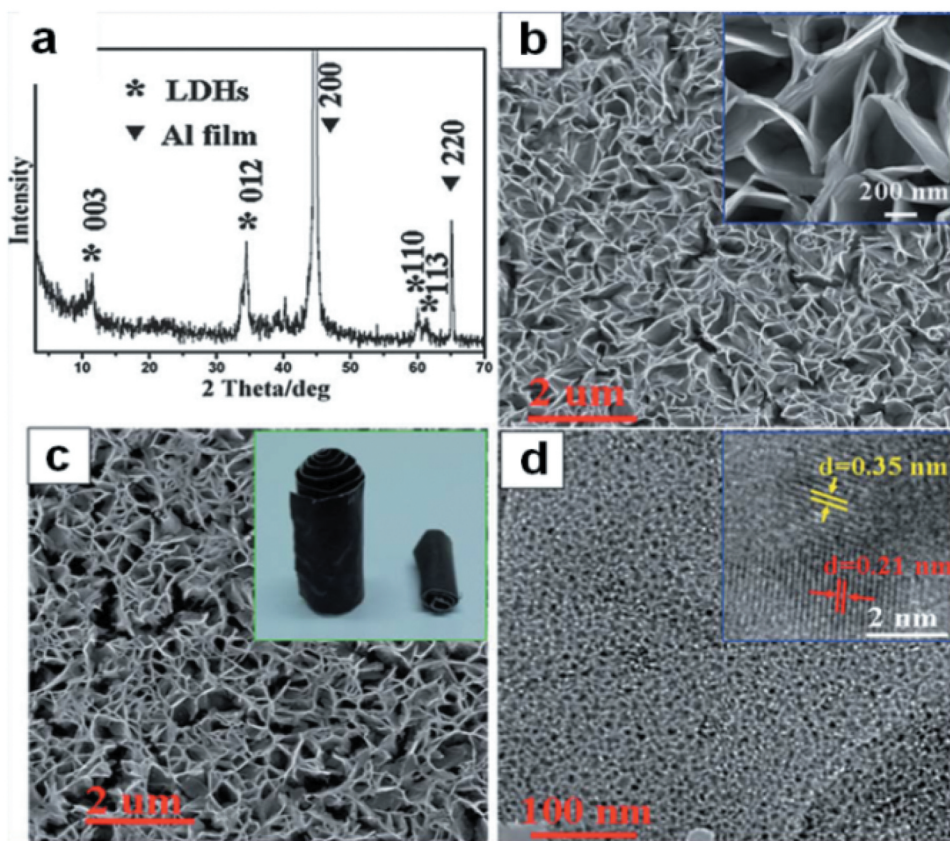
Figure 9. (A) X-ray powder diffraction (XRD) pattern of the CuCoAl-LDH precursor on an Al substrate. SEM images of (b) the CuCoAl-LDH precursor and (c) the monolithic Cu-Co catalyst. (d) TEM images of the monolithic Cu-Co catalyst (the inset shows the lattice fringes of metal Cu and spinel Co_3O_4, respectively) (Reprinted with permission from ref.[94] Copyright 2013 Royal Society of Chemistry).

times with ethanol and deionized water, and dried overnight to obtain a $Ni(OH)_2$-$Mn(OH)_2$/Ni-foam; finally, as-made sample was calcined in air to get $Ni(OH)_2$-$Mn(OH)_2$ converted into NiO-MnO_x nanocomposites. During the hydrothermal reaction, Ni^{2+} ions were first dissolved from the Ni-foam ($Ni + 2 H^+ = Ni^{2+} + H_2$) and then coprecipitated with Mn^{2+} ions ($Ni^{2+} + Mn^{2+} + 4OH^- = Ni(OH)_2 + Mn(OH)_2$) to form $Ni(OH)_2$-$Mn(OH)_2$ onto the Ni-foam.[95] The Ni-foam not only serves as the support but also provides Ni^{2+} ions for the *in-situ* growth of $Ni(OH)_2$-$Mn(OH)_2$ nanosheets. Recently, a synthesis of a monolithic Cu-Zn/Al-foam catalyst was reported.[96] The pre-treated Al-foam was immersed in an aqueous solution of cupric oxalate and zinc acetate with a solution pH of ca. 7. The system was treated at 70 °C for 24 h, and as-obtained sample was calcined in air at 350 °C for 4 h to obtain the final catalyst.

Moreover, a series of Ni-containing layers were endogenously grown onto Ni-foam by the solvothermal methods. To grow NiC_2O_4 nanorods onto the Ni-foam,[97] the oxalic acid dihydrate and NH_4Cl were dissolved in deionized water and then transferred into a Teflon-lined stainless-steel autoclave. The Ni-foam was then placed into the autoclave and hydrothermally treated at 100 °C for 24 h. After cooling to room temperature, the Ni-foam coated with a green layer of $NiC_2O_4 \cdot 2\,H_2O$ was rinsed with deionized water for several times. Finally, the resulting sample was dried in air at 80 °C to obtain a NiC_2O_4/Ni-foam. For the growth of the nickel terephthalate (Ni-Tp) nanosheets,[98] the Ni-foam was immersed into an N,N-dimethylformamide solution of terephthalic acid and $Ni(NO_3)_2 \cdot 6\,H_2O$, and then was transferred into a Teflon-lined stainless steel autoclave followed by heating at 150 °C for 24 h. After that, the resulting sample was rinsed with deionized water and absolute ethanol for several times and then dried overnight at 80 °C to obtain a Ni-Tp/Ni-foam. For the growth of the nanosheet-like $Ni(OH)_2$ onto a Ni-foam,[99] the urea and $Ni(NO_3)_2 \cdot 6\,H_2O$ were dissolved in an aqueous solution of NH_4F, the Ni-foam was immersed into the above-obtained solution, followed by heating at 100 °C for 12 h. The resulting sample was then rinsed successively with deionized water and dried overnight at 80 °C to obtain a $Ni(OH)_2$/Ni-foam.

4.6. Cross-linking molecules assistant self-organization

The core@shell nanostructure with core NPs encapsulated into oxide shells is a promising protocol to enhance the catalyst stability.[100,101] The catalytically active core NPs are isolated by the outer shell, thus preventing their sintering in the reactions at high temperature and/or with strong exothermicity. A typical model of the core@shell nanostructure is $Pt@SiO_2$ that was tailored via the colloidal synthesis of 14-nm Pt cores followed by the polymerization of 17-nm-thick SiO_2-shell around the Pt cores.[102] This nanostructure exhibited a high stability during the ethylene hydrogenation reaction, a typical strongly exothermic reaction. Recently, a hierarchical catalyst was designed and prepared in two steps[103]: pre-organization of $Pd@CeO_2$ subunits consisting of a 2 nm Pd core and a ceria (CeO_2) shell and homogeneous deposition on a modified hydrophobic alumina. The Pd cores are still isolated even after being subjected to 850 °C calcination and show an excellent stability for the CH_4 oxidation. Very recently, a new $Au@CeO_2$ catalyst was facilely synthesized using a redox-coprecipitation strategy,[104] where a redox reaction between the core and shell precursors permits spontaneous formation of a core@shell structure in one step. This catalyst shows a high durability for the alkynes semihydrogenation. However, several problems hamper their applications in heterogeneous catalysis,[105–107] such as the lack of a strategy for bulk production, complicated synthesis, and low mass/heat transfer and

high pressure drop of randomly packed catalyst bed for the strongly exo-/endo-thermic and/or high throughput reaction processes.

Based on the cross-linking molecules having multi-functional-groups, Lu et al. reported a chemically/economically affordable strategy to organize the core@-shell-like structure (core NPs encapsulated into oxide mesoporous-matrix) while firmly embedding them onto a monolithic fiber in one step.[11] The 3-aminopropyltriethoxysilane (APTES)-assisted organization of a Pd@SiO$_2$/ns-Al$_2$O$_3$/Al-fiber catalyst is taken as an example to display this strategy (Figure 10).[11,108] Typically, the AlOOH nanosheets were endogenously grown onto a 3D network of 60-μm Al-microfiber mat via the steam oxidation method (to see 4.5.2). The palladium acetate (Pd(Ac)$_2$) was dissolved into acetone, and the cross-linking agent APTES, as well as the as-made AlOOH/Al-fiber substrate was added to this solution. The chelation between the -NH$_2$ in APTES and single-metal-ion of Pd^{2+} occured; simultaneously, the silanization reaction occurred between the -Si-O-CH$_2$-CH$_3$ in APTES and -OH of AlOOH on the Al-fiber surface to form Al-O-Si bonds. Subsequently, some water was added to the system and the rest -Si-O-CH$_2$-CH$_3$ polymerized in the presence of water to form Si-O-Si bonds.[109] After treating at 100 °C for 2 h, a cross-linked organic-inorganic hybrid catalyst precursor of Pd^{2+}-APTES-AlOOH/Al-fiber with Pd^{2+} chelated in the network of APTES-AlOOH was formed, which was finally transformed into the Pd@SiO$_2$/ns-Al$_2$O$_3$/Al-fiber catalyst by calcining at 450–600 °C in air and then reducing at 150–400 °C in H$_2$.
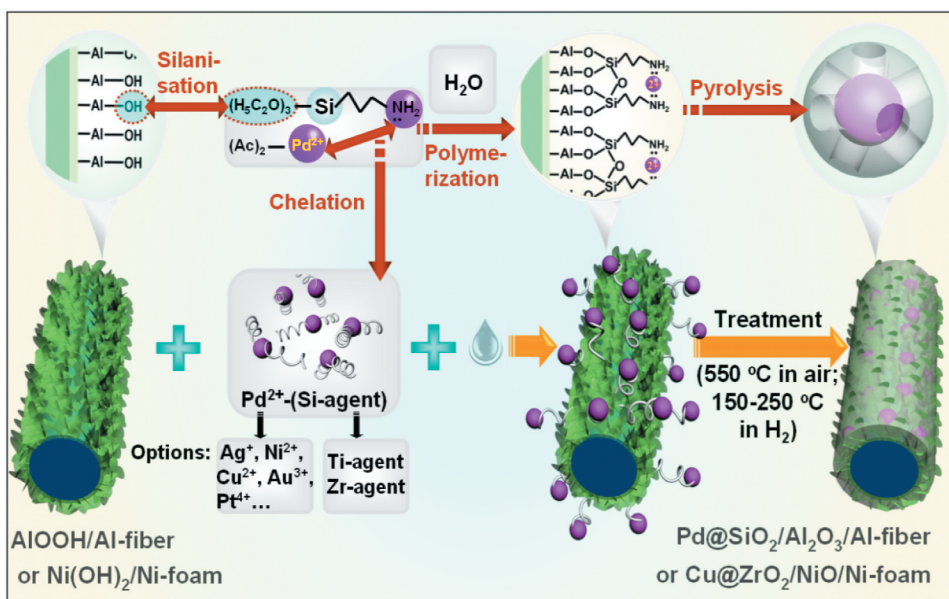
Figure 10. Schematic representation of one-step "macro-micro-nano" organization for embedding the oxide-encapsulated-nanoparticles onto monolithic-substrates with the aid of cross-linking molecules (Reprinted with permission from ref.[11] Copyright 2016 Royal Society of Chemistry).
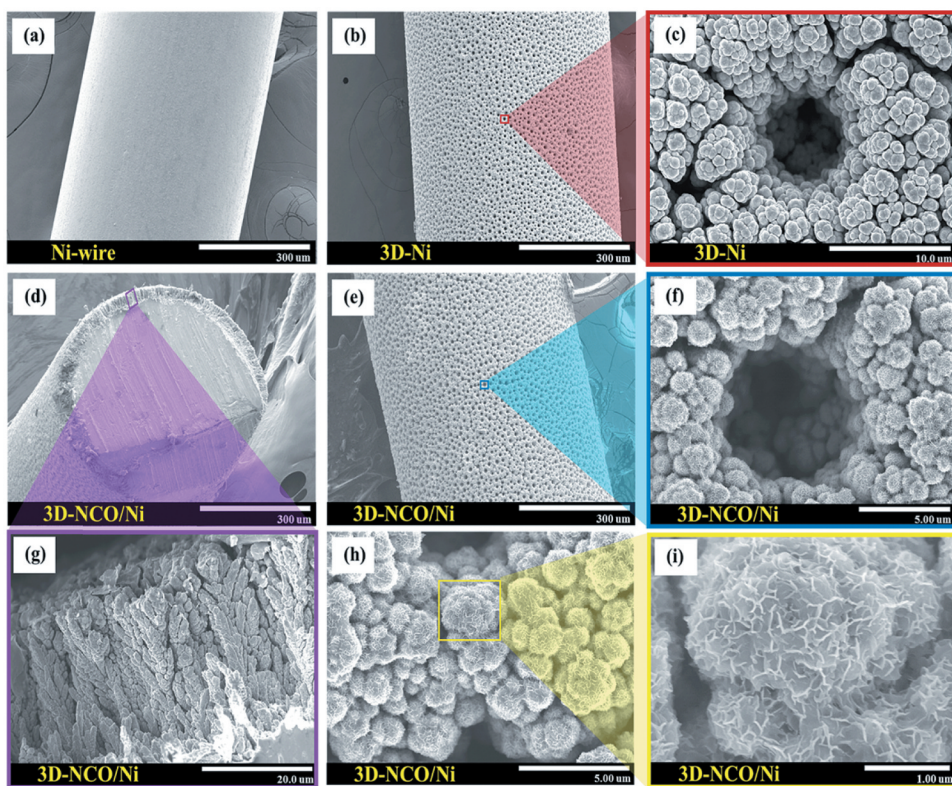
Figure 11. SEM images of (a) Ni-wire, (b-c) 3D-Ni, and (d-i) 3D-NiCo$_2$O$_4$/3D-Ni: (d,g) cross-section image. (e) Plain view images. (f-i) High magnification images (Reprinted with permission from ref.[116] Copyright 2016 Royal Society of Chemistry).

Notably, the calcination treatment also plays a pivotal role in the organization process, because the pyrolysis of remaining alkyl chains in the APTES could produce H$_2$ and CH$_4$, which facilitates the formation of mesopores inside the SiO$_2$ matrix. Expectably, these monolithic structured core@shell-like catalysts are qualified for typical harsh reactions, such as the catalytic combustion of methane and volatile organic compounds, because these catalysts uniquely combine both the advantages of the high stability of core-shell-like structures and enhanced heat/mass transfer of the monolithic metal substrates.

4.7. Reaction-induced method

Ever-increasing studies have demonstrated that the catalyst structures are sensitive to the ambient atmosphere and could even be induced into an optimum state in the reaction stream. A typical example of this observation is the Rh$_{0.5}$Pd$_{0.5}$ NPs capable of undergoing the segregation of metals, driven by the oxidizing and reducing environments[110]: in the oxidizing NO and O$_2$ environments, Rh migrated to the shell and was almost completely oxidized;

while in the reducing CO and H_2 environments, RhO_x was reduced, with Rh atoms migrating to the core and Pd atoms to the shell. Moreover, the homogeneous nanoalloy of $PdZn_x$ is induced into a heterostructure of $PdZn_y@(x-y)$ ZnO in the methanol reforming process $(CH_3OH + H_2O = 3\,H_2 + CO_2)$,[111] and the Co_3O_4-nanorod supported single-site Pt catalyst is successfully *in situ* induced into Pt_nCo_m/CoO_{1-x} for the water-gas shift reaction $(CO + H_2O = H_2 + CO_2)$.[112] Hence, it is wondered whether an optimum structure could be induced more directly from the initial precursors, nitrates for instance, by reaction itself. Recently, a monolithic catalyst of Ti-microfiber-supported binary-oxide composites was engineered from nano- to macro-scales for the gas–phase aerobic oxidation of alcohols to aldehydes.[113] The catalyst was obtained by placing the transient metal (e.g., Ni, Co, Cu, and/or Mn) nitrates onto the fiber surface by the impregnation method, and the as-supported nitrates were subsequently transformed into binary-oxide nanocomposites in the real reaction stream at 300 °C. More recently, a monolithic Al_2O_3/Al-fiber (the detailed preparation in 4.5.2) structured $InNi_3C_{0.5}$ catalyst was developed for the reverse water-gas shift reaction.[114] The Ni and In nitrates were supported onto the Al_2O_3/Al-fiber by the impregnation method, and these nitrates were transformed into a NiO-In_2O_3 binary-oxide composite after calcination. Finally, the as-obtained NiO-In_2O_3/Al_2O_3/Al-fiber was performed in the real reaction stream $(CO_2 + H_2 = CO + H_2O)$ at 500–600 °C to be transformed into the $InNi_3C_{0.5}$/Al_2O_3/Al-fiber catalyst.

## 4.8. Direct growth of needed catalytic compounds

Some monolithic fiber and foam substrates are made of transition metals, such as Ni-fiber/-foam and Cu-fiber/-foam. They not only act as the catalyst support but also can furnish the catalytic species, such as NiO in a Ni-fiber supported Au@NiO composite,[77] Cu^+ in a Cu-fiber supported $PdAuCu^+$ composite,[115] and Ni NPs in a Ni-foam supported Ni-CeO_2-Al_2O_3 composite.[81] Clearly, these elements are from the substrates and then are evolved into catalytic form either via the controllable treatment or under reaction conditions (detailed information in the following sections). More interestingly, some compounds can be grown directly on substrates. For example, the spinel/perovskite oxides, NiS_x, NiP_x, and Ni-based alloys can be controllably grown onto a Ni-foam/-fiber.

The $NiCo_2O_4$ electro-active material was grown onto a 3D-Ni/Ni-wire current collector (Figure 11).[116] The 3D-Ni was first prepared by the electro-deposition method in the presence of hydrogen bubble templates, which has porous dendritic walls with many active sites and short diffusion path length. Then, the bimetallic (Ni, Co) hydroxides were co-electrodeposited onto the 3D-Ni, followed by calcination at 300 °C to yield spinel $NiCo_2O_4$. Recently, Zhu et al.[117] reported a growth of $NiFe_2O_4$-NiO onto a Ni-foam as follows:

the Ni-foam initially underwent a hydrothermal treatment to create a porous layer of Ni(OH)$_2$ nanosheets on the foam struts; the as-obtained Ni(OH)$_2$/Ni-foam was then impregnated with an aqueous solution of iron(III) nitrate and calcined in air to produce a NiFe$_2$O$_4$-NiO/Ni-foam catalyst.

A monolithic Ni$_3$S$_2$/Ni-foam electrocatalyst was obtained via growing the highly active Ni$_3$S$_2$ nanosheets on a highly conductive Ni-foam (Figure 12).[118] The Ni-foam was ultrasonically cleaned with acetone and then with an HCl solution and subsequently washed with water and ethanol for several times. The cleaned Ni-foam was submerged into a Teflon-lined
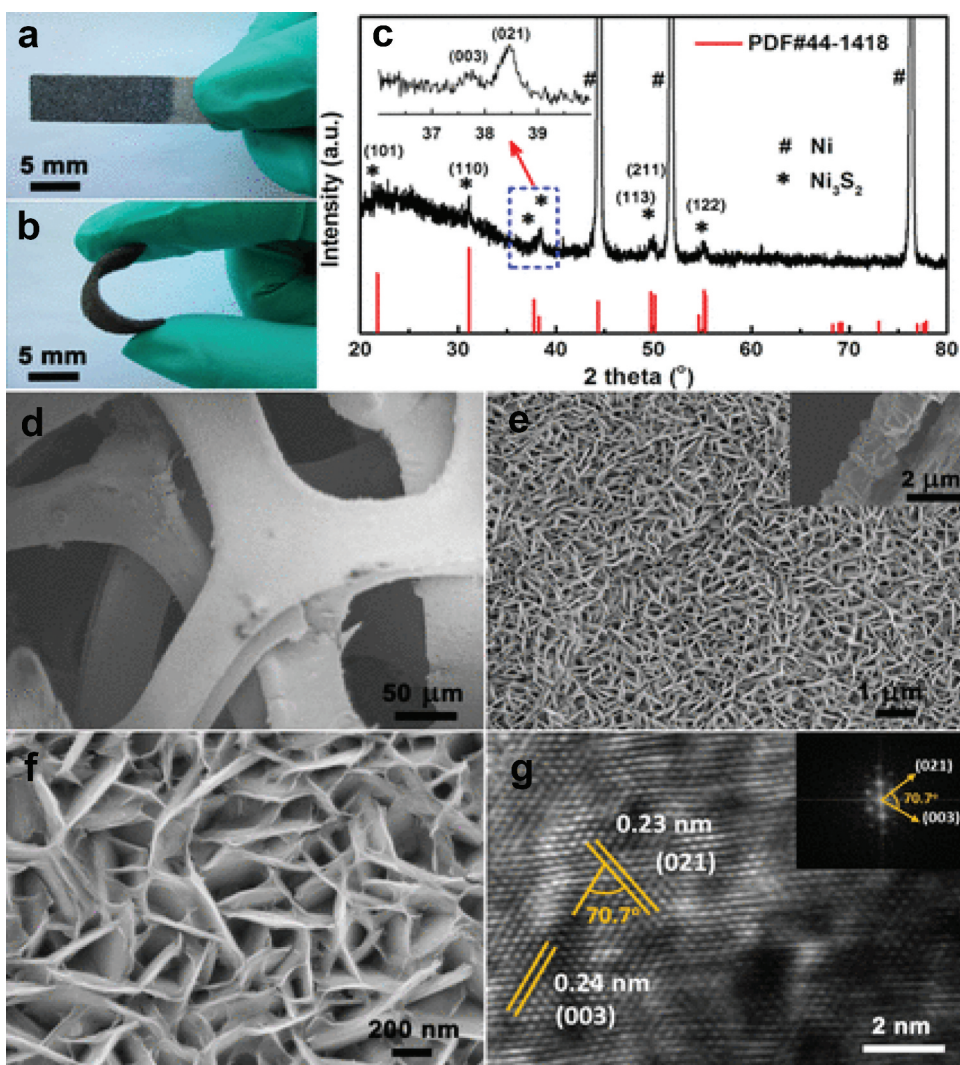
Figure 12. (A,b) Digital images, (c) XRD pattern, and (d-f) top-view SEM images of the Ni$_3$S$_2$/Ni-foam. (g) HRTEM image of the Ni$_3$S$_2$/Ni-foam (Reprinted with permission from ref.[118] Copyright 2015 American Chemical Society).

stainless steel autoclave that was filled with a thiourea solution and treated at 150 °C for 5 h. The resulting material was washed with ethanol for several times and dried in vacuum at room temperature to obtain final Ni_3S_2/Ni-foam product. Lu et al. fabricated a Ni-foam-structured Ni_xP catalyst for the gas-phase dimethyl oxalate hydrogenation to methyl glycolate.[119] In the typical synthesis, the NH_4Cl and $Ni(NO_3)_2$ were dissolved in deionized water, and the Ni-foam was cut into circular shape with a diameter of 8.0 mm. Then, the solution and Ni-foam chips were transferred into a Teflon-lined stainless steel autoclave and kept 100 °C for 3 h. After that, the resulting $Ni(OH)_2$/Ni-foam sample was washed with deionized water and dried at 100 °C for 12 h. Subsequently, the $Ni(OH)_2$/Ni-foam was placed in a quartz tube, and sodium hypophosphite was placed in its front. The phosphorization reaction was conducted in N_2 atmosphere at 300 °C for 2 h. What to be particularly noted is that phosphine, formed by the decomposition of sodium hypophosphite during the phosphorization process, is virulent and inflammable, and thus the effluent gas must be absorbed by a sodium hypochlorite solution to remove it.

4.9. Comparison on different non-dip-coating methods

Many methods for fabricating the fiber/foam-structured catalysts are presented in this review. What to be noted is that there is no a universal method appropriate for preparing all kinds of catalysts, and the different catalysts require different preparation methods. Therefore, a right method is of significance to prepare a suitable fiber/foam-structured catalyst. To facilitate the selection of an appropriate method, the advantages and disadvantages of these methods are summarized in Table 1.

5. Heterogeneous catalysis applications

Prior to reviewing the applications of as-fabricated fiber/foam-structured catalysts in heterogeneous catalysis, corresponding preparation methods, and catalytic applications of these catalysts are summarized in Table 2 for convenience.

5.1. Oxidation

5.1.1. Gas-phase oxidation of alcohols to aldehydes/ketones

The gas-phase oxidation of alcohols using oxygen (or air) in the presence of heterogeneous catalyst is a "green" process to produce "clean" aldehydes and ketones on an industrial scale. Because of the strong exothermicity of this process, the major challenge is to tailor desirable catalysts that are active and selective at low temperatures (to avoid fast catalyst deactivation) integrated with high thermal conductivity (helpful for rapidly dissipating reaction heat)

Table 1. Advantages and disadvantages of the catalytic-functionalization methods.

Method	Advantage	Disadvantage
Spray deposition method	In principle, applicable to all kinds of supporting materials sprayed onto the surface of fiber/foam substrates with high adhesion; Easy controlling of loading, porosity, and specific surface area of as-sprayed materials; Easy preparation and scaling up.	Uneven spraying at micro scale; Inapplicable to thick and/or multilayered fiber/foam substrates; Inapplicable to spraying some catalytic components.
Electrophoretic deposition method	Even deposition of supporting materials onto the surface of fiber/foam substrates with high adhesion; Easy to control loading, porosity, and specific surface area of as-deposited materials; Easy preparation and scaling up.	Inapplicable to electrophoretically depositing some catalytic components.
Galvanic replacement deposition method	In-situ growth and even deposition of catalytic components with high adhesion; Easy preparation and scaling up.	Only applicable to depositing precious metal NPs (such as Ag, Au, and Pd); Difficult to control the size and shape of catalytic components.
Chemical etching method	In-situ growth and even distribution of catalytic components with high adhesion; Easy to control loading, porosity, and specific surface area of catalytic components; Easy preparation and scaling up.	Difficult to control the size of catalytic components; Low utilization of raw materials.
In-situ growth of zeolite	In-situ growth and even distribution of zeolites with high adhesion; Easy preparation and scaling up; Easy to control loading of zeolites.	Low utilization of raw materials; Inapplicable to in-situ growth of other materials.
Endogenous growth of AlOOH/Al$_2$O$_3$	In-situ growth and even distribution of AlOOH/Al$_2$O$_3$ with high adhesion; Easy preparation and scaling up; Easy to control loading.	Low universality (only applicable to Al substrates).
In-situ growth of LDHs	In-situ growth and even distribution of LDHs with high adhesion; Easy preparation and scaling up; Easy to control loading.	Low utilization of raw materials.
Endogenous growth via hydrothermal treatment	In-situ growth and even distribution of catalytic components with high adhesion; Easy preparation and scaling up; Easy to control loading.	Too few types of catalytic components in situ grown by this method; Low utilization of raw materials.
Cross-linking molecules assisted self-organization	In-situ growth and even distribution of core@shell components with high adhesion; Easy preparation and scaling up; Easy to control loading.	Too few types of cross-linking molecules.
Reaction-induced method	In-situ growth and even distribution of catalytic components with high adhesion; Easy preparation and scaling up; Easy to control loading.	Difficult to control the size of catalytic components; Too few types of catalytic components in situ grown by this method.
Direct growth of needed catalytic compounds	In-situ growth and even distribution of catalytic components with high adhesion; Easy preparation and scaling up; Easy to control loading.	Too few types of catalytic components in situ grown by this method.

to improve their energy/production efficiency and stability. Some Ag-based catalysts such as the electrolytic Ag and supported nano-Ag catalysts have been employed for the gas-phase alcohol oxidation in a packed-bed reactor.[120–122] The electrolytic Ag has high thermal conductivity, but its catalytic activity is very low; the oxides such as Al$_2$O$_3$ and SiO$_2$ supported

Table 2. Preparation methods and applications of the fiber/foam-structured catalysts.

| Catalyst	Preparation method	Application	Ref.
Ag/LTA/Cu-grid	Seed-assisted hydrothermal synthesis of LTA zeolite, and electrolytic deposition of Ag species	Gas-phase benzyl alcohol oxidation to benzaldehyde	121
Ag/Ni-microfiber	Galvanic replacement deposition method	Gas-phase benzyl alcohol oxidation to benzaldehyde	79
Au/Cu-microfiber	Galvanic replacement deposition method	Gas-phase benzyl alcohol oxidation to benzaldehyde	78
Au/Ni-microfiber	Galvanic replacement deposition method	Gas-phase benzyl alcohol oxidation to benzaldehyde	126
$CoO@Cu_2O$/Ti-microfiber	Reaction-induced method	Gas-phase benzyl alcohol oxidation to benzaldehyde	113
$CoO@Cu_2O$/Ti-microfiber	Reaction-induced method	Gas-phase ethanol oxidation to acetaldehyde	128
$Pt/\gamma-Al_2O_3$/FeCrAl-foam	Washcoating method	Preferential oxidation of CO	130
$Au-\alpha-Fe_2O_3/ns-\gamma-Al_2O_3$/Al-fiber	Endogenous growth of Al_2O_3, hydrothermal growth of $\alpha-Fe_2O_3$, and deposition-precipitation of Au nanoparticles	CO oxidation	129
$CuO-CeO_2$/AlOOH/Al-fiber	Endogenous growth of AlOOH, hydrothermal growth of $CuO-CeO_2$	Preferential oxidation of CO	131
$Mn_2O_3-Na_2WO_4$/SiC-foam	Washcoating method	Oxidative coupling of methane	135
$CeO_2-Na_2WO_4-Mn_2O_3$/SBA-15/Al_2O_3/FeCrAl	Washcoating method	Oxidative coupling of methane	136
$TiO_2-Mn_2O_3-Na_2WO_4$/SiC-foam	Washcoating method	Oxidative coupling of methane	137
$TiO_2-Mn_2O_3-Na_2WO_4$-foam	Molding method	Oxidative coupling of methane	138
Cr/SBA-15/Al_2O_3/FeCrAl-foil	Washcoating method	Oxidative dehydrogenation of ethane	142
Nb_2O_5-NiO/Ni-foam	Endogenous $Ni(OH)_2$ growth via hydrothermal treatment followed by Nb modification and calcination treatment	Oxidative dehydrogenation of ethane	143
$InNi_3C_{0.5}/Al_2O_3$/Al-fiber	Endogenous growth of Al_2O_3, and supporting of $InNi_3C_{0.5}$	Reverse water gas shift	114
Cu-Zn/Al-foam	Hydrothermal growth method	CO_2 hydrogenation to methanol	96
Pd-Au/Cu-fiber	Galvanic replacement deposition method	Dimethyl oxalate hydrogenation to ethylene glycol	115
$InNi_3C_{0.5}$/Ni-foam	Hydrothermal growth of NiC_2O_4, and subsequent carburization to form $InNi_3C_{0.5}$	Dimethyl oxalate hydrogenation to ethylene glycol	156
$Ag-CuO_x$/Ni-foam	Galvanic replacement deposition method	Dimethyl oxalate hydrogenation to methyl glycolate	157
Ni_xP/Ni-foam	Direct growth of Ni_xP	Dimethyl oxalate hydrogenation to methyl glycolate	119
$FeNi_3-FeO_x$/Ni-foam	Direct growth of $NiFe_2O_4$-NiO followed by reduction treatment	Dimethyl oxalate hydrogenation to ethanol	117
Pd/AlOOH/Al-fiber	Endogenous growth of AlOOH, and supporting of Pd by impregnation method	Semihydrogenation of acetylene	167
$Ni-Al_2O_3$/FeCrAl-foil	Percolation-blowing method	Steam methane reforming	171
$Ni@SiO_2/Al_2O_3$/FeCrAl-fiber	Cross-linking molecules assistant self-organization method	Dry reforming of methane	176
$NiO-MgO-Al_2O_3$/FeCrAl-fiber	In-situ hydrothermal growth of LDHs followed by calcination treatment	Dry reforming of methane	177
$CeO_2-NiO-Al_2O_3$/FeCrAl-fiber	In-situ hydrothermal growth of LDHs followed by CeO_2 modification	Catalytic oxy-methane reforming	182
Rh/Al_2O_3/FeCrAl-fiber	Washcoating of Al_2O_3, and incipient wetness impregnation with Rh species	Catalytic oxy-methane reforming	183

(*Continued*)

Table 2. (Continued).

Catalyst	Preparation method	Application	Ref.
Ni/Co$_3$O$_4$/ceramic-foam	Washcoating method	Glycerol and biomass reforming	196
Ni/ceramic-foam	Washcoating method	Glycerol and biomass reforming	197
Ni-Al$_2$O$_3$/Ni-foam	Chemical etching method	CO$_2$ methanation	60
Ni-CeO$_2$-Al$_2$O$_3$/Ni-foam	Chemical etching method	CO methanation	81
HZSM-5/SS-fiber	In-situ hydrothermal growth of zeolite	Methanol to olefins	10
Hollow-B-ZSM-5/SS-fiber	In-situ hydrothermal growth of zeolite	Methanol to olefins	86
Fe-Mn-K/ns-Al$_2$O$_3$/Al-fiber	Endogenous growth of Al$_2$O$_3$, and supporting of Fe-Mn-K	Fischer-Tropsch synthesis	223
Pd/Ni-foam	Galvanic replacement deposition method	Catalytic combustion of methane	80
Pd@SiO$_2$/ns-Al$_2$O$_3$/Al-fiber	Cross-linking molecules assistant self-organization method	Catalytic combustion of methane	11
Pd-MgO-Al$_2$O$_3$/Al-fiber	In-situ hydrothermal growth of LDHs followed by calcination treatment	Catalytic combustion of methane	233
Co-MnO$_x$/ns-Al$_2$O$_3$/Al-fiber	Endogenous growth of Al$_2$O$_3$, and supporting of Co-MnOx	O$_3$ decomposition	234
Pd-Co-MnO$_x$/Al$_2$O$_3$/Al-fiber	Endogenous growth of Al2O3, stepwise supporting of Co-MnOx and Pd	O$_3$ decomposition	235
NiO-MnO$_x$/Ni-foam	Endogenous growth of Ni(OH)2-Mn(OH)x followed by calcination treatment	NH$_3$-SCR	95
Pd/Ce$_{0.66}$Zr$_{0.34}$O$_2$/TiO$_2$/Al$_2$O$_3$/WMH	Electrophoretic deposition method	NH$_3$-SCR	245
TiO$_2$@Fe$_2$O$_3$/Al$_2$O$_3$/Al-mesh	Cross-linking molecules assisted self-organization method	NH$_3$-SCR	246
Pd@SiO$_2$/ns-Al$_2$O$_3$/Al-fiber	Cross-linking molecules assisted self-organization method	Catalytic combustion of volatile organic compounds	11
Nafion-SiO$_2$/SS-fiber	Washcoating method	Benzene-HNO$_3$ nitration	249
ZSM-5/SS-fiber	In-situ hydrothermal growth of zeolite	Esterification of acetic acid with ethanol by catalytic distillation	250
Ni$_3$S$_2$/Ni-foam	Direct growth of Ni$_3$S$_2$	Oxygen evolution reaction and hydrogen evolution reaction	118
Hollow Cu-fiber	Phase-inversion/sintering method	Electroreduction of CO$_2$ to CO	257
Hollow-Ag-fiber	Phase-inversion/sintering method	Electroreduction of CO$_2$ to CO	258
NiCo$_2$O$_4$/3D-Ni/Ni-wire	Direct growth of NiCo$_2$O$_4$	Supercapacitors	116
PANi-CNTs/Ni-microfiber	Washcoating method	Supercapacitors	263

nano-Ag catalysts possess higher activity, but the weak thermal conductivity of used oxides induces hotspots in the catalyst bed, which not only severely degrade the catalyst performance but also cause the bed temperature runaway. A possible solution is to render novel catalysts that achieve the coupling of good low-temperature activity/selectivity and high thermal conductivity. To accomplish this goal, an LTA-zeolite/Cu-grid supported nano-Ag catalyst (Figure 13) is developed for the gas-phase benzyl alcohol oxidation to benzaldehyde.[121] This catalyst delivered a 60% conversion with a 90% selectivity at 320 °C. Notably, the zeolite film thickness is several micrometers, and some hotspots unavoidably emerge to some extent. In order to further enhance the catalyst heat-transfer and activity, a series of metal-microfiber-
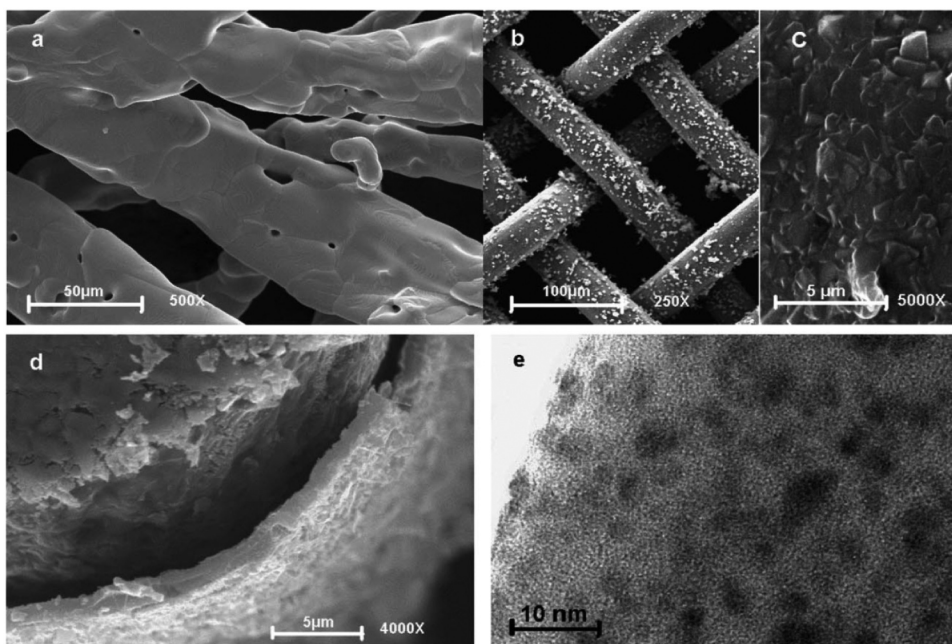
Figure 13. SEM images of the (a) bulk electrolytic Ag catalyst, (b) LTA-zeolite/Cu-grid, (c) LTA-zeolite film, and (d) Ag/LTA-zeolite/Cu-grid. (e) TEM image of the Ag/LTA-zeolite/Cu-grid (Reprinted with permission from ref.[121] Copyright 2005 Elsevier).

structured catalysts are developed by the method in 4.3. One early typical catalyst is an 8 μm Ni-microfiber-structured nano-Ag catalyst,[79] offering a 90–95% benzyl alcohol conversion with a 95–97% benzaldehyde selectivity at a relatively low temperature of 300 °C. Thanks to the high heat-transfer of Ni-microfiber, the catalyst is free of bulk-coke formation and is stable for at least 120 h.

In the last three decades, supported Au NPs catalysts have showed wide outstanding catalytic activity in many reactions.[123,124] Several nano-Au catalysts, such as Au/SiO$_2$ and Au-Cu/SiO$_2$,[125] have also been prepared for the gas-phase selective oxidation of benzyl alcohol. In consideration of the extraordinary activity of Au NPs and the enhanced heat/mass transfer of metal-microfibers, it is possible to develop a novel catalyst by embedding Au NPs onto certain metal microfiber surfaces. To check this idea, an Au/Cu-microfiber catalyst was prepared by the galvanic deposition method (for details to see in 4.3), achieving the coupling of high heat-transfer and low-temperature activity for the gas-phase benzyl alcohol oxidation (>92% benzyl alcohol conversion and 97% benzaldehyde selectivity at 250 °C).[78] The low-temperature activity stems from the "AuCu-Cu$_2$O" nanocomposites with synergistic effect between the AuCu-alloy and Cu$_2$O that were *in situ* formed during the reaction. However, its reported lifetime at 250 °C was only 50 h

because the Cu microfiber is so slender as to be easily powdered during long-term testing. In order to improve the stability, another Au/Ni-microfiber catalyst of the same type was subsequently prepared also with the aid of galvanic reaction between the $HAuCl_4$ and Ni-microfiber.[126] Via the galvanic reaction ($3Ni + 2HAuCl_4 = 2Au + 3NiCl_2 + 2HCl$), the "Au-$NiCl_2$" composites were *in situ* formed and firmly anchored onto the Ni-microfiber surface; along with activation in the reaction stream at 380 °C, the "Au-$NiCl_2$" was then transformed into "Au@NiO" nanocomposites.[77] The resulting Au/Ni-microfiber catalyst, with high thermal conductivity, is highly active, selective, and stable for the mild gas-phase oxidation of alcohols. For example, a high benzyl alcohol conversion of 94–96% with >99% benzaldehyde selectivity could be stably obtained within 700-h running at 250 °C. The X-ray photo-electron spectroscopy combined with X-ray absorption near-edge structure revealed that a Ni_2O_3-Au^+ hybrid site is formed and is the genesis of the outstanding low-temperature activity.[127]

Recently, a series of Ti-microfiber-structured binary-oxide catalysts were engineered by the method in 4.7, for the gas-phase aerobic oxidation of benzyl alcohol to benzaldehyde.[113] Among them, the CoO@Cu_2O/Ti-microfiber (with 2.5 wt% CoO and 2.5 wt% Cu_2O loadings) was found to be an outstanding catalyst, delivering a 93.5% benzyl alcohol conversion with a 99.2% benzaldehyde selectivity at 230 °C (boiling point of benzyl alcohol of 210 °C). The reaction-induced formation of "CoO@Cu_2O" ensembles (i.e., larger CoO NPs partially covered with smaller Cu_2O clusters) was revealed to account for the substantially improved low-temperature activity, in nature, due to the enhanced Cu_2O-CoO interface. Also, the CoO@Cu_2O ensembles were successfully structured on a SiC-foam via the reaction-induced method for the gas-phase ethanol oxidation to acetaldehyde (Figure 14),[128] achieving a 92% ethanol conversion with a 96% acetaldehyde selectivity at 260 °C.

5.1.2. CO oxidation

The oxidation of CO to CO_2 at low temperature plays a key role in the air cleanup, automotive emission control, and H_2 cleanup for fuel cells. In particular, in terms of gas masks and air purifiers, the catalysts with high activity and long-term stability at high gas hourly space velocity (GHSV) are needed in a wide temperature window under the harsh conditions, containing, for instance, high CO and humidity levels.[129] The Au NPs supported on FeO_x are a promising type of catalysts for the CO oxidation. One challenge for their applications in the real world is to tailor a novel monolithic catalyst to meet the fundamental criteria (such as high catalyst utilization efficiency and low pressure drop) needed for the high throughput processes.

Sirijaruphan et al.[130] reported a FeCrAl-foam-structured Pt/γ-Al_2O_3 for the CO selective oxidation in H_2. In comparison with the Pt/γ-Al_2O_3 counterpart, the foam-structured catalyst offers interesting possibilities for
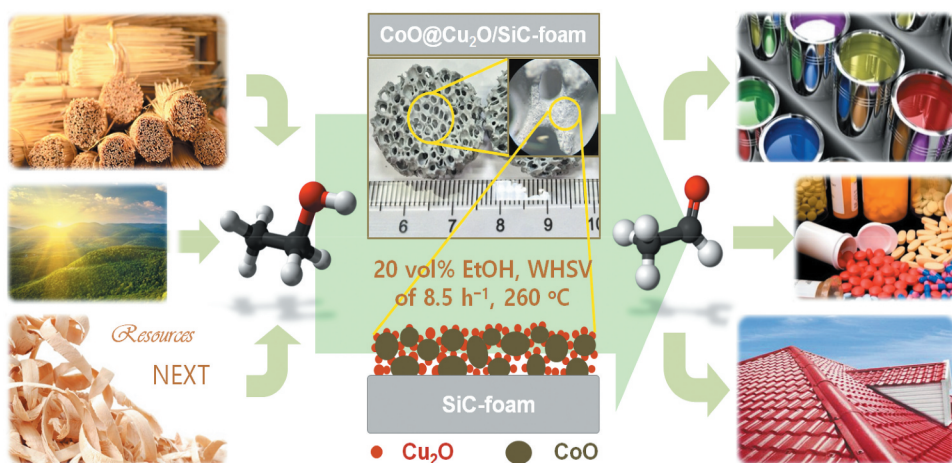
Figure 14. Reaction-induced self-assembly of CoO@Cu$_2$O nanocomposites onto SiC-foam for the gas-phase oxidation of bioethanol to acetaldehyde (Reprinted with permission from ref.[128] Copyright 2017 Wiley-VCH).

commercial application due to the low pressure drop, excellent flow characteristics through the foam, and high heat transfer properties. Tao et al.[129] prepared an active thin-felt Au-α-Fe$_2$O$_3$/ns-γ-Al$_2$O$_3$/Al-fiber catalyst by hydrothermal growth of α-Fe$_2$O$_3$ onto the ns-γ-Al$_2$O$_3$ layer structured on an Al-fiber (see 4.5.2 for detailed preparation) and subsequent Au NPs deposition via the urea-assisted deposition-precipitation method. The Au-α-Fe$_2$O$_3$/ns-γ-Al$_2$O$_3$/Al-fiber catalyst effectively couples low-temperature CO oxidation activity as well as improved water vapor tolerance with enhanced catalyst accessibility and permeability. The promising catalyst with only 0.14 wt% Au and 1.4 wt% α-Fe$_2$O$_3$ is capable of fully or 40% oxidizing CO into CO$_2$ at 25 or 0 °C for a feed gas of 2 vol% CO and 0.3 vol% water vapor in air at a high linear velocity of 0.7 cm s^{-1}, using a GHSV of 25,200 mL g$_{cat}^{-1}$ h^{-1}. Moreover, this catalyst performed robustly for at least 230 h under the changeable temperature conditions. Recently, Lu et al.[131] further employed the monolithic Al-fiber substrate to fabricate a CuO-CeO$_2$/AlOOH/Al-fiber catalyst for the preferential oxidation of CO in H$_2$, which also shows enhanced catalyst accessibility and permeability.

5.1.3. Oxidative coupling of methane

The oxidative coupling of methane (OCM) is considered to be a promising route to directly convert methane into light olefins in the presence of molecular oxygen. It has been well indicated by many studies that the OCM is a sequential process combining heterogeneous-catalysis and homogeneous-coupling to achieve the methane-to-olefins transformation.[132] Among the numerous catalysts, Mn$_2$O$_3$-Na$_2$WO$_4$/SiO$_2$ is a classic one able to convert 20–

30% CH_4 with 70–80% C_{2-3} selectivity at 800–900 °C.[133] Recently, Lu et al.-[134] reported that the TiO_2-doping of this catalyst can substantially lower the OCM light-off temperature, achieving ~20% conversion and ~70% selectivity at 650 °C; in nature, this is due to the *in-situ* formation of $MnTiO_3$ that enables the $Mn_2O_3 \leftrightarrow MnTiO_3$ redox reaction with CH_4/O_2 to be triggered at such low temperature.

However, the practical application of these catalysts still stalled, because of the strong exothermicity of this reaction ($2CH_4 + O_2 = C_2H_4 + 2 H_2O$, $\Delta H = -165$ kJ mol^{-1}) that will cause severe hotspots in packed beds and deteriorate C_{2-3} yields. To address this issue, foam-structured catalysts were developed to couple the enhanced heat transfer so as to benefit the temperature control in catalyst bed, which is a key feature for scale-up process throughout the commercial application. For example, a Mn_2O_3-Na_2WO_4/SiC-foam catalyst (Figure 15a) is developed for the OCM reaction,[135] achieving 24–25% CH_4 conversion at 850 °C with a lower CO_2 selectivity (21% vs. 24% for the Mn_2O_3-Na_2WO_4/SiO$_2$). A dual-bed reactor was constructed with upper-layer Na_2WO_4-Mn_2O_3/SiO$_2$ particulate catalyst and under-layer CeO_2-Na_2WO_4-Mn_2O_3/SBA-15/Al$_2$O$_3$/FeCrAl monolithic catalyst as well as a side tube in the interspaces of the two layers for supplementing O_2 (Figure 15b).[136] This dual-bed reactor exhibits a good OCM performance with 33.2% CH_4 conversion, 67.6% C_2 selectivity, and 22.4% C_2 yield at 800 °C, which are, respectively, increased by 6.4%, 4.1%, and 5.5% in comparison with the single-bed reactor of particulate Na_2WO_4-Mn_2O_3/SiO$_2$, and by 10.7%, 31.9%, and 17.7% compared to the CeO_2-Na_2WO_4-Mn_2O_3/SBA-15/Al$_2$O$_3$/FeCrAl monolithic
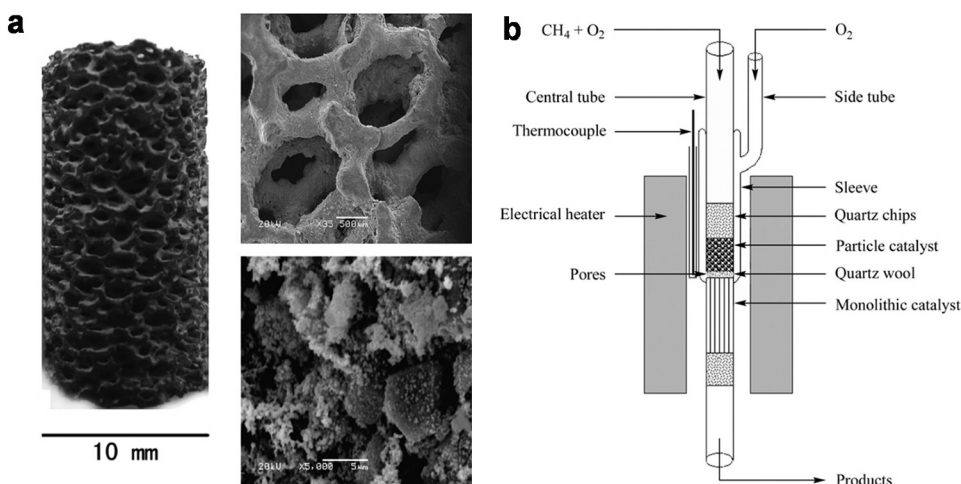
Figure 15. (A) SEM images of Na_2WO_4-Mn_2O_3/SiC-foam (Reprinted with permission from ref.[135] Copyright 2008 Elsevier). (b) Schematic diagram of dual-bed reactor (Reprinted with permission from ref.[136] Copyright 2012 Elsevier).

catalyst bed. Recently, Lu et al.[137] reported a SiC-foam-structured TiO_2-Mn_2O_3-Na_2WO_4 catalyst with strong mechanical strength and robustness stemmed from the formation of interpenetrating nanorod structure in the catalyst layer. At 0.35 MPa, an interesting OCM performance of 18% CH_4 conversion and 72% C_{2-3} selectivity could be obtained for a feed gas (no dilution) with the CH_4/O_2 molar ratio of 6.5/1, at 800 °C and a GHSV of 20,000 h^{-1}. In order to improve the catalyst activity, they further tailored a self-structured monolithic foam-catalyst by directly molding the TiO_2-Mn_2O_3-Na_2WO_4 components.[138] This self-structured catalyst can increase the number of active sites, helpful to lower the OCM reaction light-off temperature. Over the preferred catalyst, a CH_4 conversion of 25.3% with a C_{2-3} selectivity of 71.6% was achievable at 740 °C, 0.1 MPa, and a GHSV of 6000 h^{-1} for a feed gas (no dilution) with the CH_4/O_2 molar ratio of 5/1, and held unchanged for at least 100 h.

5.1.4. Oxidative dehydrogenation of ethane

Owing to one important reason that ethane is abundant in natural gas, and in particular, the shale gas revolution in recent years significantly enriches the ethane resources, ethane-to-ethylene conversion (in terms of oxidative dehydrogenation of ethane (ODE), steam cracking, and catalytic dehydrogenation) tantalizes global enthusiasm. The latter two suffer from their thermodynamic constraints and high operation temperature (>700 °C), while the ODE is thus more competitive, benefitting from its oxidative feature that can cast off the thermodynamic limitation and lower the operation temperature (350–550 °C).[139] Despite the numerous catalytic materials that have been reported, such as MoVTeNbO[140] and Nb_2O_5-NiO,[141] practical use of these materials remains a big challenge because their poor heat transfer is detrimental to the rapid dissipation of reaction heat from this strongly exothermic process ($\Delta H = -104.2$ kJ mol^{-1}). From the viewpoint of heat transfer enhancement, thus, structured catalysts are promising for applications in this reaction process.

A FeCrAl-foil structured catalyst of Cr/SBA-15/Al_2O_3/FeCrAl-foil for the ODE with CO_2 was developed according to the method in ref.[142] Ethane conversion and ethylene selectivity were 66.5% and 99.5% at 750°C, respectively, and could be stabilized for over 1130 h. The Cr^{6+} species are most likely responsible for the high activity. Recently, Lu et al.[143] developed a Ni-foam structured Nb_2O_5-NiO catalyst for the ODE with O_2. The Ni-foam was hydrothermally treated to grow $Ni(OH)_2$ nanosheets of 20 nm in thickness onto its surface (preparation method in 4.5.4) followed by Nb_2O_5 modification to obtain the Nb_2O_5-NiO/Ni-foam, which achieved a 60% conversion with an 80% selectivity and was stable for at least 240 h. It was revealed that the modification of NiO by Nb_2O_5 remarkably reduced the nonselective O_2^- species thereby substantially suppressing the combustion reaction. More

notably, the intensified heat transfer of these structured catalysts is of great benefit for practical applications.

5.2. Hydrogenation

### 5.2.1. CO_2 hydrogenation to CO and/or methanol

Global warming and ocean acidification problems caused by the CO_2 excessive emission have triggered extensive research on large-scale CO_2 reutilization via effective, economical, and sustainable technologies for the CO_2 circular economy.[144] The CO_2 hydrogenation with renewable-energy-generated H_2 to CO, named the reverse water-gas shift (RWGS) reaction, is a techno-economically viable candidate, thanks not only to its high efficiency, enabling to deal with vast amounts of CO_2, but also to the versatility of syngas $(CO + H_2)$ to produce commodity chemicals and fuels (occupying 40% CO_2 emissions[145] via the mature Fischer-Tropsch and methanol syntheses). Nevertheless, the groundbreaking catalyst represents a grand challenge. Recently, a monolithic catalyst of $InNi_3C_{0.5}/Al_2O_3/Al$-fiber (its preparation in 4.7) was developed for the RWGS reaction.[114] At 550 °C and a high GHSV of 54,000 mL g_{cat}^{-1} h^{-1}, this catalyst delivered a stable 50–55% CO_2 conversion and >95% CO selectivity for a feed gas of $H_2/CO_2/N_2$ (6/2/1, vol%) throughout the entire 140-h testing. In addition, this catalyst also offered a promising performance for the CO_2 hydrogenation to methanol. For example, at 270 °C, 4.0 MPa, and a GHSV of 21,600 mL g_{cat}^{-1} h^{-1}, a 5% CO_2 conversion with an 89% methanol selectivity can be achieved for a feed gas of $H_2/CO_2/N_2$ (6/2/1, vol%). The $InNi_3C_{0.5}(111)$ surface is dominantly exposed and gifted with dual active sites (3Ni-In and 3Ni-C), which in synergy efficiently dissociate CO_2 into CO* (on 3Ni-C) and O* (on 3Ni-In). The O* can facilely react with the 3Ni-C-offered H* to form H_2O. Interestingly, the CO* is mainly desorbed at and above 400 °C, whereas selectively hydrogenated to CH_3OH below 300 °C.

The use of methanol as a fuel and chemical feedstock becomes of great importance in the development of a sustainable society if methanol could be efficiently obtained from direct hydrogenation of CO_2. Great efforts have been made in the hydrogenation of CO_2 to methanol, and various particulate catalysts were reported, such as the Cu-based ones, oxide-based ones, and alloy-based ones.[146–151] It should be noted that the methanol selectivity is sensitive to the catalyst bed temperature, and a slight fluctuation of bed temperature causes great variation in the methanol selectivity. However, the exothermicity of CO_2-to-methanol reaction easily causes the temperature rising in catalyst bed, which is harmful to the methanol selectivity. Undoubtedly, structured catalysts are promising to address this issue. For example, a monolithic foam structured Cu-Zn/Al-foam catalyst was prepared (Figure 16a-d; preparation based on the method in 4.5.4, and detailed information in ref. [96]) and investigated in a micro-reactor for the CO_2-to-

methanol reaction.[96] Such catalyst was loaded in a flange-type micro-reactor (Figure 16e-g) in the form of packed bed to intensify this process. A high copper time yield of methanol, 7.81 g g_{Cu}^{-1} h^{-1}, was obtained at 250 °C, 3 MPa, and a GHSV of 20,000 mL g_{cat}^{-1} h^{-1} due to the high heat/mass transfer within the micro-reactor. Such catalyst combines promising catalytic performance of the Cu-Zn components with enhanced heat transfer and high permeability of the Al-foam.

5.2.2. Dimethyl oxalate hydrogenation

Dimethyl oxalate hydrogenation to ethylene glycol. Ethylene glycol (EG) is an important commodity chemical, and its production is mainly dependent on the petroleum-based ethylene. In principle, the EG can be synthesized from syngas derived from non-oil resources such as coal, through the Pd-catalyzed
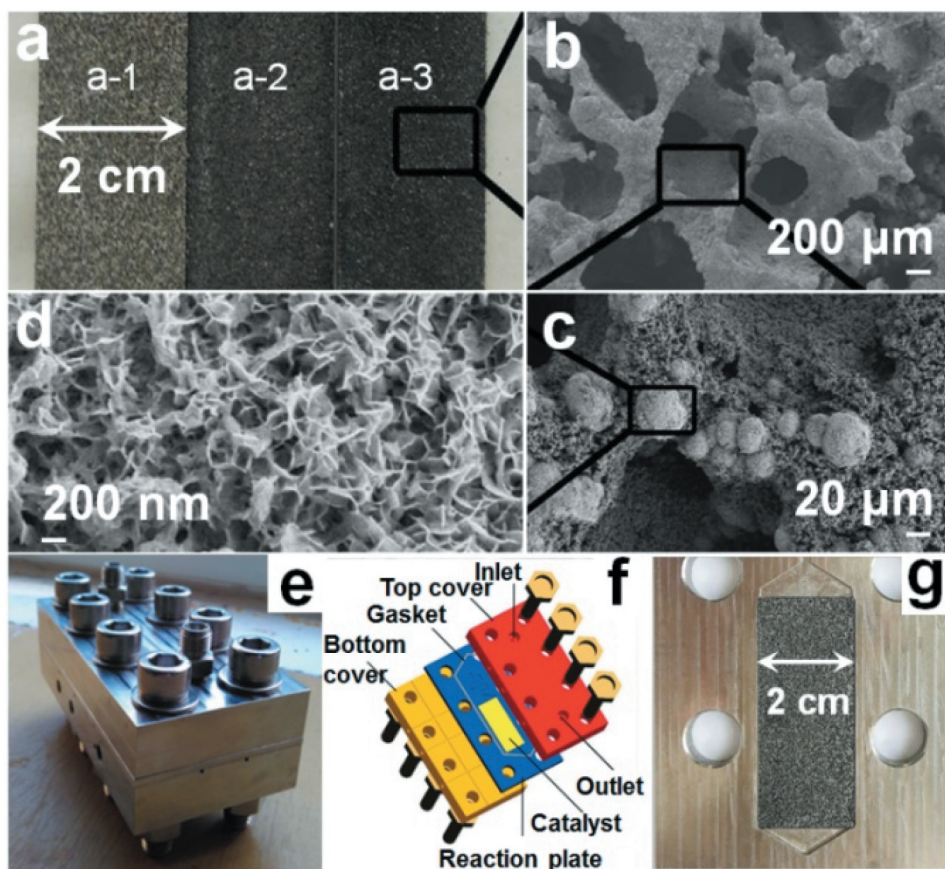
Figure 16. (A) Photograph of the macroscopic sample: (a-1) Al-foam, (a-2) catalyst after hydrothermal treatment, and (a-3) catalyst of Cu-Zn/Al-foam after calcination. (b-d) SEM images in different magnifications, showing the 3D porous structure and surface morphology of monolithic catalyst. (e) Outside view and (f) exploded view of micro-reactor. (g) Screen shots of catalyst in chamber (Reprinted with permission from ref.[96] Copyright 2017 Elsevier).

coupling of CO with methyl nitrite to dimethyl oxalate (DMO) and subsequent Cu-catalyzed gas-phase hydrogenation of DMO to EG. Whereas the commercialization of this process (called CTEG) is on the way now, the challenge is still severe. Regarding the DMO-to-EG reaction, the Cu/SiO_2 catalyst is active but highly selective only in a very narrow temperature window,[152,153] while its durability is not well qualified because of the easy sintering of copper. So, to get Cu/SiO_2 running smoothly, rapidly dissipating the reaction heat is critically required but difficult, because this is also a strongly exothermic reaction ($\Delta H = -58.73$ kJ mol^{-1}) and the catalyst is poorly thermal conductive. Therefore, the tubular reactor has to be employed. In this context, it is still calling for a new catalytic solution (such as the structured catalysts) to substantially increase the process efficiency.

A monolithic catalyst of Cu-microfiber structured Pd-Au NPs was newly developed for this process.[115] This catalyst was fabricated from nano- to macro-scales in one step by dipping Cu-microfibers into a $HAuCl_4$-$Pd(Ac)_2$ aqueous solution, and the Au-Pd NPs were galvanically co-deposited on the Cu-microfiber surface (to see the galvanic deposition method in 4.3). The as-prepared Pd-Au/Cu-fiber catalyst demonstrated high activity, selectivity, and stability, being capable of converting 97–99% DMO into EG at 90–93% selectivity with a single-run lifetime for at least 200 h at 270 °C. A ternary Pd-Au-Cu$^+$ nanocomposite was proposed, in which the Cu$^+$ acts for activating methoxy and carbonyl groups in the DMO, and the Au stabilizes Cu$^+$ to prevent its deep reduction to Cu^0, while the Au-Pd alloy synergistically promotes H_2 activation as a result of strong Au-Pd electronic interaction.

However, the optimal reaction temperature of 270 °C for this Pd-Au/Cu-fiber catalyst is much higher than the common 180–200 °C for other reported Cu-based catalysts,[152,153] and moreover, there are still other inherent problems with the Cu-based catalysts: the inevitable Cu sintering, difficult control in steady surface Cu^0/Cu$^+$ ratio, and, in particular, the narrow high-EG-selectivity temperature window. Hence, to develop and use a novel Cu-free catalyst with high performance and excellent heat transfer is particularly desirable to implement the DMO-to-EG process. Very recently, an intermetallic $InNi_3C_{0.5}$ was discovered and structured on a monolithic Ni-foam substrate (Figure 17).[154] This catalyst has high heat/mass transfer and favors EG formation with a high turnover frequency of 780 h^{-1} but is kinetically unfavorable for over-hydrogenation of EG to ethanol. A full DMO conversion with a 96% EG selectivity can be obtained stably for at least 2500 h under the industrial-relevant conditions. Another advantage of such catalyst is its much wider temperature window (200–250 °C) with high EG selectivity (>90%) than that (190–210 °C at >88%) seen with Cu/SiO_2. Moreover, this catalyst can be extended to a broad scope of carbonyl compounds hydrogenation with high yields of corresponding alcohols. The $InNi_3C_{0.5}$/Ni-foam catalyst well combines the high $InNi_3C_{0.5}$ catalytic performance with the Ni-foam
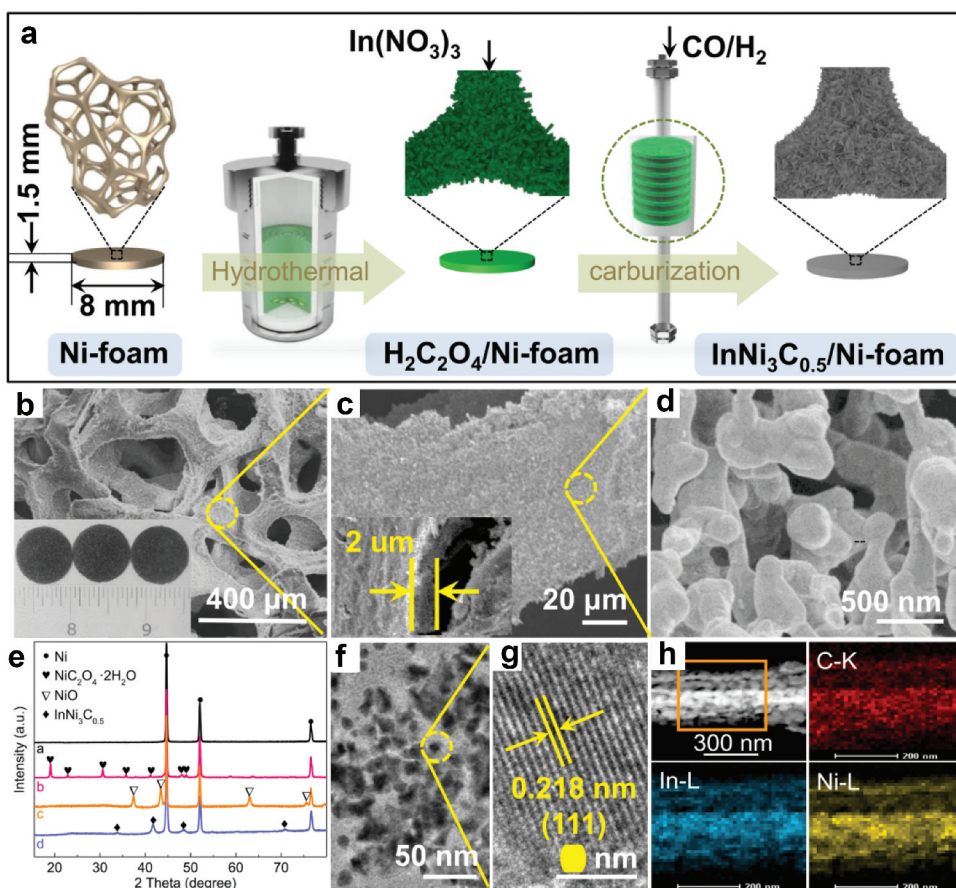
Figure 17. Catalyst preparation strategy and structural features of the InNi₃C₀.₅/Ni-foam catalyst. (A) Schematic illustration for the *in-situ* $InNi_3C_{0.5}$ growth onto the Ni-foam substrate. SEM images (B-D) and optical photograph (insert B) of the $InNi_3C_{0.5}$/Ni-foam catalyst. (E) XRD patterns of (a) Ni-foam, (b) $NiC_2O_4\cdot2H_2O$/Ni-foam, (c) In_2O_3-NiO/Ni-foam, (d) $InNi_3C_{0.5}$/Ni-foam. HRTEM images (F,G) and HAADF-STEM images (H) of the $InNi_3C_{0.5}$/Ni-foam catalyst (Reprinted with permission from ref.[154] Copyright 2021 Elsevier).

-derived high mass/heat transfer, low pressure drop, and desired mechanical robustness.

Dimethyl oxalate hydrogenation to methyl glycolate. The hydrogenation of DMO to ethylene glycol is a sequential reaction, and the intermediate is methyl glycolate (MG). Recently, selective hydrogenation of the DMO to MG is attracting growing interest because the MG can be used to synthesize PGA (polyglycolic acid, a new-generation biodegradable and thermoplastic polymer).[155,156] A hydroxyapatite-supported Cu catalyst was reported to yield a 70% MG[156]; until now, the highest MG yield of 90% was achievable over an Ag/SiO₂ catalyst.[157] Despite these promising results, the implementation of this process faces similar challenge as that for the DMO-to-EG process. From the prospective of process intensification, Chen et al.[155]

developed a foam-structured catalyst of Ag-CuO$_x$/Ni-foam by the sequential galvanic-deposition of Ag and Cu onto a Ni-foam. The preferred catalyst was capable of converting >96% DMO into the MG with >96% selectivity and was stable for at least 200 h at 210 °C and a DMO weight hourly space velocity (WHSV$_{DMO}$) of 0.25 h^{-1} for a feed of 13 wt% DMO dissolved in methanol. The Ag species shows the ability to tune the Cu$^+$/Cu^0 proportion to an appropriate scale of optimal potency for the DMO-to-MG. Nevertheless, the industrial running of this process strongly requires full DMO conversion in consideration of the high economy for the product purification. Aiming to raise the DMO conversion, Lu et al.[119] recently reported a highly active/selective and durable Ni-foam-structured Ni$_x$P catalyst for the DMO hydrogenation to MG, which was capable of converting >99.9% DMO into the MG with 95–96% selectivity and was stable for at least 1000 h without any sign of deactivation, at 230 °C and 2.5 MPa with a WHSV$_{DMO}$ of 0.44 g$_{DMO}$ g$_{cat}^{-1}$ h^{-1}.

Dimethyl oxalate hydrogenation to ethanol. As a key bulk chemical both in industry and in our daily life, ethanol (EtOH) has been extensively used as a clean fuel additive, solvent, disinfectant, and industrial intermediate. At present, the primary methods for EtOH production are based on the ethylene hydration and agricultural feedstock fermentation. However, the ethylene hydration is limited by the soaring demand for ethylene, and the fermentation of agricultural feedstock may exacerbate the food crisis and is constrained by the expensive biological processes. In this context, synthesis of EtOH from syngas via the DMO hydrogenation emerges as a promising alternative route, because the syngas can be versatilely produced from natural gas, coal, inedible biomass, and even organic wastes. Thus, development of qualified catalysts is the heart for this route.

The Cu-based heterogeneous catalysts are frequently used for this reaction owing to their high activity.[158,159] For example, the traditional Cu/SiO$_2$[153] prepared by the ammonia evaporation method offers an 83% EtOH yield at 280 °C, and the Cu/ZrO$_2$/Al$_2$O$_3$[158] provides a 97% EtOH yield at 270 °C. Despite these industrially promising EtOH yields, there are still many catalytic and technical problems to be solved. The hardest one is that the reaction temperature for obtaining high EtOH selectivity is usually above 270 °C, much higher than the Hüttig temperature of Cu nanoparticles of 134 °C, making the nano-Cu prone to be sintered.[160] In addition, the DMO hydrogenation to EtOH is strongly exothermic ($\Delta H = -145.93$ kJ mol^{-1}), and the common supports (e.g., SiO$_2$, ZrO$_2$, and Al$_2$O$_3$) have poor thermal conductivity, normally generating hotspots in the catalyst bed and thus accelerating Cu sintering. Therefore, it is particularly desirable to render a novel catalyst toward the efficient DMO-to-EtOH process.

Zhu et al.[117] demonstrated a highly qualified monolithic FeNi$_3$-FeO$_x$/Ni-foam catalyst (Figure 18) for the DMO-to-EtOH process. This catalyst was effectively and efficiently tailored by reducing the NiFe$_2$O$_4$-NiO/Ni-foam

precursor (its preparation in 4.8) and achieved a unique combination of high catalytic performance with high thermal conductivity. The preferred FeNi$_3$-FeO$_x$/Ni-foam was capable of fully converting DMO with a 98% ethanol selectivity at 230 °C and 2.5 MPa using a DMO weight hourly space velocity of 0.44 h^{-1} and a H$_2$/DMO molar ratio of 90, and particularly, was stable for at least 700 h without any sign of deactivation. It was indicated that the DMO-to-EtOH reaction, catalyzed by this catalyst, mainly follows this pathway: the DMO hydrogenation to MG followed by the MG to EG and the EG to EtOH. Moreover, the FeNi$_3$-FeO$_x$/Ni-foam catalyst has plentiful interface between FeNi$_3$ nanoalloy and FeO$_x$ fragments (acting as acid sites), achieving the synergistic catalysis to activate ester groups in the DMO as well as the as-formed hydroxyl groups, thereby leading to a marked improvement of its hydrogenation to EtOH.

5.2.3. Semihydrogenation of acetylene

The semihydrogenation of acetylene is essential in the purification of ethylene, as the acetylene is an undesired by-product in the ethylene production from thermal cracking of naphtha. Pd-based catalysts are the most effective for this reaction,[161] but suffer from high cost. In addition, this reaction is strongly exothermic ($\Delta H = -174$ kJmol^{-1}), and the traditional particulate catalysts are
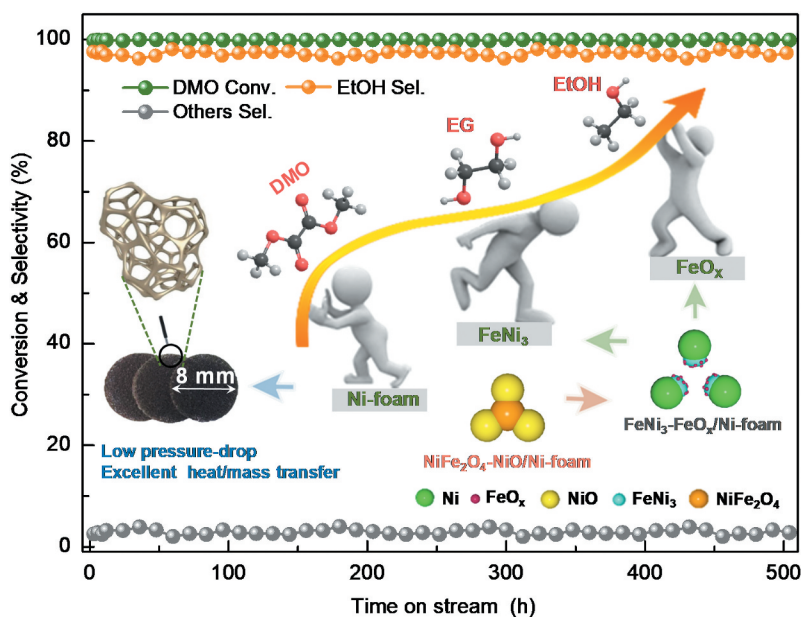
Figure 18. Optical photograph of the FeNi$_3$-FeO$_x$/Ni-foam catalyst and schematic illustration for the formation of FeNi$_3$-FeO$_x$, and the conversion and selectivity against time on stream for the DMO-to-EtOH reaction (WHSV$_{DMO}$ of 0.44 h^{-1}, n(H$_2$)/n(DMO) of 90, 2.5 MPa, 230 °C) (Reprinted with permission from ref.[117] Copyright 2020 Elsevier).

weak in the removal of reaction heat, which is harmful to the selectivity and stability of catalysts. Hence, it is still calling for a novel catalyst system toward the efficient semihydrogenation of acetylene.

For the semihydrogenation of acetylene under the front-end configuration, it is extremely desirable to avoid ethylene hydrogenation because of the high H_2 concentration in the feed gas. The modifications with Cu and Zn prove to be effective in improving the selectivity of Pd-based catalysts.[162,163] Hence, Lu et al.[164] employed brass fibers (80 μm diameter) composed of Cu and Zn to tailor a microfibrous-structured Pd-based catalyst, aiming to combine the high catalytic performance of Pd with the enhanced heat/mass transfer of brass fibers. The Pd/brass-fiber catalysts were prepared by placing Pd, via incipient impregnation method, onto the pre-calcined brass fibers with an endogenously grown ZnO-CuO$_x$ layer. Over the preferred catalyst with brass-fiber pre-calcined in air at 500 °C and Pd/brass-fiber reduced in H_2 at 250 °C, an ethylene selectivity of >90% was achieved at nearly full consumption of acetylene under the front-end conditions.

In contrast, the acetylene semihydrogenation under the back-end configuration requires a catalyst with high activity due to the low H_2 concentration. Wang et al.[165] reported a monolithic Pd/AlOOH/Al-fiber catalyst for acetylene semihydrogenation, which was obtained by dispersing Pd nanoparticles onto an AlOOH/Al-fiber support (the preparation method in 4.5.2) by the impregnation method. The preferred catalyst using the AlOOH/Al-fiber after pre-annealing at 100 °C, with a pretty low Pd loading of only 0.05 wt%, achieved a high specific activity with a turnover frequency of 0.0167 s^{-1} (measured at 40 °C), being two times as high as that (0.0083 s^{-1}) for the catalyst obtained using the AlOOH/Al-fiber after pre-annealing at 600 °C (Figure 19). In addition, this catalyst offered >99% acetylene conversion at 70 °C. The low annealing temperature for the AlOOH/Al-fiber enables the catalyst with a hydroxyl-rich surface that offers crucial Pd-hydroxyl interactions, which not only promote the adsorption of acetylene on Pd but also suppress the carbonaceous deposition and thus improve the catalyst stability by a large extent.

5.3. Reforming

5.3.1. Methane
Steam methane reforming (SMR). The CH_4 reforming has been gaining ever-increasing interests in syngas generation for the subsequent production of chemicals and fuels. The SMR is the most common reforming to produce H_2 and is highly endothermic ($CH_4 + H_2O = CO + 3 H_2$, $\Delta H = 205$ kJ mol^{-1}). The multi-tubular reactors operate from 700 to 850 °C, 5 to 15 bar, with H_2O/carbon ratio from 1/2 to 1/6. The industrial catalyst consists of Ni supported on cylindrical hollow pellets of 1–3 cm diameter.[166] The high capital costs,
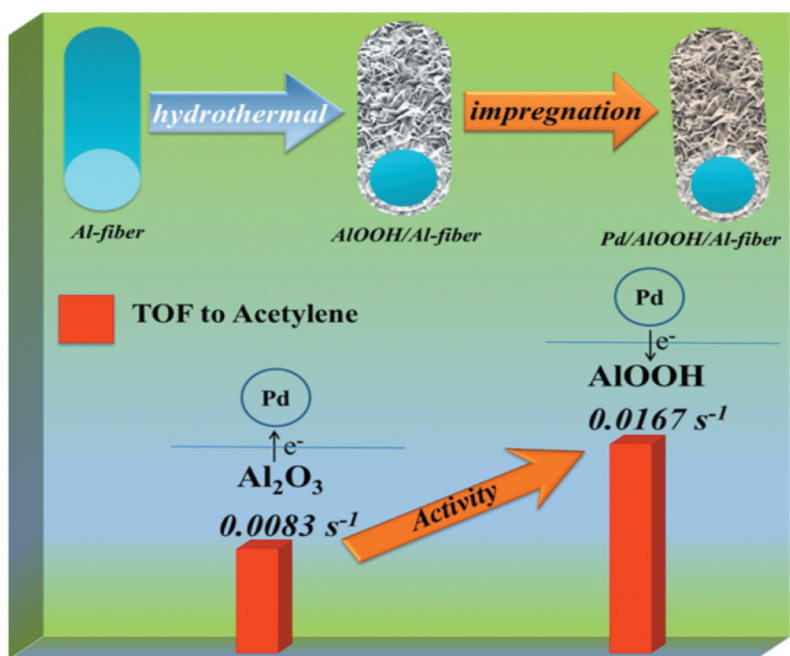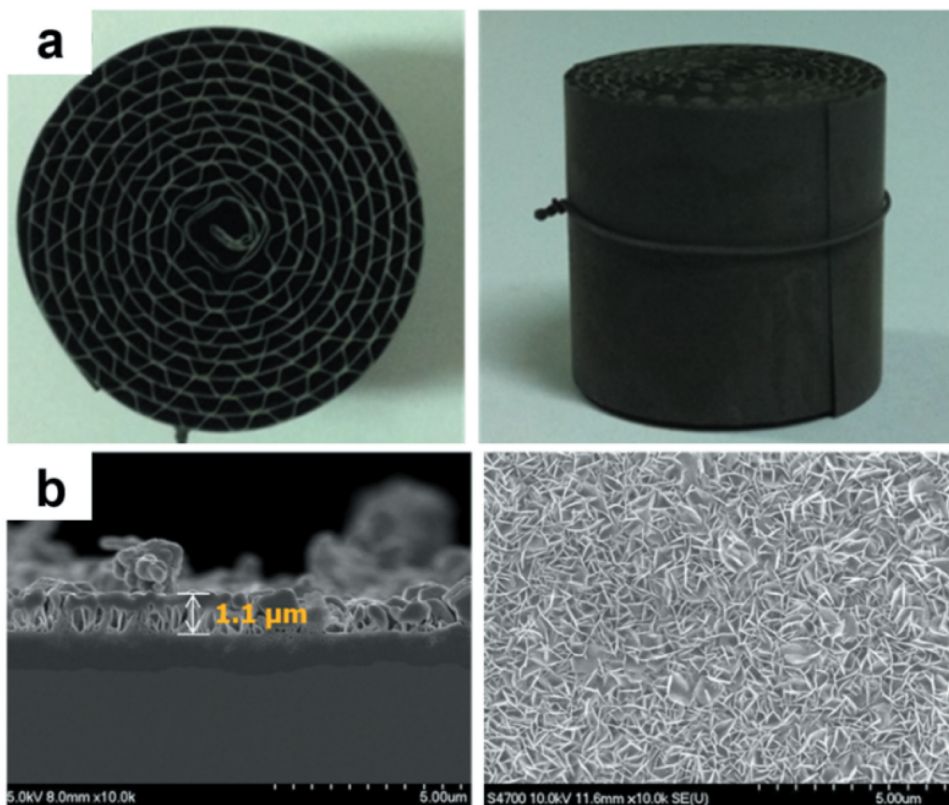
Figure 19. Schematic preparation of Pd/AlOOH/Al-fiber and turnover frequencies of catalysts respectively annealed at 600 °C (0.0083 s^{-1}, left) and 100 °C (0.0167 s^{-1}, right) (Reprinted with permission from ref.[165] Copyright 2019 American Chemical Society).

related to the large reactor volume and energy recovery units, discourage applying this technology to the small decentralized production facilities.

The FeCrAl is characterized by the high thermal conductivity and high-oxidation resistance at high temperature. These advantages are appealing and might retrofit current catalyst technology. The Ni/MgAl$_2$O$_4$, a well-known SMR catalyst, was successfully glued onto a FeCrAl-monolith (manufactured by rolling flat and corrugated FeCrAl strips into the shape of a cylinder) using the "Korea Institute of Energy Research" coating method (Figure 20a).[167] The Ni/MgAl$_2$O$_4$ layer of 1 μm thickness uniformly sprawled on the FeCrAl surface (Figure 20b), which increases the availability of active sites in this thin layer thereby leading to a higher activity and stability compared to the pellet counterparts. The Ni/MgAl$_2$O$_4$ could also be glued on the FeCrAl-foam by the percolation-blowing method,[168] enabling the SMR to reach thermodynamic equilibrium at above 450 °C even with a high GHSV of 130,000 mL g$_{cat}$$^{-1}$ h^{-1}. The Ni-Al$_2$O$_3$ glued on a micro-channel FeCrAl-foil was reported to be more active and stable compared to the particulate Ni/MgO or Ni/CeO$_2$/Al$_2$O$_3$.[169] Calcining the Ni-Al hydrotalcite-like compounds electro-deposited on a FeCrAl-foam produced a thin and strongly adherent film of NiAlO$_x$ composite oxide on the foam struts. Compared to the commercial particulate Ni-based catalysts under industrial conditions, such FeCrAl-foam-structured

Figure 20. (A) Photos of top and lateral views, and (b) SEM images of monolithic catalyst (Reprinted with permission from ref.[167] Copyright 2016 Elsevier).

catalyst delivered a higher methane conversion because of the enhanced heat-transfer ability.[170]

Dry reforming of methane (DRM). The DMR involves CH_4 reacting with CO_2 to form CO and H_2. The high carbon concentration in feed gas favors coke formation, and its formation rate is increased with the reaction pressure of particularly above 10 bar.[171] Moreover, the cold spots originated from the strong endothermicity of this reaction ($\Delta H = 247$ kJ mol^{-1}) reduce the CH_4 /CO_2 conversion and promote the coke formation.[172,173] Considering that a metal support with high thermal conductivity is helpful to minimize the thermal gradient in the catalyst bed, a thin-felt Ni@SiO$_2$/Al$_2$O$_3$/FeCrAl-fiber catalyst was fabricated by using a FeCrAl-fiber substrate via the APTES-assisted organization strategy (based on the method in 4.6, Figure 21).[174] Such catalyst was active, selective, and stable for this reaction, due to the synergistic coupling of the enhanced resistances to Ni-sintering and coke formation arising from the core-shell-like nanostructure with the high heat-transfer stemmed from FeCrAl-fiber substrate. Almost no carbon was deposited even after 500-h testing at 800 °C and a GHSV of 5000 mL g$_{cat}^{-1}$ h^{-1}.

Figure 21. A monolithic Ni@SiO$_2$/Al$_2$O$_3$/FeCrAl-fiber catalyst was fabricated by the APTES-assistant organization followed by a calcination treatment, displaying an as-expected performance for the DRM reaction (Reprinted with permission from ref.[174] Copyright 2017 Royal Society of Chemistry).

Clearly, organization of different building blocks of tunable structures and functions into the monolithic architectures based on the controllable chemical reactions represents a promising strategy to develop novel catalyst systems. Then, the same authors structured the LDHs-derived NiO-MgO-Al$_2$O$_3$ nanocomposites onto a FeCrAl-fiber substrate.[175] Differently but interestingly, the NiMgAl-LDHs were controllably grown onto a FeCrAl-fiber through the γ-Al$_2$O$_3$/water interface-assisted method.[175] By combining the homogeneous distribution of LDHs-derived NiO-MgO-Al$_2$O$_3$ and the enhanced heat transfer, this catalyst delivered satisfying performance with the enhanced sintering/coke resistances in the DRM reaction. At 800°C and a GHSV of 5000 mL g$_{cat}$$^{-1}$ h^{-1}, the CH$_4$/CO$_2$ conversion is maintained almost constant at 91%/89% within the initial 90 h and then moved in a smooth downturn (to 80/85%) within another 180 h.
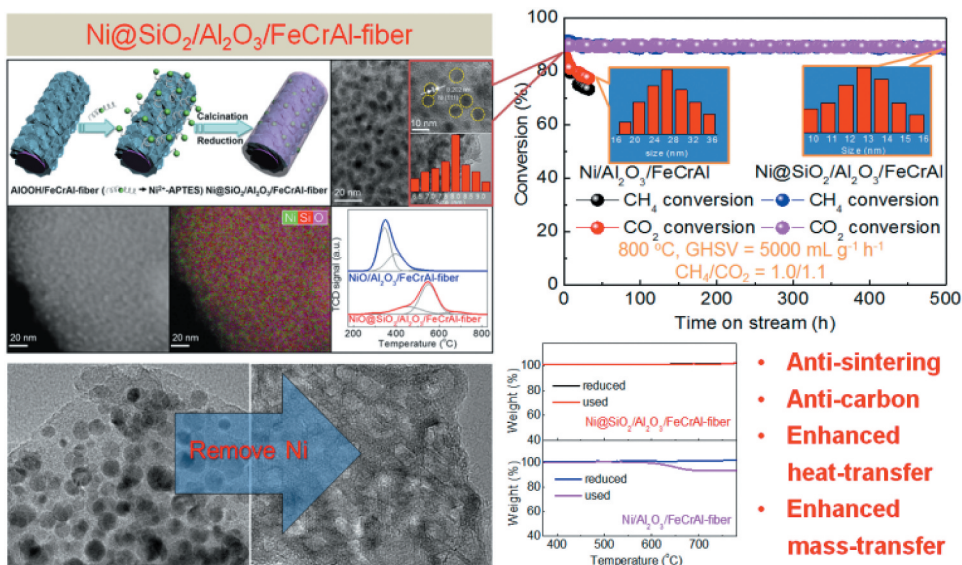
Catalytic oxy-methane reforming (COMR). Profiting from the high production efficiency, and especially the suitable H$_2$/CO ratio (2/1) for the downstream processes (e.g., the Fischer-Tropsch and methanol syntheses), the COMR has been attracting more and more attention as a compact and energy-efficient process.[176] Notably, this is a high-throughput reaction, being able to proceed at a very short contact time of milliseconds.[177] Whereas this is a mild exothermic reaction, the high-temperature "hot-spots" formation is inevitable at the top of catalyst bed because syngas is formed through COMR via the CH$_4$ combustion and subsequent CH$_4$ reforming with CO$_2$ and H$_2$O.[177] In this

context, it is worthwhile to try to use the metal and SiC fiber/foam substrates to fabricate catalysts with the synergistic coupling of high heat transfer and high permeability for application in this high-throughput COMR reaction process.[178] A monolithic catalyst of Ni-CeAlO$_3$-Al$_2$O$_3$/FeCrAl-fiber was fabricated by thermally decomposing NiAl-LDHs/FeCrAl-fiber (NiAl-LDHs growth based on the method in 4.5.3, and detailed information in ref. [179]) to a NiO-Al$_2$O$_3$/FeCrAl-fiber, followed by CeO$_2$-modification and H$_2$-reduction.[179] The preferred catalyst, with 5 wt% Al$_2$O$_3$, 5 wt% Ni, and 2 wt% CeO$_2$, exhibited high activity, high selectivity, and particularly prolonged stability. At a GHSV of 100,000 mL g$_{cat}^{-1}$ h^{-1} and 700 °C, the CH$_4$ conversion and H$_2$/CO selectivity could be stably maintained at 86% and 96/92% for a feed gas with CH$_4$/O$_2$ molar ratio of 2/1 within the 350-h test, due to the enhanced Ni-sintering and carbon resistance. Furthermore, a catalytic module (Figure 22) of Rh/Al$_2$O$_3$/FeCrAl-fiber has both radial and axial intermixing to increase the heat/mass transfer. This configuration is less expensive and more accessible in the market. The coating of Al$_2$O$_3$ enables a high dispersion of catalytic species, such as Rh. The composite architecture ensures the maintenance of high Rh dispersion despite operating above 900 °C for 20 h on stream with four start-up/shut-down cycles.[180] Clearly from these assays, the fiber/foam-structured catalysts are expectable as the new-generation catalysts to stimulate their commercial exploration for the COMR reaction.

5.3.2. Glycerol and biomass

In recent years, biodiesel as an alternative to the nonrenewable resource has been developed rapidly.[181] Glycerol is produced as a major by-product in the biodiesel
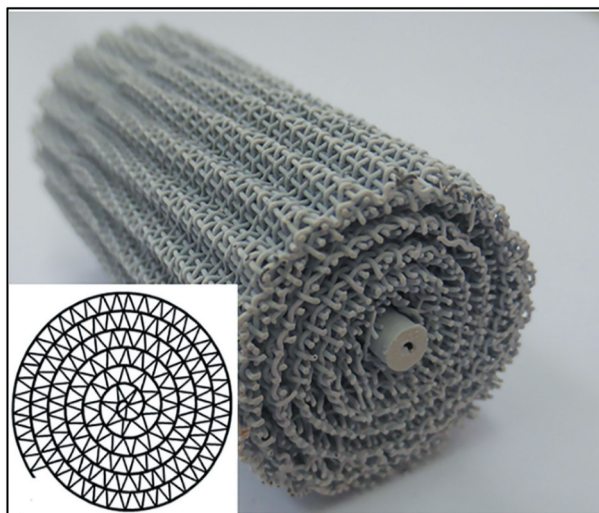
Figure 22. Overview and cross sections of the Rh/Al$_2$O$_3$/FeCrAl-fiber catalyst (Reprinted with permission from ref.[180] Copyright 2019 Elsevier).

production but it has been thrown out as a waste, so the effective technique for glycerol reforming is attracting more and more attention. And till now, many research institutes have made great efforts on the steam reforming of glycerol.[182,183] Recently, the glycerol reforming on charcoal has been studied in a fixed-bed reactor.[184] The results indicated that the charcoal not only had a high activity for this process but could also decrease the cost of syngas production. The syngas yield, glycerol conversion, and H_2/CO ratio could reach $1.37 \, m^3 \, kg^{-1}$, 76.8%, and 3.04, respectively, for a feed with the steam/carbon molar ratio of 4 at 800 °C and a weight hourly space velocity of $2 \, h^{-1}$. It is indicated that the coke from glycerol polymerization might be in an amorphous state, which is the main cause for the reduction of surface area and average pore size of charcoal. A Ni-foam-structured catalyst was developed for the glycerol-steam reforming,[185] achieving a higher glycerol conversion than those over the Al_2O_3 and SBA-15 supported catalysts. This Ni-foam catalyst shows a more homogeneous thermal distribution over its surface as it has higher thermal conductivity than the oxides-supported catalysts.

Biomass is a carbon neutral resource, which can be used to produce renewable energy, fuels, and high-value materials. Biomass pyrolysis oil (bio-oil) can be produced from thermal-chemical decomposition of the biomass in the absence of oxygen at around 500 °C. Converting bio-oil into syngas is attracting substantial attention,[186] and the catalytic steam bio-oil reforming to produce hydrogen has been explored extensively.[187–190] Development of an efficient catalyst is one of the key challenges for this process. The Ni-based catalysts are considered as the most popular candidates because of their high catalytic activity in relation to the hydrogen production and cost. For example, Czernik[191] studied Ni catalyst for the steam reforming of bio-oil in a fluidized-bed and a high yield of hydrogen (12.9 g H_2/100 g bio-oil) was obtained. The catalyst support plays a significant role in developing nano-Ni-based catalysts. The ceramic-foam has been employed to structure a Ni/CeO_2 catalyst for hydrogen production from the steam biogas reforming.[192]

The ceramic-foam was also used to structure a Ni/Co_3O_4 catalyst for hydrogen production from the catalytic steam reforming of methane, ethanol, and fermentation products.[193] Compared to the particulate catalyst, the ceramic-foam-structured catalyst achieves not only a higher conversion of raw material but also a higher H_2 selectivity. Recently, the catalytic reforming of bio-oil was carried out using a nano-Ni/ceramic-foam catalyst in a fixed-bed reactor,[194] yielding H_2 with a capacity of $44.4–89.2 \, g_{H2} \, kg_{bio-oil}^{-1}$ at 500–800 °C.

5.4. Syngas conversion

5.4.1. CO and/or CO$_2$ methanation

The production of substitute natural gas (SNG) via CO and/or CO_2 methanation is a promising way toward effective and clean usage of coal and

biomass.[195,196] The CO and/or CO_2 methanations are strongly exothermic (CO +3 H_2 = CH_4 + H_2O, ΔH = −206 kJ mol^{-1}; CO_2 +4 H_2 = CH_4 +2 H_2O, ΔH = −165 kJ mol^{-1}) and require high throughput operation. Hence, the qualified catalysts should achieve synergistic coupling of high activity/selectivity and good durability with high mass/heat transfer (for effective temperature management) and high permeability (to reduce pressure drop). In pioneered Ru catalysts both in pellet and in honeycomb form,[197] the latter demonstrated a much lower pressure drop and also a much higher selectivity, by taking advantage of high voidage and short diffusion length for the reactant and product molecules. However, the low heat transfer of honeycomb support is insufficient to rapidly dissipate the reaction heat released in the catalyst bed, and moreover, their parallel and unconnected channels prohibit mass mixing in radial direction.

Given the high voidage, continuously interconnected open pores, and high thermal conductivity of the monolithic metal foams, a novel Ni-foam-structured catalyst of Ni-Al_2O_3/Ni-foam was tailored for the CO_2 methanation reaction.[60] A uniform NiO-Al_2O_3 nanocomposite catalytic layer (ca. 3 μm thickness) was formed onto the Ni-foam surface by using the wet chemical etching method (in 4.4). The resulting parent NiO-Al_2O_3/Ni-foam catalyst was reduced in a H_2 flow to form the Ni-Al_2O_3/Ni-foam, which was capable of converting ~90% CO_2 into CH_4 with ~99.9% selectivity for a feed gas of H_2/CO_2 (4/1) at 320 °C, 0.1 MPa, and a GHSV of 5000 h^{-1}. In particular, this catalyst was stable throughout the entire 1200 h with 10.2 mL catalyst usage.

Subsequently, a same kind of Ni-foam-structured catalyst of Ni-CeO_2-Al_2O_3/Ni-foam to be used in the CO methanation was tailored also by the chemical etching method.[81] The as-obtained NiO-CeO_2-Al_2O_3/Ni-foam (Figure 23) was reduced in H_2 to form the Ni-CeO_2-Al_2O_3/Ni-foam catalyst, which achieved a high CO conversion of >99.9% with a 94% CH_4 selectivity. In particular, this catalyst stably ran throughout the entire 1500-h testing. The experiments and computational fluid dynamics calculations consistently showed a dramatic reduction of the "hot-spot" temperature in catalyst bed due to its enhanced heat transfer stemmed from the Ni-foam.

5.4.2. Methanol to olefins

Light olefins are extensively utilized as crucial petrochemical feedstocks in the modern chemical industry, which are mainly produced by the steam cracking of naphtha or as the by-products of oil refining processes. The methanol to olefins (MTO) process has been attracting great attention for light olefin production as an alternative route from non-oil sources, such as biomass, natural gas, and coal.[198] At present, an industrial implementation of this process has been achieved in ethylene production on the SAPO-34 zeolite in a fluidized-bed reactor. Moreover, the fast-growing global demand of propylene is spurring worldwide impetus on the exploration of methanol to
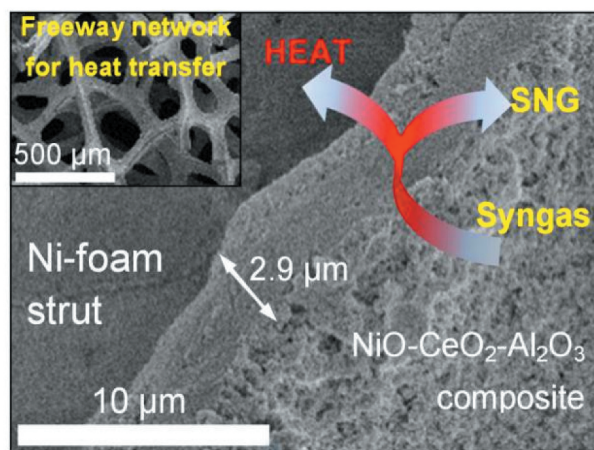
Figure 23. Monolithic Ni-CeO₂-Al₂O₃/Ni-foam catalyst developed by modified wet chemical etching of Ni-foam followed by calcination in air, providing unique combination of high activity/selectivity, excellent stability, and enhanced heat transfer (Reprinted with permission from ref.[81] Copyright 2015 Wiley and Sons).

propylene (MTP). Lurgi's MTP process has been industrially demonstrated by using a ZSM-5 particulate catalyst in a packed bed,[198] and then extensive studies have still been conducted to further improve the propylene selectivity and stability of this catalyst. Most efforts have been focused on the ZSM-5 modification such as acidity tuning, size and/or morphology controllable synthesis, and hierarchical design of pore structure.[199,200] Despite these advances, the practical use of ZSM-5 as catalysts in the fixed-bed reactor is still facing some challenges, as the micro-granules or extruded pellets of a few millimeters are required in the real world rather than the as-made powders. In turn, some frustrating problems emerge including the mass and heat transfer limitations, high pressure drop, non-regular flow pattern, and adverse effects of the binders used, always reducing the intrinsic catalyst selectivity and activity.

Owing to the improved hydrodynamics in combination with the enhanced heat/mass transfer of structured catalysts,[8,201] structuring zeolites onto monolithic substrates (such as the fibers and foams) is becoming a source of inspiration. However, only a few studies have reported the synthesis of ZSM-5 on SiC-foam for the MTP process.[202,203] The simulation calculations also showed that the micro-structured design of ZSM-5 could promote C_{2-4} olefin selectivity up to 71% with a high propylene selectivity up to 49%.[204] In the last several years, Lu et al.[10,85,86] improved the catalyst selectivity and stability for the MTP process, just via a strategy of microfibrous-structured design rather than the pore-tuning and chemical-modification of HZSM-5. In 2014, they first presented a 3D stainless steel microfibers (SS-fiber, 20-μm in diameter)

structured catalyst of HZSM-5/SS-fiber, which could be obtainable on a macroscopic scale by direct growth of ZSM-5 shell onto an SS-fiber (growth method in 4.5.1).[10] This approach effectively combines the high heat/mass transfer, large void volume, hierarchical porous structure from micro- to macro-sizes, binder-free *in-situ* hydrothermal synthesis, and good rigidity/ robustness. Thanks to this beneficial combination, such microfibrous structured design exhibited a remarkable improvement of C_{2-4} olefins (especially to propylene) selectivity and life-time for the MTP process compared with the particulate zeolite. Using a feed of 30 vol% methanol in N_2 and at 480 °C, a high propylene selectivity of ~46% could be obtainable with a total C_{2-4} olefin selectivity of ~70%, much higher than that (~37%, with C_{2-4} olefin selectivity of ~64%) for the particulate catalyst; the life-time is at least for 210 h, almost threefold longer than that of 60 h for the particulate one. In nature, this unprecedented improvement originates from the propagation of olefin methylation-cracking cycle over the aromatic-based cycle in the methanol-to-hydrocarbon catalysis.

Moreover, the kinetic and modeling studies also displayed higher internal-diffusion efficiency and narrower distribution of residence time of reactants in the zeolite shell, not only promoting the propylene formation but also improving the utilization efficiency of HZSM-5.[31] It is widely accepted that hierarchical tailoring is a promising strategy to improve ZSM-5 lifetime due to the shortened internal-diffusion path length.[199] To accomplish this goal, various methods have been studied to create intra-crystalline mesopores like desilication and dual-templating.[205–208] More recently, Lu et al.[86] developed a hollow-B-ZSM-5/SS-fiber catalyst (Figure 24; preparation method in 4.5.1). The core@shell nanocomposite of silicalite-1@B-ZSM-5 was first *in situ* structured onto a thin felt of 20 μm SS-fiber by the seed-assisted dry gel vapor-phase transport method. Then, the hollow structure was created through alkali leaching of the silicalite-1 cores. The as-obtained catalyst showed a remarkable stability improvement in the MTP reaction (lifetime of 109 h for this catalyst vs. 40 h for the catalyst in ref. [10] at a high WHSV of $10 h^{-1}$) because of the nano-hollow-structure enhanced diffusion.[86,209] Boron incorporation is essential for preventing the framework dealumination during the alkali leaching. These findings will initiate the attempts to develop microfibrous-structured catalysts, and further inspire research activities concerning in-depth understanding of the promotion effect stemming from the zeolite-modifications in combination with the fibrous-structured design.

5.4.3. Fischer-tropsch synthesis

The Fischer-Tropsch synthesis (FTS) process is strongly exothermic ($\Delta H = -165 kJ mol^{-1}$ of CH_2).[53,54] The earnest endeavors to enhance heat-transfer efficiency inside the reactor have been made in terms of developing fluidized-bed reactors,[210] slurry reactors,[211] metal-monolith catalysts,[212] and
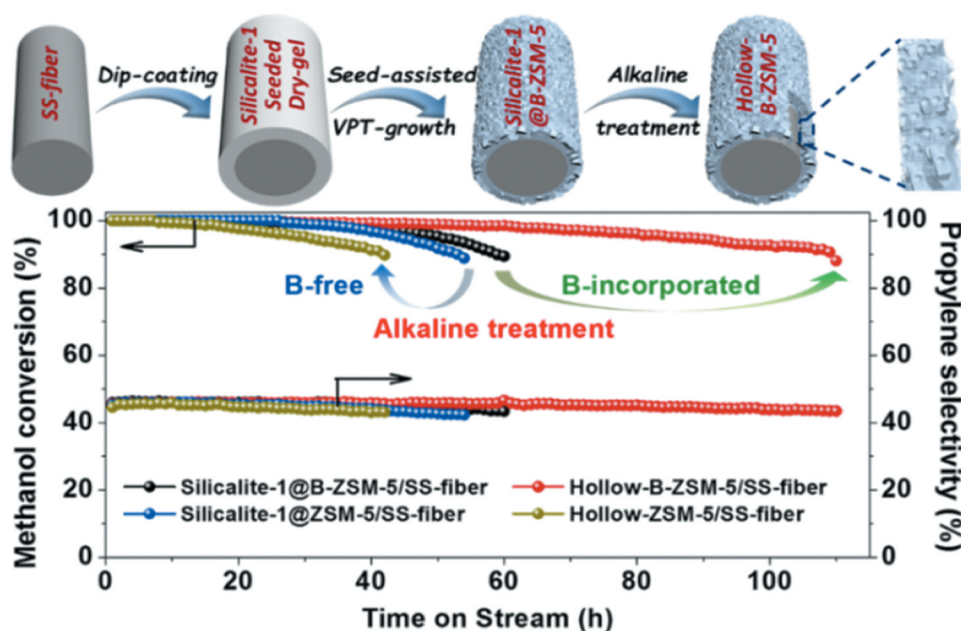
Figure 24. Thin-felt hollow-B-ZSM-5/SS-fiber catalyst was tailored through alkaline leaching of silicalite-1, showing dramatic MTP stability improvement due to the enhanced diffusion with stabilized framework aluminum (Reprinted with permission from ref.[86] Copyright 2017 Royal Society of Chemistry).

corrugated packings with open/close cross flow structures.[213] Despite some successful applications of these methods, they still carry some disadvantages. The catalyst density in a fluidized-bed reactor and slurry reactor is relatively low.[214] Monoliths need washcoating to load catalytic species,[215] unsuitable for the pre-manufactured catalysts. Corrugated packing, compatible with both washcoating and pre-manufactured catalyst particles, has been proven to have a poor conductive contribution to heat transfer,[216] so that a gas or liquid recycle is usually applied to improve the convective component to achieve an enhanced intra-bed heat transfer. Based on the high heat-transfer of metal-fibers, Tatarchuk et al.[58,61,217,218] prepared a series of microfibrous entrapped particulate catalysts (MFEPC; preparation information in corresponding references) to maintain a stable reaction temperature for the FTS process. The porous structure of MFEPC can entrap any pre-manufactured catalyst particles. Typically, the Cu-microfibers entrapped particulate catalyst of Fe/Al_2O_3©Cu-fiber (Figure 25) demonstrated an excellent intra-bed heat transfer for the FTS thermal management.[218] The FTS was carried out in a large tubular reactor (34.0 mm inner diameter) packed with the Fe/Al_2O_3 ©Cu-fiber, showing a radial temperature gradient of <5 °C and similar reactivity/selectivity as those obtained in a small FTS reactor (9.5 mm). In contrast, the particulate Fe/Al_2O_3 bed (34.0 mm), with the same catalyst loading density

and under identical conditions, reached a radial temperature gradient around 54 °C. The apparent reaction rate constant and productivity of the Fe/Al$_2$O$_3$ ©Cu-fiber at a 27.7% CO conversion were 167 mmol$_{(H2+CO)}$ g$_{cat}^{-1}$ h^{-1} and 0.30 g$_{C5+}$ g$_{cat}^{-1}$ h^{-1}, respectively, which are comparable to the most active unsupported Fe-based catalyst. It was also found that the Fe/Al$_2$O$_3$©Cu-fiber required negligible amount of time to reach its steady state compared with the particulate Fe/Al$_2$O$_3$ bed. These advantages show that the MFEPC approach is a promising alternative to the particulate-packing bed for exothermic reactions such as FTS.

Besides the MTP process for light olefins production (to see 8.2), the Fischer-Tropsch process (named as FTO) is another alternative production from syngas, but in a direct manner. To date, various catalytic components (such as Fe, Co, or Ru at bulk- or nano-scales), supports (ranging from oxides and molecular sieves to carbonaceous materials, such as Al$_2$O$_3$, MgO, SiO$_2$, or carbon nanotubes), and promoters (Ag, Mn, or K) have been widely studied to optimize the FTO performance.[219] Despite some promising results, further industrial applications still remain particularly challenging, because, on the one hand, the extruded pellets or microgranules are required in the real world rather than as-made powders, and on the other hand, the FTO process is strongly exothermic. Therefore, it is desirable to render a catalyst with good heat conductivity for rapidly dissipating the reaction heat from the catalyst bed. Recently, a microfibrous structured FTO catalyst of Fe-Mn-K/ns-Al$_2$O$_3$ /Al-fiber was reported.[220] Firstly, the ns-Al$_2$O$_3$/Al-fiber support was prepared according to the method in 4.5.2,[87,88] and the active components of Fe and Mn as well as additive K were then placed onto the surface of ns-Al$_2$O$_3$ /Al-fiber by the incipient wetness impregnation method. By combining the
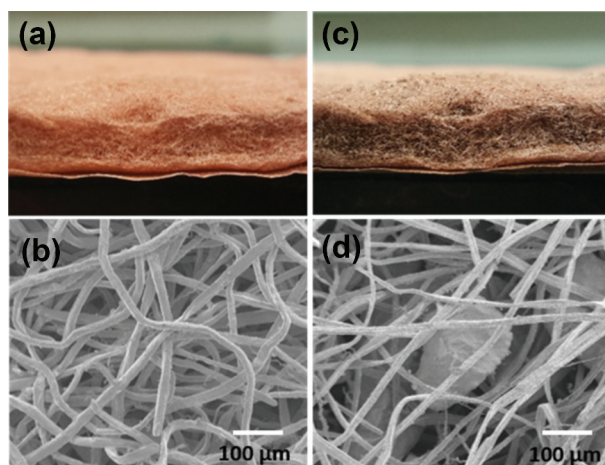
Figure 25. (A) Picture and (b) SEM image of Cu-fiber. (c) Picture and (d) SEM image of Fe/Al$_2$O$_3$ ©Cu-fiber (Reprinted with permission from ref.[218] Copyright 2019 Elsevier).

enhanced heat/mass transfer, large void volume, and entirely open network structure, this catalyst delivered a high iron time yield of 206.9 μmol_{CO} g_{Fe}^{-1} s^{-1} at a 90% CO conversion with a 40% selectivity to C_2-C_4 olefins at 350 °C, 4.0 MPa, and a GHSV of 10,000 mL g_{cat}^{-1} h^{-1}. Very recently, another micro-fibrous structured catalyst of Fe-Mn-K/ns-Al_2O_3/Al-fiber of the same type was fabricated via the surface impregnation combustion method.[221] The catalyst prepared under the air atmosphere delivered a very high iron time yield of 202.3 μmol_{CO} g_{Fe}^{-1} s^{-1} with an 89.6% CO conversion and a 42.1% selectivity to C_{2-4} olefins at 350 °C, 4.0 MPa, and a GHSV of 10,000 mL g_{cat}^{-1} h^{-1}. The hydrocarbon distribution over this catalyst remained constant throughout the entire 225-h testing, with a CH_4 selectivity of ~16%, lower olefins of ~38%, and C_5^+ hydrocarbon of ~35%.

5.5. Environmental protection

5.5.1. Catalytic combustion of methane

Catalytic combustion of methane under O_2-lean condition. The catalytic CH_4 combustion is an important reaction for coal-bed gas upgrading (under O_2-lean condition), environment protection, and energy production (under CH_4-lean condition). Obviously, the strong exothermicity ($\Delta H_{298} = -802.7$ kJ mol^{-1}) and high throughput operation for these processes require the catalyst to be highly active/selective/stable, thermally conductive, and highly permeable. To this end, the honeycomb monoliths of short channel length and high channel density have been catalytically functionalized with high surface area coatings.[222] The buildup of boundary layer between gas flow and coating surface could be avoided, thus greatly enhancing the internal diffusion of reactant within coatings, but such kind of catalysts still face the lack of radial mixing of reactants and relatively low heat transfer.[37,223,224] Fortunately, Ni-foam (typically 100 pores per inch) has beneficial features to fabricate the structured catalysts, such as the high void fraction, excellent thermal conductivity, and enhanced mechanical strength; more interestingly, a novel Pd/Ni-foam catalyst for the deoxygenation of coal-bed gas can be facilely prepared by the method in 4.3.[80] This catalyst integrated the high catalytic performance with as-expected high heat/mass transfer and low pressure drop, thus offering a good stability for at least 500 h with >95% O_2 conversion and 100% CO_2 selectivity at 320–350 °C.

Catalytic combustion of low-concentration methane. The monolithic Pd@SiO_2/ns-Al_2O_3/Al-fiber catalyst prepared by the method in 4.6 was applied in the catalytic combustion of methane under the methane-lean condition,[11] and delivered a high activity owing to the high dispersion of Pd NPs (2–3 nm). The CH_4 conversion was gradually increased to 10% at 275 °C, 50% at 325 °C, 90% at 365 °C, and 100% at 400 °C, using a high GHSV of 72,000 mL g_{cat}^{-1} h^{-1} for a feed gas of 1.0 vol% CH_4 in air. The other advantage

of this catalyst is the high permeability from its entirely open network structure with a high void volume. Therefore, this fiber-structured catalyst, with complete CH_4 conversion at 445 °C, generated a very low pressure drop of only 4000 Pa m^{-1} even at a high GHSV of 100,000 mL g$_{cat}^{-1}$ h^{-1}. Moreover, this catalyst assured the activity maintenance throughout a 1000-h test, and the Pd-encapsulation into SiO_2 matrix plays a pivotal role in preventing Pd NPs from sintering.

Recently, Zhao et al.[225] developed a thin-sheet microfiber-structured Pd-MgO-Al_2O_3/Al-fiber catalyst for this reaction. Notably, the feed gas contains 3–15 vol% water vapor, as the exhaust gas from compressed natural gas vehicles has a large amount of water vapor of 3–15% as well as a low CH_4 concentration of ca. 0.1–1 vol %.[226] The ideal catalysts for the CH_4 combustion should be able to couple the high activity/stability and high resistance to water-vapor poisoning with the high permeability for a low pressure drop. A high-performance Pd-MgO-Al_2O_3/Al-fiber catalyst was tailored by hydrothermally growing the Mg-Al mixed-oxide precursors (e.g., layered double hydroxides (LDHs) plus $MgCO_3$; growth method based on the method in 4.5.3, and details in ref. [225]) on the Al-fiber surface followed by placing 0.5 wt% Pd on the as-obtained substrate by the wet impregnation method. The MgO in Pd-MgO-Al_2O_3 composites enhances the catalyst basicity and electron density of metallic Pd, thus weakening the support of electrophilicity and stabilizing PdO against the formation of inactive Pd^{4+} species. This catalyst could stably run for a feed gas of 1 vol% methane and 3–15 vol% water vapor in air.

5.5.2. O$_3$ decomposition

The O_3 layer in upper atmosphere prevents the short-wavelength ultraviolet light from reaching the Earth surface, but the indoor O_3 of higher than 0.1 ppm can cause severe health problems, such as dizziness, headache, and fatigue, along with various other symptoms. Therefore, the research on O_3 decomposition are important from the point of view of public health and indoor environmental protection. The honeycomb-structured catalysts are usually implemented to achieve such goal,[2] but the dip-coating technology for the honeycomb catalysts always suffer from high cost of their production. Lu et al.[227] tailored a highly efficient structured catalyst of Co-MnO$_x$/ns-Al$_2$O$_3$/Al-fiber (Figure 26) with the unique form factor and high permeability for the catalytic O_3 decomposition. The Co and Mn species were placed onto the ns-γ-Al$_2$O$_3$/Al-fiber chips (whose preparation is in 4.5.2) by the incipient wetness co-impregnation method, being able to achieve full O_3 conversion at 25 °C for a feed gas containing 1000 ppm O_3 at a high GHSV of 48,000 mL g$_{cat}^{-1}$ h^{-1}; a full O_3 conversion was retained in the absence of moisture until the end of testing after 720 min; in case with a relative humidity of 50%, the O_3 conversion declined from the initial 88% to a flat of ~66% within 90 min. In order to improve the catalyst moisture resistance, the above catalyst was

modified by Pd to get a Pd-Co-MnO$_x$/Al$_2$O$_3$/Al-fiber.[228] The preferred catalyst remained full O$_3$ conversion for at least 4 h at 25°C for a feed gas with 1500 ppm O$_3$ even at a high relative humidity of 70% and a GHSV of 48,000 mL g$_{cat}^{-1}$ h^{-1}; the full O$_3$ conversion quickly moved to a flat of ~96% during the 4-h testing at 90% relative humidity, whereas it was retrievable immediately after switching into the dry feed gas. The remarkable improvement in activity, stability, and moisture resistance by the Pd-modification is due to the greatly improved and stabilized oxygen vacancies and markedly weakened H$_2$O adsorption on the catalyst surface.

5.5.3. NO$_x$ removal

The nitrogen oxides (NO$_x$) emitted from combustion of coal and oil can cause great environmental pollution, including acid rain, photochemical smog, and greenhouse effect.[229,230] At present, the selective catalytic reduction of NO by ammonia (NH$_3$-SCR) has been recognized as the most effective and economical method for the removal of NO$_x$ from the mobile and stationary
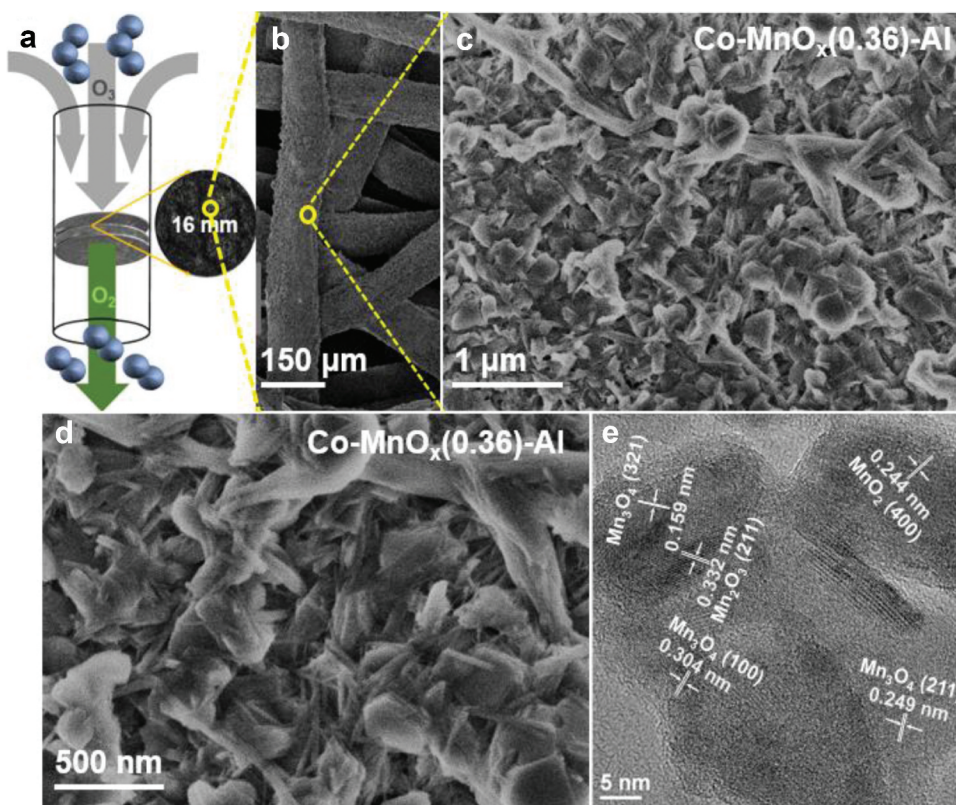
Figure 26. Geometry, morphology and structure features of the representative Co-MnO$_x$/ns-Al$_2$O$_3$/Al-fiber catalyst from nano- to macro-scale: (a) optical photograph, (b-d) SEM and (e) TEM images (Reprinted with permission from ref.[227] Copyright 2015 Wiley and Sons).

sources.[231,232] For decades, V_2O_5-MoO_3/TiO_2 and V_2O_5-WO_3/TiO_2 were used in many countries as the industrially adopted NH_3-SCR catalysts,[233] but suffered from high operation temperature and low N_2 selectivity as well as V toxicity to the environment and human health. Recently, many studies have been conducted on the Mn-based catalysts,[234–236] and the NiO-MnO_x acted as a promising candidate.[236] For practical applications, active components were usually immobilized on the surface or adsorbed to the channel walls of ceramic monoliths or parallel passage reactors by the wash-coating, dip-coating, impregnation, or extrusion technique.[237] However, their actual operations face the problems of random distribution of active components, low interphase mass transfer, and blockage of channels. The fiber/foam-structured ones are attractive alternatives.

The Ni-foam can be taken as a new prospective support due to its high porosity, high mass/heat transfer, and high mechanical strength. By integrating the highly active NiO-MnO_x nanocomposites with the Ni-foam support, Zhang et al.[95] tailored a Ni-foam-structured NiO-MnO_x catalyst by a simple hydrothermal treatment and calcination process (partially described in 4.5.4 and totally illustrated in Figure 27). Such catalyst gave high catalytic activity, good stability, and a wide temperature window of >80% NO conversion ranged from 245 to 360 °C; a maximum NO conversion of 91% was obtained at 270°C, while the NO conversion was maintained at ca. 90% for at least 16 h without any sign of deactivation.

A Pd/$Ce_{0.66}Zr_{0.34}O_2$/TiO_2/Al_2O_3/WMH (WMH: wire-mesh-honeycomb) was prepared by the electrophoretic deposition method (described in 4.2).[238] This WMH structured catalyst exhibited a higher NO_x conversion at lower temperatures and could establish the steady state more quickly than the ceramic monolithic catalyst, for applications in the unsteady-state cases. This catalyst also exhibited a characteristic of fast light-off. In addition, the WMH-structured V_2O_5-WO_3-TiO_2 catalyst was also prepared for the NH_3-SCR.[74,75] The mass transfer of such WMH-type catalysts was investigated, and the results revealed that they had not only a high catalyst utilization relative to the geometric surface area and catalyst weight but also a low pressure drop. Moreover, the resistances to H_2O, SO_2, and dust were investigated for the WMH catalyst. The results showed that above 95% NO_x conversion could be kept in a broad temperature window (250–425 °C) and nearly 92% NO_x conversion was achieved during a durability test in the presence of H_2O and SO_2. Furthermore, little dust of 2.9 g m^{-2} was deposited on catalyst during a 40-h dust exposure, which is the guarantee of good maintenance of nearly 90% NO_x conversion. By comparison, the dust amount deposited on the ceramic honeycomb catalyst with the same cell density reached up to 6.7 g m^{-2}, thus leading to a large reduction of the NO_x conversion to 58%. The high dust resistance of WMH catalyst might be attributed to its entirely open 3D porous structure.
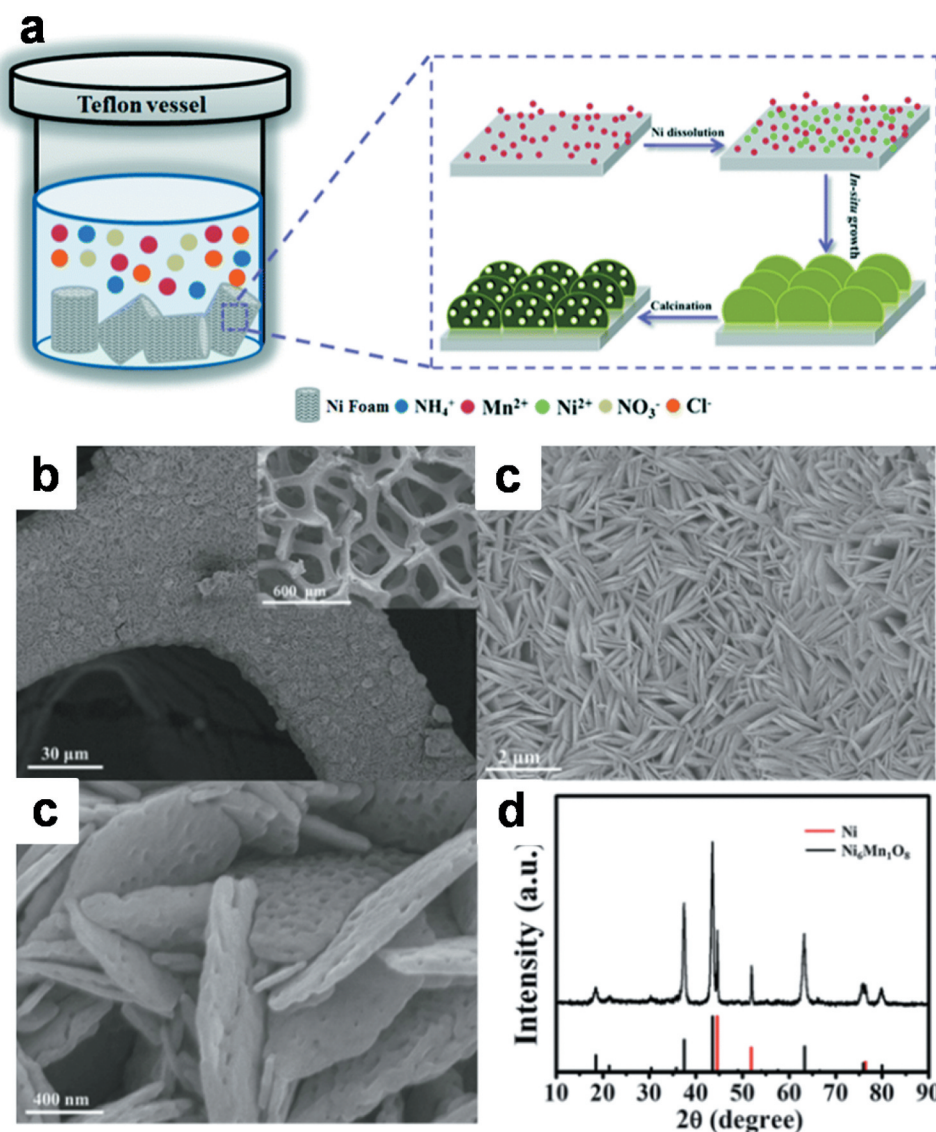
Figure 27. (A) Schematic representation of the synthesis route to NiO-MnO$_x$/Ni-foam catalyst. (b-d) SEM images and (e) XRD pattern of the NiO-MnO$_x$/Ni-foam catalyst (Reprinted with permission from ref.[95] Copyright 2014 Royal Society of Chemistry).

It is an intractable issue to improve the low-temperature SO$_2$-tolerant NH$_3$-SCR performance because as-deposited sulfates are difficult to be decomposed below 300 °C. Han et al.[239] tailored a low-temperature self-prevention structured catalyst of TiO$_2$@Fe$_2$O$_3$/Al$_2$O$_3$/Al-mesh against the sulfate deposition. This catalyst was prepared via a one-pot self-assembly method using the titanate cross-linking molecule (titanium bis(triethanolamine)-diisopropoxide; preparation based on the method in 4.6 and details in

ref.[239]), delivering a superior SO_2 tolerance at 260 °C and a broad window of 220–420 °C with the NO conversion above 90%. The mesoporous TiO_2-shell effectively restrained the deposition of $FeSO_4$ and NH_4HSO_4 because of the weakened SO_2 adsorption and promoted NH_4HSO_4 decomposition on the mesoporous-TiO_2.

5.5.4. Catalytic combustion of volatile organic compounds

Some mesh-structured catalysts were prepared by the spray deposition method (described in 4.1) and used to burn away different pollutants in the flue gases from fuel combustion, e.g., CO, propylene, terpenes, and tar.[66,67] In most cases relevant to the particulate catalysts, the combustion is severely limited by the limited external mass transfer. However, the combustion performing with this FeCrAl-wire mesh catalyst revealed that its performance in the mass-transfer controlled domain was superior.[66] Moreover, a numerical model was also developed to compare the performance of wire-mesh, monolith, and pellet catalysts,[67] together with a model describing the resistance to internal/external mass/heat transfer and the effects of axial dispersion. The results revealed that such wire-mesh catalysts take advantage of high mass/heat transfer, moderate pressure drop, insignificant effects of pore diffusion and axial dispersion, good thermal and mechanical strength, geometric flexibility, excellent thermal response, and simplicity in the catalyst recovery.

The above-mentioned $Pd@SiO_2$/ns-Al_2O_3/Al-fiber for the CH_4 combustion in 5.5.1 was also promising for the catalytic abatement of volatile organic compounds, including hydrocarbons, alcohols, aldehydes, and esters.[11] Under conditions of 1000 ppm of single organic compound in air and GHSV of 72,000 mL g_{cat}^{-1} h^{-1}, T_{90} was 267 °C for toluene, 200 °C for propylene, 200 °C for ethane, 138 °C for methyl formate, 100 °C for formaldehyde, and 60 °C for methanol. The wire-mesh-honeycomb (WMH) catalysts exhibit better flow distribution and higher interphase mass transfer than the ceramic honeycomb ones. The Al_2O_3-coated WMH (coated method in 4.2) was deposited with Pt/TiO_2 for the ethyl acetate oxidation.[76] The mass-transfer coefficient in the WMH module was found to be quite different from that in the ceramic honeycomb one. After deposition of V_2O_5-TiO_2 by the impregnation method onto the WMH surface, the resulting catalyst was applied for the catalytic oxidation of 1,2-dichlorobenzene,[240] showing better catalytic performance than the ceramic honeycomb catalyst due to the reduced mass-transfer resistance by the existence of holes in the mesh sheet. The kinetic study showed that the better performance of WMH catalysts is due to an improved external mass-transfer because of the existence of additional flow across the channel walls of the wire mesh.

5.6. Others

5.6.1. Liquid-liquid mixing reaction

The sintered-locked microfibrous structures were also used as micro-agitators toward the process intensification of liquid–liquid mixing reactions, such as the benzene nitration that suffers from strong heat/mass transfer and high risk of explosion, because of the benefits from their 3D open network for micro-scale segmentation and rapid mixing of fluids. Based on the thin-felt packing consisting of 20-μm SS-fiber, Li et al.[241] designed a micro-reactor with the unique integration of micro-mixing, reaction, and heat exchange (Figure 28) and investigated the fast and highly exothermic liquid–liquid two-phase mixing benzene-HNO$_3$ nitration reaction. This reaction can be facilitated in a short time with a benzene conversion of 91.7% and a nitrobenzene selectivity of 99.4%. For the purpose of eliminating the use of H$_2$SO$_4$ as catalyst in this reaction, Yang et al.[242] developed a microfibrous-structured Nafion-SiO$_2$/SS-fiber catalyst with a voidage of 60%–75%, by engineering the Nafion solid acid particles onto a thin-felt SS-fiber packing. Its catalytic performance for the H$_2$SO$_4$-free benzene nitration was tested on a micro-reactor (Figure 28), achieving a 44.7% benzene conversion with a nitrobenzene selectivity of 99.9% at 75 °C. The catalytic efficiency of per unit acid site of the Nafion-SiO$_2$/SS-fiber packing is nearly 600 times higher than that of H$_2$SO$_4$ (used in the traditional batch stirred reactor) at comparable benzene conversion.

5.6.2. Catalytic distillation

The esterification of acetic acid with ethanol to ethyl acetate (EA) is a typical equilibrium reaction with limited EA formation. The catalytic distillation (CD) integrates catalysis and distillation to separate EA from the reaction system timely, making a positive shift of equilibrium. Lai et al.[243] investigated the EA production by the CD method using particulate Amberlyst 35 (acidic ion exchange resin) at a pilot-plant scale, and high-purity EA of higher than 99% selectivity could be obtainable with an acetic acid impurity of less than 100 ppm. Despite this interesting result, some challenges still exist regarding this catalyst, such as the high pressure drop and limited heat/mass transfer.[244] To solve these problems, some monolithic metal-structures (such as MULTIPAK®,[245] KATAPAK®-SP,[246] and SCPI[247]) have been adopted to arrange the particulate catalyst in arrays of these structures (namely to fabricate the arranged catalyst packings). However, these arranged catalyst packings are complex and costly exercised with no guarantee of catalyst durability due to the inherent usage of particulate catalysts even though in the arranged form.

Deng et al.[248] reported the acetic acid-ethanol esterification by the CD method using a microfibrous-structured ZSM-5/SS-fiber CD packing, which was prepared by directly growing ZSM-5 onto the θ-ring-like analogues of SS-fiber (preparation method in 4.5.1; Figure 29). High total (95.9%) and actual
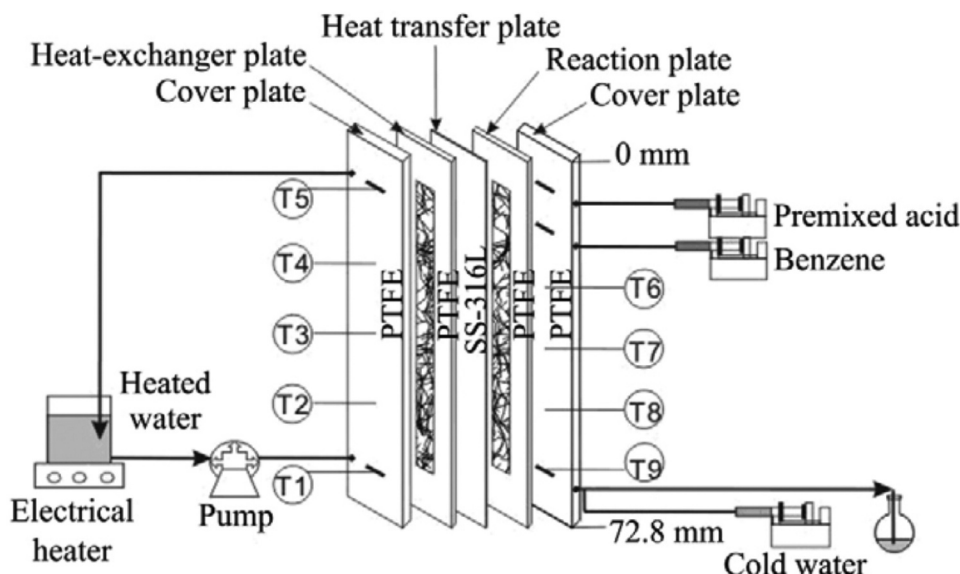
Figure 28. Micro-reactor structure and reaction flow chart (PTFE: polytetrafluoroethylene; T1-T9: temperature measurement points) (Reprinted with permission from ref.[242] Copyright 2007 Elsevier).

(90.9%) yields of EA with an 89.8% purity were achievable, while the high CD efficiency was well preserved after 30 consecutive batch runs for at least 240 h. This packing achieved a unique combination of good stability, adequate Bronsted acid sites, and high mass/heat transfer.

5.6.3. Electrocatalysis

The electrocatalysis is a hot topic in the current international academic frontier. It has a broad prospect in many reactions, such as splitting water to produce hydrogen and catalyzing CO_2-H_2O to synthesize CO and oxygen-containing hydrocarbons. From the perspective of application, the self-supporting and efficient-diffusion electrode catalysts are very important for electrocatalysis. The fine construction of self-supporting electrode catalysts based on the metal fiber/foam matrix has been reported continuously.

For example, the hydrogen production via water-splitting is a sustainable way in catalysis and renewable energy. Noble metals are still the best catalysts for the two half-reactions in the water-splitting (oxygen evolution (OER) reaction and hydrogen evolution (HER) reaction), but suffer from high cost and low natural abundance. Some non-noble metal catalysts have been investigated, but the catalytic efficiency of many of them (*e.g.*, MoS_2) is greatly limited by the low electrical conductivity.[249] A monolithic Ni_3S_2/Ni-foam electrocatalyst (Figure 12) is fabricated via *in situ* growth of the highly active Ni_3S_2 nanosheets on the highly conductive metal Ni-foam (preparation details in 4.8).[118] This catalyst can serve as a highly active, binder-free, bifunctional
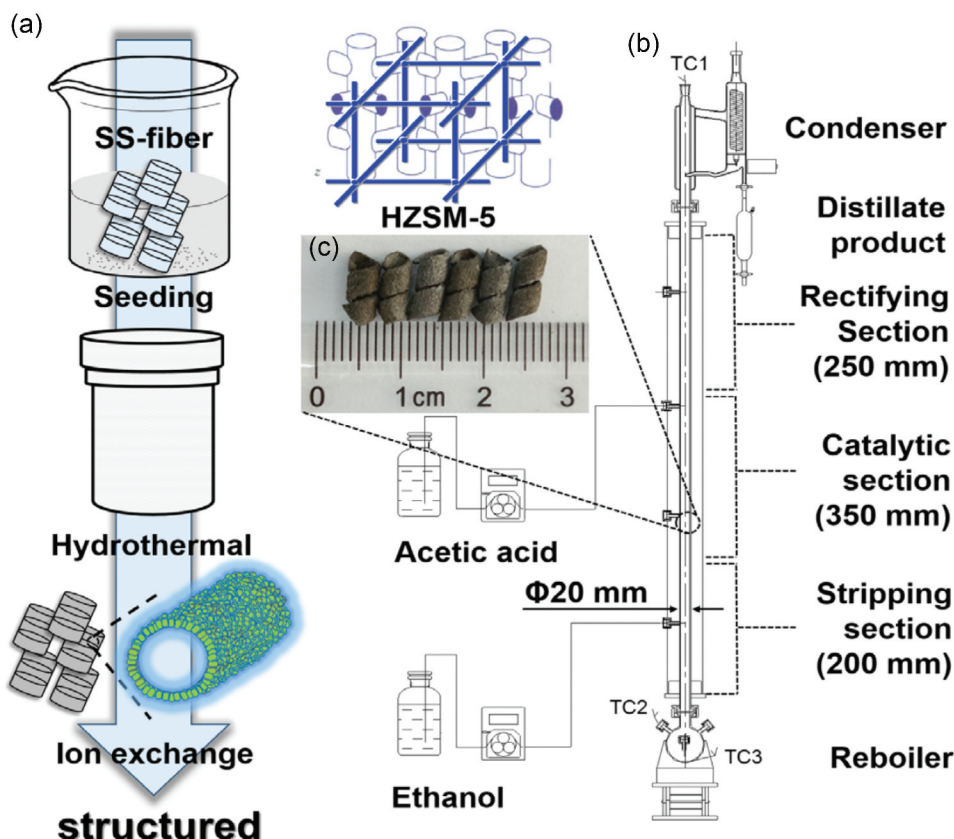
Figure 29. (A) Schematic illustration of the preparation of microfibrous-structured ZSM-5/SS-fiber catalyst packings. (b) CD apparatus with optical photograph of θ-ring analogues of ZSM-5/SS-fiber (TC1, TC2: thermocouples for monitoring the temperatures at column top and in flask, respectively; TC3: thermocouple for controlling reboiler duty). (c) Macroscopic photograph of the ZSM-5/SS-fiber (50) catalyst (Reprinted with permission from ref.[248] Copyright 2016 Royal Society of Chemistry).

electrocatalyst for both the HER and OER. The Ni_3S_2/Ni-foam delivered 100% Faradaic yield toward both the HER and OER and showed a remarkable catalytic stability for at least 200 h, in nature, due to the combination of high catalytic performance of the Ni_3S_2-nanosheet arrays with high electrical conductivity of the Ni-foam.

Although the electrocatalytic reduction of CO_2 is a prospective strategy to address both carbon emission abatement and sustainable energy development, the efficient CO_2 conversion remains a big challenge in the aqueous CO_2 electroreduction because of the low solubility and intrinsic inertness of CO_2. Chen et al.[250] reported a hollow Cu-fiber of gas-diffusion electrode catalyst for the CO_2 reduction to formate. The considerable faradaic efficiency (80%) at a high current density (210 mA cm^{-2}) could be achievable over this electrode catalyst, with its formate yield (2677 μmol h^{-1} cm^{-2}) about 30 times that

of the Cu-foil. The CO_2 molecules are forced to penetrate through porous wall of the hollow Cu-fiber electrode, resulting in CO_2 effective activation and compulsive interaction with the active sites, which synergistically facilitates the formate formation. Moreover, Chen et al.[251] successfully constructed a high-performance hollow-silver-fiber electrode catalyst (Figure 30) through combining the phase transformation with the electrochemical *in-situ* activation. At 25 °C, 0.1 MPa, and a high GHSV of ≥30000 mL g_{cat}^{-1} h^{-1}, a single-running CO_2 conversion of ≥50% was obtained with ≥90% Faraday efficiency of CO and a current density of 1200 mA cm^{-2}, showing a great application potential.

5.6.4. Supercapacitors

The supercapacitors structured on carbon cloth, metal sheets, papers, and plastic substrates are widely employed as the portable and wearable energy-storage devices.[252] In order to further increase their compatibility but with decreased size, the fiber and cable supercapacitors were considered as a promising strategy. Recently, Wang et al.[253] tailored a coaxial fiber supercapacitor based on the $NiCo_2O_4$ nanosheets, giving a volumetric capacitance of 10.3 F cm^{-3} at 0.08 mA. In addition, a supercapacitor integrating the planar $ZnCo_2O_4$ nano-arrays and carbon-fiber offers a capacitance of 0.6 F g^{-1} at 1 A g^{-1}.[254]

Despite these interesting results, further studies still need to be carried out to improve their performance for the practical applications. For example, most supercapacitors are based on metal wire current collectors, which have smooth surface, low surface area, and low porosity, thus causing large contact resistance between the current collector substrate and active materials. Hence, the internal resistance should be reduced for faster charge transport, and the active
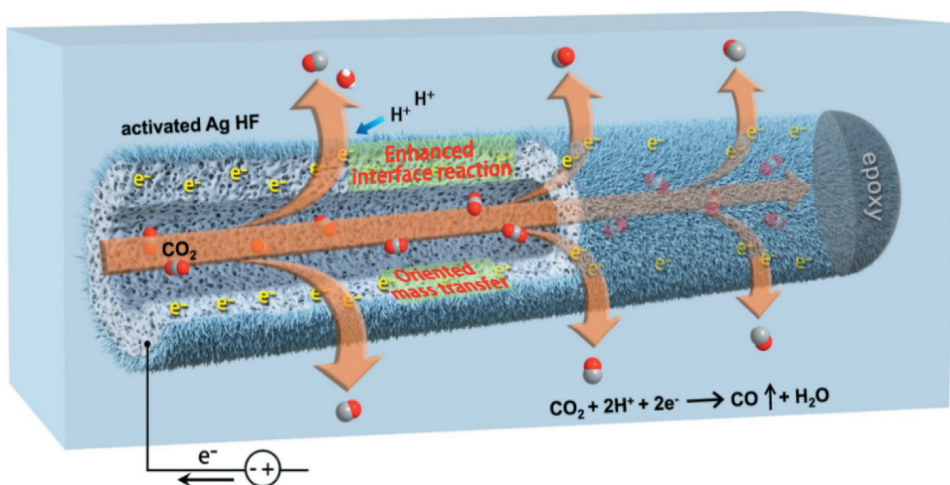
Figure 30. Schematic diagram of high-efficiency electroreduction of CO_2 with micro/nano structure hollow fiber silver electrode (Reprinted with permission from ref.[251] Copyright 2022 Springer Nature).

surface area should be increased to permit easy access for electrolyte ions. A $NiCo_2O_4$ electroactive material was grown onto a 3D-Ni/Ni-wire current collector by the method described in 4.8.[116] As-prepared $NiCo_2O_4$/3D-Ni /Ni-wire exhibited an outstanding volumetric capacitance of 29.7 F cm^{-3} with a good rate capability of 97.5% at 20 mA.

The carbon nanotubes (CNTs) and carbon aerogel (CAG) are promising nano-carbon-based materials but encounter molding problems when used in batteries and supercapacitors. The use of traditional polymer adhesives will not only sacrifice the specific surface area and destroy the structural characteristics of carbon materials but also lead to a high resistance of charge conduction and ion transfer. Therefore, the cross-scale preparation of binder-free nano-carbon materials has attracted great attention. Based on the large voidage, open network, and unique shape factor of the thin-sheet Ni-microfiber substrate, Jiang et al.[255] successfully prepared a CNTs/Ni-microfiber composite (8.0 cm in diameter) by growing CNTs on the fiber surface via the chemical vapor deposition method. The overall structure was intact, and the CNTs were evenly distributed with CNTs loading as high as 60 wt%. The charge transfer and ion transfer resistances of such composites were very small, and the specific capacitance measured in a 5 M KOH aqueous solution electrolyte could reach 47 F g^{-1}. Furthermore, Li et al.[256] used the above-obtained CNTs/Ni-microfiber composite as the substrate to prepare a self-supporting electrode material of PANi-CNTs/Ni-microfiber by the
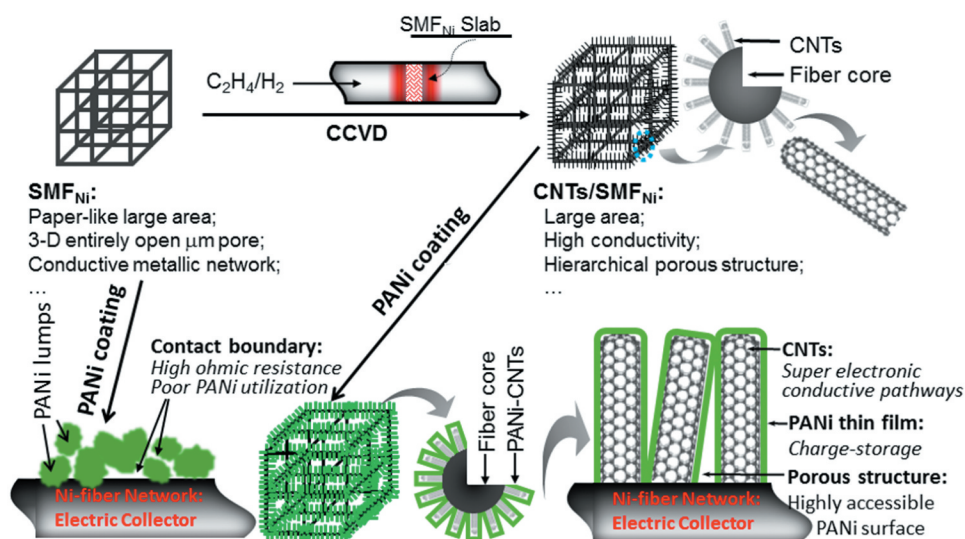
Figure 31. Schematic diagram of self-supporting three-dimensional CNT-PANi/Ni-microfiber electrode material, with metal fiber network as collector, CNTs as conductor-nanowire, PANi as chemical energy storage active material, and spanning macro-micro-nano scales (Reprinted with permission from ref.[256] Copyright 2012 Royal Society of Chemistry).

polyaniline (PANi) coating method. In this electrode, Ni-microfiber acts as the current collector, with CNTs as the conductor-nanowire and PANi as the chemical energy storage active material, with spanning macro-, meso-, and nano-scales (Figure 31). This electrode exhibited promising electrochemical properties, chemical capacitance energy storage performance, and good charge-discharge cycle stability. In nature, the electronic interactions generated by the π-π stacking interactions between the PANi and CNTs not only promote the electrochemical activity of PANi but may also have a stabilizing effect on the PANi, thus improving the charge-discharge cycle stability. The above results demonstrate that the fabricated devices possess excellent potentials for flexible, portable, and wearable applications in energy-storage devices.

6. Conclusions and future outlook

The exploration of heterogeneous catalysis based on the structured catalysts has experienced a rich history for decades of years, and clearly, their progress to date has proven the superiority to the particulate catalysts that are randomly packed in reactor. This review is only a snapshot of the current states of non-dip-coating fabrication of the fiber/foam catalysts for energy and environmental catalysis, and the production of fine chemicals. However, there is still enough room for further improvement in multi-aspects.

The first is to render more advanced methods to effectively and efficiently structure the nanocomposites onto the fiber/foam substrates. Some strategies such as the galvanic deposition and chemical etching have been applied but are still junior because the size, shape, and distribution of building blocks are hard to be controlled. Hence, more advanced methods based on the modern nanosynthesis techniques should be exigently developed to resolve these problems. Secondly, it is urgent to structure the nanocomposites with adequate resistance to sintering and coke for the ultrahigh-temperature reactions such as the catalytic oxy-methane reforming (700–800 °C) and steam methane reforming (800–1000 °C). To achieve this goal, the substrates (such as SiC-foam and SiC-fiber) should be modified to be endowed with the high-temperature stability and coke-resistance properties. Therefore, new methods need to be found to catalytically functionalize these supports via *in-situ* growth of the catalytic components. Next, the fiber/foam catalysts will find the place in other applications such as catalytic distillation for the cyclohexyl acetate production from cyclohexene and acetic acid over the structured solid-acid catalysts. Moreover, the knowledge of flow and transport phenomena as detailed as possible is needed to model the three-phase structured reactors, and their design and modeling for the three-phase processes should be intensively conducted. Fifth, other functional materials (such as metal-organic framework, ionic liquid, grapheme, and biocompatible materials)

are also welcome to be structured onto the monoliths to construct more advanced structured catalysts or biomaterials. Sixth, shape design and other features prediction of the desirable structured catalysts should be developed on the basis of computational calculations. However, it is unfortunate that there are no correlations between the key parameters (such as pressure drop and heat/mass transfer) and the different structures for catalyst design, and there should be a more intense focus on description of the hydrodynamics and transport properties. Last but not least, great challenges still exist in the applications of the fiber/foam-structured catalysts in industrial scale. The methods summarized in Table 1 possess substantial potential to prepare the fiber/foam catalysts on a large scale, but the actual experiments of their scale-up preparation are still lacking. In addition, there are also few studies of the fiber/foam catalysts involving applications at industrial scale, such as process and reactor design, stability test, deactivation mechanism, and regeneration. Moreover, the mass and heat transfer behavior in the amplified process also needs to be studied urgently. In one word, the issues involving their industrial-scale applications are in urgent need of study. Anyhow, a close collaboration among chemistry, materials, engineering, mathematics, and computer science is highly urgent in order to develop more advanced structured catalysts and materials, which might lead to improved or new-advantageous structures attractive for heterogeneous catalysis and other new fields like biomedicine.

Acknowledgments

Disclosure statement

No potential conflict of interest was reported by the author(s).

ORCID

Yong Lu ⓘ //orcid.org/0000-0002-5126-1476

References

[1] Ertl, G.; Knözinger, H.; Schüth, F.; Weitkamp, J.; Ertl, G.; Knözinger, H.; Schüth, F.; Weitkamp, J. *Handbook of Heterogeneous Catalysis*, 2nd; Weinheim: Wiley-VCH, 2008. DOI: 10.1002/9783527610044

[2] Cybulski, A.; Moulijn, J. A.; Cybulski, A.; Moulijn, J. A. *Structured Catalysts and Reactors*. Marcel Dekker (Ed.), New York, 2006. DOI: 10.1201/9781420028003

[3] Zhao, G.; Liu, Y.; Lu, Y. Foam/fiber-Structured Catalysts: Non-Dip-Coating Fabrication Strategy and Applications in Heterogeneous Catalysis. *Sci. Bull.* 2016, *61*, 745–748. DOI: 10.1007/s11434-016-1074-2.

[4] Dautzenberg, F. M.; Mukherjee, M. Process Intensification Using Multifunctional Reactors. *Chem. Eng. Sci.* 2001, *56*, 251–267. DOI: 10.1016/S0009-2509(00)00228-1.

[5] European Roadmap for Process Intensification, June 2008 (https:////www.senternovem.nl/energytransition/downloads).

[6] Westmoreland, P. R. Chemical Engineering in the Next 25 Years. *Chem. Eng. Prog.* 2008, *104*, 31–41.

[7] Science and Technology Roadmap on Catalysis for Europe, July 2016 (https:////www.euchems.eu/roadmap-on-catalysis-for-europe).

[8] Renken, A.; Kiwi-Minsker, L. Microstructured Catalytic Reactors. *Adv. Catal.* 2010, *53*, 47–122. DOI: 10.1016/S0360-0564(10)53002-5.

[9] Montebelli, A.; Visconti, C. G.; Groppi, G.; Tronconi, E.; Cristiani, C.; Ferreirac, C.; Kohlerd, S. Methods for the Catalytic Activation of Metallic Structured Substrates. *Catal. Sci. Technol.* 2014, *4*(9), 2846–2870. DOI: 10.1039/C4CY00179F.

[10] Wang, X.; Wen, M.; Wang, C.; Ding, J.; Sun, Y.; Liu, Y.; Lu, Y. Microstructured Fiber@HZSM-5 Core–Shell Catalysts with Dramatic Selectivity and Stability Improvement for the Methanol-To-Propylene Process. *Chem. Commun.* 2014, *50*(48), 6343–6345. DOI: 10.1039/C3CC49567A.

[11] Zhang, Q.; Zhao, G.; Zhang, Z.; Han, L.; Fan, S.; Chai, R.; Li, Y.; Liu, Y.; Huang, J.; Lu, Y. From Nano-To Macro-Engineering of Oxide-Encapsulated-Nanoparticles for Harsh Reactions: One-Step Organization via Cross-Linking Molecules. *Chem. Commun.* 2016, *52*(80), 11927–11930. DOI: 10.1039/C6CC05804C.

[12] Berglin, T.; Herrman, W. Cryosurgical Treatment of the Eyelids and Lacrimal Drainage Ducts of the Rhesus Monkey. *EP.* 1984, *102*(6), 934 A2. DOI: 10.1001/archopht.1984.01040030754040.

[13] Deshmukh, S. R.; Tonkovich, A. L. Y.; Jarosch, K. T.; Schrader, L.; Fitzgerald, S. P.; Kilanowski, D. R.; Lerou, J. J.; Mazanec, T. J. Scale-Up of Microchannel Reactors for Fischer–tropsch Synthesis. *Ind. Eng. Chem. Res.* 2010, *49*(21), 10883–10888. DOI: 10.1021/ie100518u.

[14] Markowz, G.; Schirrmeister, S.; Albrecht, J.; Becker, F.; Schütte, R.; Caspary, K. J.; Klemm, E. Microstructured Reactors for Heterogeneously Catalyzed Gas-Phase Reactions on an Industrial Scale. *Chem. Eng. Technol.* 2005, *28*(4), 459–464. DOI: 10.1002/ceat.200407146.

[15] Farrauto, R. J.; Voss, K. E. Monolithic Diesel Oxidation Catalysts. *Appl. Catal. B.* 1996, *10*, 29–51. DOI: 10.1016/0926-3373(96)00022-7.

[16] Heck, R. M.; Farrauto, R. J. *Catalytic Air Pollution Control: Commercial Technology*, 2nd ed.; Wiley: New York, 2002.

[17] Farrauto, R. J.; Heck, R. M. Catalytic Converters: State of the Art and Perspectives. *Catal. Today.* 1999, *51*(3–4), 351–360. DOI: 10.1016/S0920-5861(99)00024-3.

[18] König, A.; Herding, G.; Hupfeld, B.; Richter, T.; Weidmann, K. Current Tasks and Challenges for Exhaust Aftertreatment Research. A Viewpoint from the Automotive Industry. *Top. Catal.* 2001, *16*(1/4), 23–31. DOI: 10.1023/A:1016666327542.

[19] Kašpar, J.; Fornasiero, P.; Hickey, N. Automotive Catalytic Converters: Current Status and Some Perspectives. *Catal. Today.* 2003, *77*(4), 419–449. DOI: 10.1016/S0920-5861(02)00384-X.

[20] Cybulski, A.; Moulijn, J. A. Monoliths in Heterogeneous Catalysis. *Catal. Rev. Sci. Eng.* 1994, *36*, 179–270. DOI: 10.1080/01614949408013925.

[21] Nijhuis, T. A.; Kreutzer, M. T.; Romijn, A. C. J.; Kapteijn, F.; Moulijn, J. A. Monolithic Catalysts as Efficient Three-Phase Reactors. *Chem. Eng. Sci.* 2001, *56*, 823–829. DOI: 10.1016/S0009-2509(00)00294-3.

[22] Nijhuis, T. A.; Kreutzer, M. T.; Romijn, A. C. J.; Kapteijn, F.; Moulijn, J. A. Monolithic Catalysts as More Efficient Three-Phase Reactors. *Catal. Today.* 2001, *66*(2–4), 157–165. DOI: 10.1016/S0920-5861(00)00621-0.

[23] Banhart, J. Manufacture Characterization and Application of Cellular Metals and Metal Foams. *Prog. Mater. Sci.* 2001, *46*(6), 559–632. DOI: 10.1016/S0079-6425(00)00002-5.

[24] Richardson, J. T.; Remue, D.; Hung, J.-K. Properties of Ceramic Foam Catalyst Supports: Mass and Heat Transfer. *Appl. Catal. A.* 2003, *250*, 319–329. DOI: 10.1016/S0926-860X(03)00287-4.

[25] Giani, L.; Groppi, G.; Tronconi, E. Heat Transfer Characterization of Metallic Foams. *Ind. Eng. Chem. Res.* 2005, *44*(24), 9078–9085. DOI: 10.1021/ie050598p.

[26] Harris, D. K.; Cahela, D. R.; Tatarchuk, B. J. Wet Layup and Sintering of Metal Containing Microfibrous Composites for Chemical Processing Opportunities. *Compos. A.* 2001, *32*(8), 1117–1126. DOI: 10.1016/S1359-835X(01)00059-8.

[27] Lu, Y.; Wang, H.; Liu, Y.; Xue, Q.; Chen, L.; He, M. Novel Microfibrous Composite Bed Reactor: High Efficiency H_2 Production from NH_3 with Potential for Portable Fuel Cell Power Supplies. *Lab. Chip.* 2007, *7*(1), 133–140. DOI: 10.1039/B608555E.

[28] Zhang, H.; Gao, L.; Hu, X. Preparation of Microfibrous Entrapped Activated Carbon Composite. *Sep. Purif. Technol.* 2009, *67*, 149–151. DOI: 10.1016/j.seppur.2009.03.023.

[29] Sonstrom, P.; Adam, M.; Wang, X.; Wilhelm, M.; Grathwohl, G.; Baumer, M. Colloidal Nanoparticles Embedded in Ceramers: Toward Structurally Designed Catalysts. *J. Phys. Chem. C.* 2010, *114*(33), 14224–14232. DOI: 10.1021/jp1058897.

[30] Tomašić, V.; Jović, F. State-Of-The-Art in the Monolithic Catalysts/Reactors. *Appl. Catal. A.* 2006, *311*, 112–121. DOI: 10.1016/j.apcata.2006.06.013.

[31] Wen, M.; Ding, J.; Wang, C.; Li, Y.; Zhao, G.; Liu, Y.; Lu, Y. High-Performance SS-Fiber@ HZSM-5 Core-Shell Catalyst for Methanol-To-Propylene: A Kinetic and Modeling Study. *Micropor. Mesopor. Mater.* 2016, *221*, 187–196. DOI: 10.1016/j.micromeso.2015.09.039.

[32] Irandoust, S.; Andersson, B. Monolithic Catalysts for Nonautomobile Applications. *Catal. Rev. - Sci. Eng.* 1988, *30*(3), 341–392. DOI: 10.1080/01614948808080809.

[33] Murkin, C.; Brightling, J. Eighty Years of Steam Reforming. *Johnson Matthey Technol. Rev.* 2016, *60*(4), 263–269. DOI: 10.1595/205651316X692923.

[34] Albers, R. E.; Nyström, M.; Siverström, M.; Sellin, A.; Dellve, A.-C.; Andersson, U.; Herrmann, W.; Berglin, T. Development of a Monolith-Based Process for H_2O_2 Production: From Idea to Large-Scale Implementation. *Catal. Today.* 2001, *69*(1–4), 247–252. DOI: 10.1016/S0920-5861(01)00376-5.

[35] Ishii, T.; Mitsui, K.; Sano, K.; Shishida, K.; Shiota, Y. Catalyst for Treating Wastewater, Process for Producing It, and Process for Treating Wastewater with the Catalyst, U.S. Patent 5 374 599, 1994.

[36] Deng, T.; Li, Y.; Zhao, G.; Zhang, Z.; Liu, Y.; Lu, Y. Catalytic Distillation for Ethyl Acetate Synthesis Using Microfibrous-Structured Nafion–SiO$_2$/SS-Fiber Solid Acid Packings. *Reaction Chem. Eng.* 2016, *1*(4), 409–417. DOI: 10.1039/C6RE00088F.

[37] Heck, R. M.; Gulati, S.; Farrauto, R. J. The Application of Monoliths for Gas Phase Catalytic Reactions. *Chem. Eng. J.* 2001, *82*, 149–156. DOI: 10.1016/S1385-8947(00) 00365-X.

[38] Patcas, F. C.; Garrido, G. I.; Kraushaar-Czarnetzki, B. CO Oxidation Over Structured Carriers: A Comparison of Ceramic Foams, Honeycombs and Beads. *Chem. Eng. Sci.* 2007, *62*, 3984–3990. DOI: 10.1016/j.ces.2007.04.039.

[39] Reichelt, E.; Jahn, M. Generalized Correlations for Mass Transfer and Pressure Drop in Fiber-Based Catalyst Supports. *Chem. Eng. J.* 2017, *325*, 655–664. DOI: 10.1016/j.cej. 2017.05.119.

[40] Aghaei, P.; Visconti, C. G.; Groppi, G.; Tronconi, E. Development of a Heat Transport Model for Open-Cell Metal Foams with High Cell Densities. *Chem. Eng. J.* 2017, *321*, 432–446. DOI: 10.1016/j.cej.2017.03.112.

[41] Yang, K. S.; Mul, G.; Choi, J. S.; Moulijn, J. A.; Chung, J. S. Development of TiO$_2$/Ti Wire-Mesh Honeycomb for Catalytic Combustion of Ethyl Acetate in Air. *Appl. Catal. A.* 2006, *313*, 86–93. DOI: 10.1016/j.apcata.2006.07.008.

[42] Matatov-Meytal, Y.; Sheintuch, M. Catalytic Fibers and Cloths. *Appl. Catal. A.* 2002, *231*, 1–16. DOI: 10.1016/S0926-860X(01)00963-2.

[43] Twigg, M. V.; Richardson, J. T. Fundamentals and Applications of Structured Ceramic Foam Catalysts. *Ind. Eng. Chem. Res.* 2007, *46*(12), 4166–4177. DOI: 10.1021/ie061122o.

[44] Kryca, J.; Iwaniszyn, M.; Piątek, M.; Jodłowski, P. J.; Jędrzejczyk, R.; Pędrys, R.; Wróbel, A.; Łojewska, J.; Kołodziej, A. Structured Foam Reactor with CuSSZ-13 Catalyst for SCR of NO$_x$ with Ammonia. *Top. Catal.* 2016, *59*(10–12), 887–894. DOI: 10.1007/s11244-016-0564-4.

[45] Heddrich, M. P.; Reichelt, M.; Jahn, E.; Michaelis, A. Fiber Based Structured Materials for Catalytic Applications. *Appl. Catal. A.* 2014, *476*, 78–90. DOI: 10.1016/j.apcata.2014. 02.021.

[46] Groppi, G.; Tronconi, E.; Bozzano, G.; Dente, M. Experimental and Theoretical Study of Gas/Solid Mass Transfer in Metallic Filters as Supports for Micro-Structured Catalysts. *Chem. Eng. Sci.* 2010, *65*, 392–397. DOI: 10.1016/j.ces.2009.06.038.

[47] Huu, T. T.; Lacroix, M.; Huu, C. P.; Schweich, D.; Edouard, D. Towards a More Realistic Modeling of Solid Foam: Use of the Pentagonal Dodecahedron Geometry. *Chem. Eng. Sci.* 2009, *64*, 5131–5142. DOI: 10.1016/j.ces.2009.08.028.

[48] Inayat, A.; Freund, H.; Zeiser, T.; Schwieger, W. Determining the Specific Surface Area of Ceramic Foams: The Tetrakaidecahedra Model Revisited. *Chem. Eng. Sci.* 2011, *66*, 1179–1188. DOI: 10.1016/j.ces.2010.12.031.

[49] Lu, T.; Stone, H.; Ashby, M. Heat Transfer in Open-Cell Metal Foams. *Acta. Mater.* 1998, *46*, 3619–3635. DOI: 10.1016/S1359-6454(98)00031-7.

[50] Gibson, L. J.; Ashby, M. F. *Cellular Solids, Structures and Properties*; Pergamon Press: Oxford, 1988; pp. 915–925.

[51] Garrido, G. I.; Patcas, F. C.; Lang, S.; Kraushaar-Czarnetzki, B. Mass Transfer and Pressure Drop in Ceramic Foams: A Description for Different Pore Sizes and Porosities. *Chem. Eng. Sci.* 2008, *63*, 5202–5217. DOI: 10.1016/j.ces.2008.06.015.

[52] Bracconi, M.; Ambrosetti, M.; Maestri, M.; Groppi, G.; Tronconi, E. A Fundamental Investigation of Gas/Solid Mass Transfer in Open-Cell Foams Using a Combined Experimental and CFD Approach. *Chem. Eng. J.* 2018, *352*, 558–571. DOI: 10.1016/j. cej.2018.07.023.

[53] Kölbel, H.; Ralek, M. The Fischer-Tropsch Synthesis in the Liquid Phase. *Catal. Rev. - Sci. Eng.* 1980, *21*(2), 255–274. DOI: 10.1080/03602458008067534.

[54] Sie, S. T.; Krishna, R. Fundamentals and Selection of Advanced Fischer–Tropsch Reactors. *Appl. Catal. A.* 1999, *186*(1–2), 55–70. DOI: 10.1016/S0926-860X(99)00164-7.

[55] Davis, B. H. Fischer–Tropsch Synthesis: Overview of Reactor Development and Future Potentialities. *Top. Catal.* 2005, *32*(3–4), 143–168. DOI: 10.1007/s11244-005-2886-5.

[56] Groppi, G.; Tronconi, E. Design of Novel Monolith Catalyst Supports for Gas/Solid Reactions with Heat Exchange. *Chem. Eng. Sci.* 2000, *55*, 2161–2171. DOI: 10.1016/S0009-2509(99)00440-6.

[57] Boger, T.; Heibel, A. K.; Sorensen, C. M. Monolithic Catalysts for the Chemical Industry. *Ind. Eng. Chem. Res.* 2004, *43*(16), 4602–4611. DOI: 10.1021/ie030730q.

[58] Sheng, M.; Yang, H.; Cahela, D. R.; Tatarchuk, B. J. Novel Catalyst Structures with Enhanced Heat Transfer Characteristics. *J. Catal.* 2011, *281*, 254–262. DOI: 10.1016/j.jcat.2011.05.006.

[59] Chen, W.; Sheng, W.; Cao, F.; Lu, Y. Microfibrous Entrapment of Ni/Al_2O_3 for Dry Reforming of Methane: Heat/Mass Transfer Enhancement Towards Carbon Resistance and Conversion Promotion. *Ind. Eng. Chem. Res.* 2012, *37*, 18021–18030. DOI: 10.1016/j.ijhydene.2012.09.080.

[60] Li, Y.; Zhang, Q.; Chai, R.; Zhao, G.; Liu, Y.; Lu, Y.; Cao, F. Ni-Al 2 O 3 /ni-Foam Catalyst with Enhanced Heat Transfer for Hydrogenation of CO 2 to Methane. *AIChE. J.* 2015, *61* (12), 4323–4331. DOI: 10.1002/aic.14935.

[61] Sheng, M.; Cahela, D. R.; Yang, H.; Gonzalez, C. F.; Yantz, W. R., Jr; Harris, D. K.; Tatarchuk, B. J. Effective Thermal Conductivity and Junction Factor for Sintered Microfibrous Materials. *Int. J. Heat Mass Tran.* 2013, *56*(1–2), 10–19. DOI: 10.1016/j.ijheatmasstransfer.2012.08.015.

[62] Lee, J.-S.; Yano, T. Fabrication of Short-Fiber-Reinforced SiC Composites by Polycarbosilane Infiltration. *J. Eur. Ceram. Soc.* 2004, *24*, 25–31. DOI: 10.1016/S0955-2219(03)00125-0.

[63] Dul'nev, G.; Muratova, B. Thermal Conductivity of Fibrous Systems. *J. Eng. Thermophys.* 1968, *14*(1), 29–35. DOI: 10.1007/BF00826965.

[64] Mantle, W. J.; Chang, W. S. Effective Thermal Conductivity of Sintered Metal Fibers. In *Proceedings of the 24th Intersociety Energy Conversion Engineering Conference.* Washington: IEEE. 1989; pp. 1871–1877. DOI: 10.1109/IECEC.1989.74727.

[65] Chung, K.-S.; Jiang, Z.; Gill, B.-S.; Chung, J.-S. Oxidative Decomposition of O Dichlorobenzene Over V_2O_5/TiO_2 Catalyst Washcoated Onto Wire-Mesh Honeycombs. *Appl. Catal. A.* 2002, *237*(1–2), 81–89. DOI: 10.1016/S0926-860X(02)00303-4.

[66] Ahlström-Silversand, A.; Odenbrand, C. I. Thermally Sprayed Wire-Mesh Catalysts for the Purification of Flue Gases from Small-Scale Combustion of Bio-Fuel Catalyst Preparation and Activity Studies. *Appl. Catal. A.* 1997, *153*(1–2), 177–201. DOI: 10.1016/S0926-860X(96)00329-8.

[67] Ahlström-Silversand, A. F.; Odenbrand, C. U. I. Modelling Catalytic Combustion of Carbon Monoxide and Hydrocarbons Over Catalytically Active Wire Meshes. *Chem. Eng. J.* 1999, *73*, 205–216. DOI: 10.1016/S1385-8947(99)00029-7.

[68] Meille, V.; Pallier, S.; Bustamante, G. V. S. C.; Roumanie, M.; Reymond, J.-P. Deposition of γ-Al_2O_3 Layers on Structured Supports for the Design of New Catalytic Reactors. *Appl. Catal. A.* 2005, *286*(2), 232–238. DOI: 10.1016/j.apcata.2005.03.028.

[69] Specchia, S.; Ahumada Irribarra, M. A.; Palmisano, P.; Saracco, G.; Specchia, V. Aging of Premixed Metal Fiber Burners for Natural Gas Combustion Catalyzed with Pd/LaMno 3 ·2zro 2. *Ind. Eng. Chem. Res.* 2007, *46*(21), 6666–6673. DOI: 10.1021/ie061665y.

[70] Ugues, D.; Specchia, S.; Saracco, G. Optimal Microstructural Design of a Catalytic Premixed FeCralloy Fiber Burner for Methane Combustion. *Ind. Eng. Chem. Res.* 2004, *43*(9), 1990–1998. DOI: 10.1021/ie034202q.

[71] Civera, A.; Negro, G.; Specchia, S.; Saracco, G.; Specchia, V. Optimal Compositional and Structural Design of a LaMnO$_3$/ZrO$_2$/Pd-Based Catalyst for Methane Combustion. *Catal. Today.* 2005, *100*(3–4), 275–281. DOI: 10.1016/j.cattod.2004.09.062.

[72] Vorob'eva, M.; Greish, A.; Ivanov, A.; Kustov, L. Preparation of Catalyst Carriers on the Basis of Alumina Supported on Metallic Gauzes. *Appl. Catal. A.* 2000, *199*, 257–261. DOI: 10.1016/S0926-860X(99)00563-3.

[73] Sun, H.; Quan, X.; Chen, S.; Zhao, H.; Zhao, Y. Preparation of Well-Adhered γ-Al$_2$O$_3$ Washcoat on Metallic Wire Mesh Monoliths by Electrophoretic Deposition. *Appl. Surf. Sci.* 2007, *253*, 3303–3310. DOI: 10.1016/j.apsusc.2006.07.044.

[74] Sun, H.; Shu, Y.; Quan, X.; Chen, S.; Pang, B.; Liu, Z. Experimental and Modeling Study of Selective Catalytic Reduction of NO$_x$ with NH$_3$ Over Wire Mesh Honeycomb Catalysts. *Chem. Eng. J.* 2010, *165*, 769–775. DOI: 10.1016/j.cej.2010.09.057.

[75] Shu, Y.; Sun, H.; Quan, X.; Chen, S. Improvement of Water-, Sulfur Dioxide-, and Dust-Resistance in Selective Catalytic Reduction of NO$_x$ with NH$_3$ Using a Wire-Mesh Honeycomb Catalyst. *Ind. Eng. Chem. Res.* 2012, *51*(23), 7867–7873. DOI: 10.1021/ie300832d.

[76] Jiang, Z.; Chung, K.-S.; Kim, G.-R.; Chung, J.-S. Mass Transfer Characteristics of Wire-Mesh Honeycomb Reactors. *Chem. Eng. Sci.* 2003, *58*, 1103–1111. DOI: 10.1016/S0009-2509(02)00546-8.

[77] Zhao, G.; Huang, J.; Jiang, Z.; Zhang, S.; Chen, L.; Lu, Y. Microstructured Au/Ni Fiber Catalyst for Low-Temperature Gas-Phase Alcohol Oxidation: Evidence of Ni$_2$O$_3$-Au$^+$ Hybrid Active Sites. *Appl. Catal. B.* 2013, *140-141*, 249–247. DOI: 10.1016/j.apcatb.2013.04.015.

[78] Zhao, G.; Hu, H.; Deng, M.; Ling, M.; Lu, Y. Au/cu-Fiber Catalyst with Enhanced Low-Temperature Activity and Heat Transfer for the Gas-Phase Oxidation of Alcohols. *Green. Chem.* 2011, *13*(1), 55–58. DOI: 10.1039/C0GC00679C.

[79] Deng, M.; Zhao, G.; Xue, Q.; Chen, L.; Lu, Y. Microfibrous-Structured Silver Catalyst for Low-Temperature Gas-Phase Selective Oxidation of Benzyl Alcohol. *Appl. Catal. B.* 2010, *99*, 222–228. DOI: 10.1016/j.apcatb.2010.06.023.

[80] Zhang, Q.; Wu, X.-P.; Zhao, G.; Li, Y.; Wang, C.; Liu, Y.; Gong, X.-Q.; Lu, Y. High Performance PdNi Alloy Structured in situ on Monolithic Metal Foam for Coalbed Methane Deoxygenation via Catalytic Combustion. *Chem. Commun.* 2015, *51*(63), 12613–12616. DOI: 10.1039/C5CC04389A.

[81] Li, Y.; Zhang, Q.; Chai, R.; Zhao, G.; Liu, Y.; Lu, Y. Structured Ni-CeO 2 -Al 2 O 3 /ni-Foam Catalyst with Enhanced Heat Transfer for Substitute Natural Gas Production by Syngas Methanation. *ChemCatchem.* 2015, *7*(9), 1427–1431. DOI: 10.1002/cctc.201500086.

[82] Chai, R.; Li, Y.; Zhang, Q.; Zhao, G.; Liu, Y.; Lu, Y. Monolithic Ni-MO$_x$/Ni-Foam (M = Al, Zr or Y) Catalysts with Enhanced Heat/Mass Transfer for Energy-Efficient Catalytic Oxy-Methane Reforming. *Catal. Commun.* 2015, *70*, 1–5. DOI: 10.1016/j.catcom.2015.07.007.

[83] Ding, J.; Fan, S.; Chen, P.; Deng, T.; Liu, Y.; Lu, Y. Vapor-Phase Transport Synthesis of Microfibrous-Structured SS-Fiber@ ZSM-5 Catalyst with Improved Selectivity and Stability for Methanol-To-Propylene. *Catal. Sci. Technol.* 2017, *7*(10), 2087–2100. DOI: 10.1039/C7CY00283A.

[84] Persson, A.; Schoeman, B.; Sterte, J.; Otterstedt, J.-E. The Synthesis of Discrete Colloidal Particles of TPA-Silicalite-1. *Zeolites*. 1994, *14*(7), 557–567. DOI: 10.1016/0144-2449(94)90191-0.

[85] Ding, J.; Zhang, Z.; Han, L.; Wang, C.; Chen, P.; Zhao, G.; Liu, Y.; Lu, Y. A Self-Supported SS-Fiber@meso-HZSM-5 Core–Shell Catalyst via Caramel-Assistant Synthesis Toward Prolonged Lifetime for the Methanol-To-Propylene Reaction. *R.S.C. Adv*. 2016, *6*(54), 48387–48395. DOI: 10.1039/C6RA08944E.

[86] Ding, J.; Jia, Y.; Chen, P.; Zhao, G.; Liu, Y.; Lu, Y. Thin-Felt Hollow-B-ZSM-5/SS-Fiber Catalyst for Methanol-To-Propylene: Toward Remarkable Stability Improvement from Mesoporosity-Dependent Diffusion Enhancement. *Chem. Eng. J*. 2019, *361*, 588–598. DOI: 10.1016/j.cej.2018.12.108.

[87] Wang, C.; Han, L.; Zhang, Q.; Li, Y.; Zhao, G.; Liu, Y.; Lu, Y. Endogenous Growth of 2D AlOoh Nanosheets on a 3D Al-Fiber Network via Steam-Only Oxidation in Application for Forming Structured Catalysts. *Green. Chem*. 2015, *17*(7), 3762–3765. DOI: 10.1039/C5GC00530B.

[88] Wang, C.; Han, L.; Chen, P.; Zhao, G.; Liu, Y.; Lu, Y. H.-P. Low Pd Loading Microfibrous-Structured Al-Fiber@ns-AlOoh@pd Catalyst for CO Coupling to Oimethyl Oxalate. *J. Catal*. 2016, *337*, 145–156. DOI: 10.1016/j.jcat.2016.02.008.

[89] Evans, D. G.; Duan, X. Preparation of Layered Double Hydroxides and Their Applications as Additives in Polymers, as Precursors to Magnetic Materials and in Biology and Medicine. *Chem. Commun*. 2006, *6*(5), 485–496. DOI: 10.1039/B510313B.

[90] He, L.; Huang, Y.; Wang, A.; Wang, X.; Chen, X.; Delgado, J. J.; Zhang, T. A Noble-Metal-Free Catalyst Derived from Ni-Al Hydrotalcite for Hydrogen Generation from N2h4·h2o Decomposition. *Angew. Chem. Int. Ed*. 2012, *51*(25), 6191–6194. DOI: 10.1002/anie.201201737.

[91] Gardner, G. P.; Go, Y. B.; Robinson, D. M.; Smith, P. F.; Hadermann, J.; Abakumov, A.; Greenblatt, M.; Dismukes, G. C. Structural Requirements in Lithium Cobalt Oxides for the Catalytic Oxidation of Water. *Angew. Chem. Int. Ed*. 2012, *51*(7), 1616–1619. DOI: 10.1002/anie.201107625.

[92] Sun, J.; Li, Y.; Liu, X.; Yang, Q.; Liu, J.; Sun, X.; Evans, D. G.; Duan, X. Hierarchical Cobalt Iron Oxide Nanoarrays as Structured Catalysts. *Chem. Commun*. 2012, *48*(28), 3379–3381. DOI: 10.1039/C2CC17368A.

[93] Chen, H.; Zhang, F.; Chen, T.; Xu, S.; Evans, D. G.; Duan, X. Comparison of the Evolution and Growth Processes of Films of M/al-Layered Double Hydroxides with M= Ni or Zn. *Chem. Eng. Sci*. 2009, *64*, 2617–2622. DOI: 10.1016/j.ces.2009.02.034.

[94] Li, C.; Zhou, J.; Gao, W.; Zhao, J.; Liu, J.; Zhao, Y.; Wei, M.; Evans, D. G.; Duan, X. Binary Cu–Co Catalysts Derived from Hydrotalcites with Excellent Activity and Recyclability Towards NH3BH3 Dehydrogenation. *J. Mater. Chem. A*. 2013, *1*(17), 5370–5376. DOI: 10.1039/C3TA10424A.

[95] Cai, S.; Zhang, D.; Shi, L.; Xu, J.; Zhang, L.; Huang, L.; Li, H.; Zhang, J. Porous Ni–Mn o_x ide Nanosheets in situ Formed on Nickel Foam as 3D Hierarchical Monolith de-NO$_x$ Catalysts. *Nanoscale*. 2014, *6*(13), 7346–7353. DOI: 10.1039/C4NR00475B.

[96] Liang, Z.; Gao, P.; Tang, Z.; Lv, M.; Sun, Y. Three Dimensional Porous Cu-Zn/al Foam Monolithic Catalyst for CO_2 Hydrogenation to Methanol in Microreactor. *J. CO2 Util*. 2017, *21*, 191–199. DOI: 10.1016/j.jcou.2017.05.023.

[97] Zhang, Z.; Zhao, G.; Chai, R.; Zhu, J.; Liu, Y.; Lu, Y. L.-T. Low-Temperature, Highly Selective, Highly Stable Nb 2 O 5 –NiO/ni-foam Catalyst for the Oxidative Dehydrogenation of Ethane. *Catal. Sci. Technol*. 2018, *8*(17), 4383–4389. DOI: 10.1039/C8CY01041B.

[98] Chen, Q.; Lei, S.; Deng, P.; Ou, X.; Chen, L.; Wang, W.; Xiao, Y.; Cheng, B. Direct Growth of Nickel Terephthalate on Ni Foam with Large Mass-Loading for High Performance Supercapacitors. *J. Mater. Chem. A.* 2017, 5(36), 19323–19332. DOI: 10.1039/C7TA05373H.

[99] Huang, M.; Li, F.; Ji, J. Y.; Zhang, Y. X.; Zhao, X. L.; Gao, X. Facile Synthesis of Single-Crystalline NiO Nanosheet Arrays on Ni Foam for High-Performance Supercapacitors. *CrystEngcomm.* 2014, 16(14), 2878–2884. DOI: 10.1039/C3CE42335B.

[100] Schärtl, W. Current Directions in Core–Shell Nanoparticle Design. *Nanoscale.* 2010, 2(6), 829–843. DOI: 10.1039/C0NR00028K.

[101] Alayoglu, S.; Nilekar, A. U.; Mavrikakis, M.; Eichhorn, B. Ru–Pt Core–Shell Nanoparticles for Preferential Oxidation of Carbon Monoxide in Hydrogen. *Nat. Mater.* 2008, 7(4), 333–338. DOI: 10.1038/nmat2156.

[102] Joo, S. H.; Park, J. Y.; Tsung, C.-K.; Yamada, Y.; Yang, P.; Somorjai, G. A. Thermally Stable Pt/Mesoporous Silica Core–Shell Nanocatalysts for High-Temperature Reactions. *Nat. Mater.* 2009, 8(2), 126–131. DOI: 10.1038/nmat2329.

[103] Cargnello, M.; Jaén, J. D.; Garrido, J. H.; Bakhmutsky, K.; Montini, T.; Gámez, J. C.; Gorte, R.; Fornasiero, P. Exceptional Activity for Methane Combustion Over Modular $Pd@CeO_2$ Subunits on Functionalized Al_2O_3. *Science.* 2012, 337(6095), 713–717. DOI: 10.1126/science.1222887.

[104] Mitsudome, T.; Yamamoto, M.; Maeno, Z.; Mizugaki, T.; Jitsukawa, K.; Kaneda, K. One-Step Synthesis of Core-Gold/shell-Ceria Nanomaterial and Its Catalysis for Highly Selective Semihydrogenation of Alkynes. *J. Am. Chem. Soc.* 2015, 137(42), 13452–13455. DOI: 10.1021/jacs.5b07521.

[105] Cargnello, M.; Wieder, N. L.; Montini, T.; Gorte, R. J.; Fornasiero, P. Synthesis of Dispersible $Pd@CeO_2$ Core–shell Nanostructures by Self-Assembly. *J. Am. Chem. Soc.* 2010, 132(4), 1402–1409. DOI: 10.1021/ja909131k.

[106] Zhou, H.; Wu, H.; Shen, J.; Yin, A.; Sun, L.; Yan, C. Thermally Stable Pt/CeO_2 Hetero-Nanocomposites with High Catalytic Activity. *J. Am. Chem. Soc.* 2010, 132(14), 4998–4999. DOI: 10.1021/ja101110m.

[107] Lu, J.; Fu, B.; Kung, M. C.; Xiao, G.; Elam, J. W.; Kung, H. H.; Stair, P. C. Coking-And Sintering-Resistant Palladium Catalysts Achieved Through Atomic Layer Deposition. *Science.* 2012, 335(6073), 1205–1208. DOI: 10.1126/science.1212906.

[108] Kim, J.; Lee, D. Synthesis and Properties of Core-Shell Metal-Ceramic Microstructures and Their Application as Heterogeneous Catalysts. *ChemCatchem.* 2014, 6(9), 2642–2647. DOI: 10.1002/cctc.201402274.

[109] Lechevallier, S.; Hammer, P.; Caiut, J. M.; Mazeres, S.; Mauricot, R.; Verelst, M.; Dexpert, H.; Ribeiro, S. J.; Dexpert-Ghys, J. APTES-Modified RE_2O_3: Eu^{3+} Luminescent Beads: Structure and Properties. *Langmuir.* 2012, 28(8), 3962–3971. DOI: 10.1021/la204469f.

[110] Tao, F.; Grass, M. E.; Zhang, Y.; Butcher, D. R.; Renzas, J. R.; Liu, Z.; Chung, J. Y.; Mun, B. S.; Salmeron, M.; Somorjai, G. A. Reaction-Driven Restructuring of Rh-Pd and Pt-Pd Core-Shell Nanoparticles. *Science.* 2008, 322(5903), 932–934. DOI: 10.1126/science.1164170.

[111] Friedrich, M.; Penner, S.; Heggen, M.; Armbrüster, M. High CO_2 Selectivity in Methanol Steam Reforming Through ZnPd/ZnO Teamwork. *Angew. Chem. Int. Ed.* 2013, 52(16), 4389–4392. DOI: 10.1002/anie.201209587.

[112] Zhang, S.; Shan, J.; Zhu, Y.; Frenkel, A. I.; Patlolla, A.; Huang, W.; Yoon, S. J.; Wang, L.; Yoshida, H.; Takeda, S. WGS Catalysis and in situ Studies of CoO_{1-x}, $PtCo_n/Co_3O_4$, and $Pt_mCo_{m'}/CoO_{1-x}$ Nanorod Catalysts. *J. Am. Chem. Soc.* 2013, 135(22), 8283–8393. DOI: 10.1021/ja401967y.

[113] Zhao, G.; Fan, S.; Tao, L.; Chai, R.; Zhang, Q.; Liu, Y.; Lu, Y. Titanium- Microfiber-Supported Binary-Oxide Nanocomposite with a Large Highly Active Interface for the Gas-Phase Selective Oxidation of Benzyl Alcohol. *ChemCatchem*. 2016, *8*(2), 313–317. DOI: 10.1002/cctc.201500991.

[114] Chen, P.; Zhao, G.; Shi, X.-R.; Zhu, J.; Ding, J.; Lu, Y. Nano-Intermetallic $InNi_3C_{0.5}$ Compound Discovered as a Superior Catalyst for CO_2 Reutilization. *iScience*. 2019, *17*, 315–324. DOI: 10.1016/j.isci.2019.07.006.

[115] Zhang, L.; Han, L.; Zhao, G.; Chai, R.; Zhang, Q.; Liu, Y.; Lu, Y. Structured Pd–Au/cu-fiber Catalyst for Gas-Phase Hydrogenolysis of Dimethyl Oxalate to Ethylene Glycol. *Chem. Commun*. 2015, *51*(52), 10547–10550. DOI: 10.1039/C5CC03009A.

[116] Ramadoss, A.; Kang, K.; Ahn, H.; Kim, S.; Ryu, S.; Jang, J. Realization of High Performance Flexible Wire Supercapacitors Based on 3-Dimensional $NiCo_2O_4$/Ni Fibers. *J. Mater. Chem. A*. 2016, *4*(13), 4718–4727. DOI: 10.1039/C5TA10781D.

[117] Zhu, J.; Zhao, G.; Sun, W.; Nie, Q.; Wang, S.; Xue, Q.; Liu, Y.; Lu, Y. Superior $FeNi_3$-FeO_x/Ni-Foam Catalyst for Gas-Phase Hydrogenation of Dimethyl Oxalate to Ethanol. *Appl. Catal. B*. 2020, *270*, 118873. DOI: 10.1016/j.apcatb.2020.118873.

[118] Feng, L.; Yu, G.; Wu, Y.; Li, G.; Li, H.; Sun, Y.; Asefa, T.; Chen, W.; Zou, X. High-Index Faceted Ni_3S_2 Nanosheet Arrays as Highly Active and Ultrastable Electrocatalysts for Water Splitting. *J. Am. Chem. Soc.* 2015, *137*(44), 14023–14026. DOI: 10.1021/jacs.5b08186.

[119] Zhu, J.; Cao, L.; Li, C.; Zhao, G.; Zhu, T.; Hu, W.; Sun, W.; Lu, Y. Nanoporous Ni_3P Evolutionarily Structured Onto a Ni Foam for Highly Selective Hydrogenation of Dimethyl Oxalate to Methyl Glycolate. *ACS Appl. Mater. Interfaces*. 2019, *11*(41), 37635–37643. DOI: 10.1021/acsami.9b11703.

[120] Yamamoto, R.; Sawayama, Y.; Shibahara, H.; Ichihashi, Y.; Nishiyama, S.; Tsuruya, S. Promoted Partial Oxidation Activity of Supported Ag Catalysts in the Gas Phase Catalytic Oxidation of Benzyl Alcohol. *J. Catal.* 2005, *234*(2), 308–317. DOI: 10.1016/j.jcat.2005.06.032.

[121] Shen, J.; Shan, W.; Zhang, Y.; Du, J.; Xu, H.; Fan, K.; Shen, W.; Tang, Y. Gas Phase Selective Oxidation of Alcohols: In situ Electrolytic Nano-Silver/zeolite Film/Copper Grid Catalyst. *J. Catal.* 2006, *237*(1), 94–101. DOI: 10.1016/j.jcat.2005.10.027.

[122] Magaev, O.; Knyazev, A.; Vodyankina, O.; Dorofeeva, N.; Salanov, A.; Boronin, A. Active Surface Formation and Catalytic Activity of Phosphorous-Promoted Electrolytic Silver in the Selective Oxidation of Ethylene Glycol to Glyoxal. *Appl. Catal. A*. 2008, *344*, 142–149. DOI: 10.1016/j.apcata.2008.04.007.

[123] Chen, M.; Goodman, D. The Structure of Catalytically Active Gold on Titania. *Science*. 2004, *306*(5694), 252–255. DOI: 10.1126/science.1102420.

[124] Min, B. K.; Friend, C. M. Heterogeneous Gold-Based Catalysis for Green Chemistry: Low-Temperature CO Oxidation and Propene Oxidation. *Chem. Rev.* 2007, *107*(6), 2709–2724. DOI: 10.1021/cr050954d.

[125] Pina, D. C.; Falletta, E.; Rossi, M. Highly Selective Oxidation of Benzyl Alcohol to Benzaldehyde Catalyzed by Bimetallic Gold–Copper Catalyst. *J. Catal.* 2008, *260*(2), 384–386. DOI: 10.1016/j.jcat.2008.10.003.

[126] Zhao, G.; Hu, H.; Deng, M.; Lu, Y. Microstructured Au/ni-Fiber Catalyst for Low-Temperature Gas-Phase Selective Oxidation of Alcohols. *Chem. Commun.* 2011, *47*(34), 9642–9644. DOI: 10.1039/C1CC12964C.

[127] Zhao, G.; Hu, H.; Chen, W.; Jiang, Z.; Zhang, S.; Huang, J.; Lu, Y. Ni 2 O 3 –Au + Hybrid Active Sites on NiO X @au Ensembles for Low-Temperature Gas-Phase Oxidation of Alcohols. *Catal. Sci. Technol.* 2013, *3*(2), 404–408. DOI: 10.1039/C2CY20579C.

[128] Zhao, G.; Fan, S.; Pan, X.; Chen, P.; Liu, Y.; Lu, Y. Reaction-Induced Self-Assembly of CoO@cu $_2$ O Nanocomposites in Situ Onto SiC-Foam for Gas-Phase Oxidation of Bioethanol to Acetaldehyde. *ChemSuschem.* 2017, *10*(7), 1380–1384. DOI: 10.1002/cssc.201601848.

[129] Tao, L.; Zhao, G.; Chen, P.; Zhang, Z.; Liu, Y.; Lu, Y. Thin-Felt Microfibrous Structured Au-α-Fe$_2$O$_3$/ns-γ-Al$_2$O$_3$/Al-Fiber Catalyst for High-Throughput CO Oxidation. *Appl. Catal. A.* 2018, *556*, 180–190. DOI: 10.1016/j.apcata.2018.03.003.

[130] Sirijaruphan, A.; Goodwin, J. G., Jr; Rice, R. W.; Wei, D.; Butcher, K. R.; Roberts, G. W.; Spivey, J. J. Metal Foam Supported Pt Catalysts for the Selective Oxidation of CO in Hydrogen. *Appl. Catal. A.* 2005, *281*, 1–9. DOI: 10.1016/j.apcata.2004.10.019.

[131] Wei, Y.; Gao, Y.; Xu, X.; Si, J.; Sun, W.; Zhao, G.; Liu, Y.; Lu, Y. High Jolt-Resistance Monolithic CuO–CeO$_2$/AlOOH/Al-fiber Catalyst for CO-PROX: Influence of AlOoh/al-Fiber Calcination on Cu–Ce Interaction. *Int. J. Hydrogen. Energy.* 2022, *47*(26), 13030–13043. DOI: 10.1016/j.ijhydene.2022.02.068.

[132] Driscoll, D. J.; Martir, W.; Wang, J. X.; Lunsford, J. H. Formation of Gas-Phase Methyl Radicals Over Magnesium Oxide. *J. Am. Chem. Soc.* 1985, *107*(1), 58–63. DOI: 10.1021/ja00287a011.

[133] Fang, X.; Li, S.; Lin, J.; Gu, J.; Yang, D. Preparation and Characterization of Catalyst for Oxidative Coupling of Methane. *J. Mol. Catal. (China).* 1992, *6*, 254–262.

[134] Wang, P.; Zhao, G.; Wang, Y.; Lu, Y. MnTiO$_3$-Driven Low-Temperature Oxidative Coupling of Methane Over TiO$_2$-Doped Mn$_2$O$_3$-Na$_2$WO$_4$/SiO$_2$ Catalyst. *Sci. Adv.* 2017, *3*(6), e1603180. DOI: 10.1126/sciadv.1603180.

[135] Liu, H.; Yang, D.; Gao, R.; Long, C.; Zhang, S.; Wang, X. A Novel Na2WO4–Mn/sic Monolithic Foam Catalyst with Improved Thermal Properties for the Oxidative Coupling of Methane. *Catal. Commun.* 2008, *9*(6), 1302–1306. DOI: 10.1016/j.catcom.2007.11.022.

[136] Wang, W.; Zhang, Z.; Ji, S. Particle/metal-Based Monolithic Catalysts Dual Bed Reactor with Beds-Interspace Supplementary Oxygen: Construction and Performance for Oxidative Coupling of Methane. *J. Nat. Gas. Chem.* 2012, *21*(4), 400–406. DOI: 10.1016/S1003-9953(11)60382-4.

[137] Liu, J.; Zhao, G.; Si, J.; Sun, W.; Liu, Y.; Lu, Y. Binder-Free Dip-Coating of Mn$_2$O$_3$-Na$_2$WO$_4$-TiO$_2$ Catalyst Onto Monolithic SiC-Foam Towards Efficient Oxidative Coupling of Methane. *Fuel.* 2021, *305*, 121560. DOI: 10.1016/j.fuel.2021.121560.

[138] Zhao, G.; Liu, J.; Si, J.; Ni, J.; Sun, W.; Liu, Y.; Lu, Y. Self-Structured Monolithic TiO$_2$-Mn$_2$O$_3$-Na$_2$WO$_4$-Foam Catalyst Towards Efficient Oxidative Coupling of Methane. *Fuel.* 2022, *327*, 125193. DOI: 10.1016/j.fuel.2022.125193.

[139] Heynderickx, G.; Schools, E.; Marin, G. Coke Combustion and Gasification Kinetics in Ethane Steam Crackers. *AIChE. J.* 2005, *51*(5), 1415–1428. DOI: 10.1002/aic.10401.

[140] Nieto, J. L.; Botella, P.; Vázquez, M.; Dejoz, A. The Selective Oxidative Dehydrogenation of Ethane Over Hydrothermally Synthesised MoVtenb Catalysts. *Chem. Commun.* 2002. 17, 1906–1907. DOI: 10.1039/B204037A.

[141] Zhu, H.; Ould-Chikh, S.; Anjum, D. H.; Sun, M.; Biausque, G.; Basset, J. M.; Caps, V. Nb Effect in the Nickel Oxide-Catalyzed Low-Temperature Oxidative Dehydrogenation of Ethane. *J. Catal.* 2012, *285*, 292–303. DOI: 10.1016/j.jcat.2011.10.005.

[142] Shi, X.; Ji, S.; Wang, K.; Li, C. Oxidative Dehydrogenation of Ethane with CO$_2$ Over Novel Cr/SBA-15/Al$_2$O$_3$/FeCrAl Monolithic Catalysts. *Energy. Fuels.* 2008, *22*(6), 3631–3638. DOI: 10.1021/ef800567v.

[143] Zhang, Z.; Zhao, G.; Sun, W.; Liu, Y.; Lu, Y. Oxidative Dehydrogenation of Ethane: Superior Nb$_2$O$_5$-NiO/Ni-Foam Catalyst Tailored by Tuning Morphology of NiO-Precursors Grown on a Ni-Foam. *iScience.* 2019, *20*, 90–99. DOI: 10.1016/j.isci.2019.09.021.

[144] Olah, G. A.; Geoppert, A.; Prakash, G. K. S. *Beyond Oil and Gas: The Methanol Economy.* Weinheim; Wiley-VCH: Germany, 2006.

[145] Zhang, X.; Zhu, X.; Lin, L.; Yao, S.; Zhang, M.; Liu, X.; Wang, X.; Li, Y.; Shi, C.; Ma, D. Highly Dispersed Copper Over β-Mo$_2$C as an Efficient and Stable Catalyst for the Reverse Water Gas Shift (RWGS) Reaction. *ACS. Catal.* 2017, *7*(1), 912–918. DOI: 10.1021/acscatal.6b02991.

[146] Jiang, X.; Nie, X.; Guo, X.; Song, C.; Chen, J. G. Recent Advances in Carbon Dioxide Hydrogenation to Methanol via Heterogeneous Catalysis. *Chem. Rev.* 2020, *120*(15), 7984–8034. DOI: 10.1021/acs.chemrev.9b00723.

[147] Wang, J.; Li, G.; Li, Z.; Tang, C.; Feng, Z.; An, H.; Liu, H.; Liu, T.; Li, C. A Highly Selective and Stable ZnO-ZrO$_2$ Solid Solution Catalyst for CO$_2$ Hydrogenation to Methanol. *Sci. Adv.* 2017, *3*(10), e1701290. DOI: 10.1126/sciadv.1701290.

[148] Studt, F.; Sharafutdinov, I.; Abild-Pedersen, F.; Elkjær, C. F.; Hummelshøj, J. S.; Dahl, S.; Chorkendorff, I.; Nørskov, J. K. Discovery of a Ni-Ga Catalyst for Carbon Dioxide Reduction to Methanol. *Nat. Chem.* 2014, *6*(4), 320–324. DOI: 10.1038/nchem.1873.

[149] Meng, C.; Zhao, G.; Shi, X.; Chen, P.; Liu, Y.; Lu, Y. Oxygen-Deficient Metal Oxides Supported Nano-Intermetallic InNi$_3$C$_{0.5}$ Toward Efficient CO$_2$ Hydrogenation to Methanol. *Sci. Adv.* 2021, *7*(32), eabi6012. DOI: 10.1126/sciadv.abi6012.

[150] Meng, C.; Zhao, G.; Shi, X.; Nie, Q.; Liu, Y.; Lu, Y. Electronic Modulation of InNi$_3$C$_{0.5}$ /Fe$_3$O$_4$ by Support Precursor Toward Efficient CO$_2$ Hydrogenation to Methanol. *Appl. Catal. B.* 2022, *316*, 121699. DOI: 10.1016/j.apcatb.2022.121699.

[151] Chen, P.; Zhao, G.; Liu, Y.; Lu, Y. Monolithic Ni$_5$Ga$_3$/SiO$_2$/Al$_2$O$_3$/Al-Fiber Catalyst for CO$_2$ Hydrogenation to Methanol at Ambient Pressure. *Appl. Catal. A.* 2018, *562*, 234–240. DOI: 10.1016/j.apcata.2018.06.021.

[152] Chen, L. F.; Guo, P. J.; Qiao, M. H.; Yan, S. R.; Li, H. X.; Shen, W.; Xu, H. L.; Fan, K. N. Cu/SiO$_2$ Catalysts Prepared by the Ammonia-Evaporation Method: Texture, Structure, and Catalytic Performance in Hydrogenation of Dimethyl Oxalate to Ethylene Glycol. *J. Catal.* 2008, *257*, 172–180. DOI: 10.1016/j.jcat.2008.04.021.

[153] Gong, J.; Yue, H.; Zhao, Y.; Zhao, S.; Zhao, L.; Lv, J.; Wang, S.; Ma, X. Synthesis of Ethanol via Syngas on Cu/SiO 2 Catalysts with Balanced Cu 0 –Cu + Sites. *J. Am. Chem. Soc.* 2012, *134*(34), 13922–13925. DOI: 10.1021/ja3034153.

[154] Zhu, J.; Zhao, G.; Meng, C.; Chen, P.; Shi, X.; Lu, Y. Superb Ni-Foam Structured Nano-Intermetallic InNi$_3$C$_{0.5}$ Catalyst for Hydrogenation of Dimethyl Oxalate to Ethylene Glycol. *Chem. Eng. J.* 2021, *426*, 130857. DOI: 10.1016/j.cej.2021.130857.

[155] Chen, Y.; Han, L.; Zhu, J.; Chen, P.; Fan, S.; Zhao, G.; Liu, Y.; Lu, Y. High Performance Ag-CuO$_x$ Nanocomposite Catalyst Galvanically Deposited Onto a Ni Foam for Gas-Phase Dimethyl Oxalate Hydrogenation to Methyl Glycolate. *Catal. Commun.* 2017, *96*, 58–62. DOI: 10.1016/j.catcom.2017.04.001.

[156] Wen, C.; Cui, Y.; Chen, X.; Zong, B.; Dai, W. Reaction Temperature Controlled Selective Hydrogenation of Dimethyl Oxalate to Methyl Glycolate and Ethylene Glycol Over Copper-Hydroxyapatite Catalysts. *Appl. Catal. B.* 2015, *162*, 483–493. DOI: 10.1016/j. apcatb.2014.07.023.

[157] Yin, A.; Guo, X.; Dai, W.; Fan, K. High Activity and Selectivity of Ag/SiO$_2$ Catalyst for Hydrogenation of Dimethyl Oxalate. *Chem. Commun.* 2010, *46*(24), 4348–4350. DOI: 10.1039/C0CC00581A.

[158] Zhu, Y.; Kong, X.; Zhu, S.; Dong, F.; Zheng, H.; Zhu, Y.; Li, Y. Construction of Cu/ZrO$_2$ /Al$_2$O$_3$ Composites for Ethanol Synthesis: Synergies of Ternary Sites for Cascade Reaction. *Appl. Catal. B.* 2015, *166-167*, 551–559. DOI: 10.1016/j.apcatb.2014.12.015.

[159] Zhao, S.; Yue, H.; Zhao, Y.; Wang, B.; Geng, Y.; Lv, J.; Wang, S.; Gong, J.; Ma, X. Chemoselective Synthesis of Ethanol via Hydrogenation of Dimethyl Oxalate on

Cu/SiO$_2$: Enhanced Stability with Boron Dopant. *J. Catal.* 2013, *297*, 142–150. DOI: 10.1016/j.jcat.2012.10.004.

[160] Yue, H.; Zhao, Y.; Zhao, L.; Lv, J.; Wang, S.; Gong, J.; Ma, X. Hydrogenation of Dimethyl Oxalate to Ethylene Glycol on a Cu/SiO$_2$/Cordierite Monolithic Catalyst: Enhanced Internal Mass Transfer and Stability. *AIChE. J.* 2012, *58*(9), 2798–2809. DOI: 10.1002/aic.12785.

[161] Ravanchi, M. T.; Sahebdelfar, S.; Komeili, S. Acetylene Selective Hydrogenation: A Technical Review on Catalytic Aspects. *Rev. Chem. Eng.* 2018, *34*(2), 215–237. DOI: 10.1515/revce-2016-0036.

[162] Kruppe, C. M.; Krooswyk, J. D.; Trenary, M. Selective Hydrogenation of Acetylene to Ethylene in the Presence of a Carbonaceous Surface Layer on a Pd/Cu(111) Single-Atom Alloy. *ACS. Catal.* 2017, *7*(12), 8042–8049. DOI: 10.1021/acscatal.7b02862.

[163] Zhou, H.; Yang, X.; Li, L.; Liu, X.; Huang, Y.; Pan, X.; Wang, A.; Li, J.; Zhang, T. PdZn Intermetallic Nanostructure with Pd–Zn–Pd Ensembles for Highly Active and Chemoselective Semi-Hydrogenation of Acetylene. *ACS. Catal.* 2016, *6*(2), 1054–1061. DOI: 10.1021/acscatal.5b01933.

[164] Wang, S.; Zhu, J.; Si, J.; Zhao, G.; Liu, Y.; Lu, Y. High-Performance Pd/Brass Fiber Catalyst for Selective Hydrogenation of Acetylene: Effect of Calcination-Assisted Endogenous Growth of ZnO-CuO$_x$ on Brass-Fiber. *J. Catal.* 2020, *382*, 295–304. DOI: 10.1016/j.jcat.2019.12.027.

[165] Wang, S.; Zhao, G.; Liu, Y.; Lu, Y. Microfibrous-Structured Pd/AlOoh/Al Fiber with Hydroxyl-Enriched Surfaces for the Catalytic Semihydrogenation of Acetylene. *Ind. Eng. Chem. Res.* 2019, *58*(36), 16431–16441. DOI: 10.1021/acs.iecr.9b02784.

[166] Rostrup-Nielsen, J. R.; Sehested, J.; Nørskov, J. K. Hydrogen and Synthesis Gas by Steam-And CO$_2$ Reforming. *Adv. Catal.* 2002, *47*, 65–139. DOI: 10.1016/S0360-0564(02)47006-X.

[167] Koo, K. Y.; Eom, H. J.; Jung, U. H.; Yoon, W. L. Ni Nanosheet-Coated Monolith Catalyst with High Performance for Hydrogen Production via Natural Gas Steam Reforming. *Appl. Catal. A.* 2016, *525*, 103–109. DOI: 10.1016/j.apcata.2016.07.016.

[168] Cristiani, C.; Finocchio, E.; Latorrata, S.; Visconti, C. G.; Bianchi, E.; Tronconi, E.; Groppi, G.; Pollesel, P. Activation of Metallic Open-Cell Foams via Washcoat Deposition of Ni/MgAl$_2$O$_4$ Catalysts for Steam Reforming Reaction. *Catal. Today.* 2012, *197*(1), 256–264. DOI: 10.1016/j.cattod.2012.09.003.

[169] De Miguel, N.; Manzanedo, J.; Thormann, J.; Pfeifer, P.; Arias, P. L. Ni Catalyst Coating on Fecralloy Â® Microchanneled Foils and Testing for Methane Steam Reforming. *Chem. Eng. Technol.* 2010, *33*(1), 155–166. DOI: 10.1002/ceat.200900439.

[170] Ryu, J.; Lee, K.; La, H.; Kim, H.; Yang, J.; Jung, H. Ni Catalyst Wash-Coated on Metal Monolith with Enhanced Heat-Transfer Capability for Steam Reforming. *J. Power Sources.* 2007, *171*(2), 499–505. DOI: 10.1016/j.jpowsour.2007.05.107.

[171] Schulz, L. A.; Kahle, L. C.; Delgado, K. H.; Schunk, S. A.; Jentys, A.; Deutschmann, O.; Lercher, J. A. On the Coke Deposition in Dry Reforming of Methane at Elevated Pressures. *Appl. Catal. A.* 2015, *504*, 599–607. DOI: 10.1016/j.apcata.2015.03.002.

[172] Zhang, J.; Li, F. Coke-Resistant Ni@SiO$_2$ Catalyst for Dry Reforming of Methane. *Appl. Catal. B.* 2015, *176-177*, 513–521. DOI: 10.1016/j.apcatb.2015.04.039.

[173] Peng, H.; Zhang, X.; Zhang, L.; Rao, C.; Lian, J.; Liu, W.; Ying, J.; Zhang, G.; Wang, Z.; Zhang, N. One-Pot Facile Fabrication of Multiple Nickel Nanoparticles Confined in Microporous Silica Giving a Multiple-Cores@ Shell Structure as a Highly Efficient Catalyst for Methane Dry Reforming. *ChemCatchem.* 2017, *9*(1), 127–136. DOI: 10.1002/cctc.201601263.

[174] Chai, R.; Zhao, G.; Zhang, Z.; Chen, P.; Liu, Y.; Lu, Y. High Sintering-/coke-Resistance Ni@sio 2 /Al 2 O 3 /fecral-Fiber Catalyst for Dry Reforming of Methane: One-Step,

Macro-To-Nano Organization via Cross-Linking Molecules. *Catal. Sci. Technol.* 2017, *23* (23), 5500–5504. DOI: 10.1039/C7CY01491K.

[175] Chai, R.; Fan, S.; Zhang, Z.; Chen, P.; Zhao, G.; Li, Y.; Yong, L. Free-Standing NiO-MgO-Al$_2$O$_3$ Nanosheets Derived from Layered Double Hydroxides Grown Onto FeCral-Fiber as Structured Catalysts for Dry Reforming of Methane. *ACS Sustainable Chem. Eng.* 2017, *5*(6), 4517–4522. DOI: 10.1021/acssuschemeng.7b00717.

[176] Choudhary, T. V.; Choudhary, V. R. Energy-Efficient Syngas Production Through Catalytic Oxy-Methane Reforming Reactions. *Angew. Chem. Int. Ed.* 2008, *47*(10), 1828–1847. DOI: 10.1002/anie.200701237.

[177] York, A. P. E.; Xiao, T.; Green, M. L. H. Brief Overview of the Partial Oxidation of Methane to Synthesis Gas. *Top. Catal.* 2003, *22*(3/4), 345–358. DOI: 10.1023/A:1023552709642.

[178] Chai, R.; Li, Y.; Zhang, Q.; Fan, S.; Zhang, Z.; Chen, P.; Zhao, G.; Liu, Y.; Lu, Y. Foam-Structured NiO-MgO-Al 2 O 3 Nanocomposites Derived from NiMgal Layered Double Hydroxides in Situ Grown Onto Nickel Foam: A Promising Catalyst for High-Throughput Catalytic Oxymethane Reforming. *ChemCatchem.* 2017, *9*(2), 268–272. DOI: 10.1002/cctc.201601167.

[179] Zhao, G.; Chai, R.; Zhang, Z.; Sun, W.; Liu, Y.; Lu, Y. High-Performance Ni-CeAlO$_3$-Al$_2$O$_3$/FeCrAl-Fiber Catalyst for Catalytic Oxy-Methane Reforming to Syngas. *Fuel.* 2019, *258*, 116102. DOI: 10.1016/j.fuel.2019.116102.

[180] Rogozhnikov, V.; Snytnikov, P.; Salanov, A.; Kulikov, A.; Ruban, N.; Potemkin, D.; Sobyanin, V.; Kharton, V. Rh/θ-Al$_2$O$_3$/FeCrAlloy Wire Mesh Composite Catalyst for Partial Oxidation of Natural Gas. *Mater. Lett.* 2019, *236*, 316–319. DOI: 10.1016/j.matlet.2018.10.133.

[181] Biodiesel 2020: Global Market Survey, Feedstock Trends and Forecasts. Emerging Markets Online, Multi-Client Study, 2008 (https:////www.healthtech.com/biodiesel2020/).

[182] Lin, Y. Catalytic Valorization of Glycerol to Hydrogen and Syngas. *Ind. Eng. Chem. Res.* 2013, *37*, 209–226. DOI: 10.1016/j.ijhydene.2012.12.079.

[183] Czernik, S.; French, R.; Feik, C.; Chornet, E. Hydrogen by Catalytic Steam Reforming of Liquid Byproducts from Biomass Thermoconversion Processes. *Ind. Eng. Chem. Res.* 2002, *41*(17), 4209–4215. DOI: 10.1021/ie020107q.

[184] Qi, W.; Xu, Q.; Yan, Y. Preparation of Syngas by Reforming of Biological Glycerol on Charcoal Catalyst. *Envir. Prog. Sustain.* 2016, *35*(6), 1765–1771. DOI: 10.1002/ep.12388.

[185] Kim, T.; Park, D. Preparation and Characterization of Ni Nanostructures Coated on the Substrates for Glycerol Steam Reforming. *J. Nanosci. Nanotechnol.* 2017, *17*(4), 2478–2481. DOI: 10.1166/jnn.2017.13353.

[186] Rennard, D.; French, R.; Czernik, S.; Josephson, T.; Schmidt, L. Production of Synthesis Gas by Partial Oxidation and Steam Reforming of Biomass Pyrolysis Oils. *Ind. Eng. Chem. Res.* 2010, *35*, 4048–4059. DOI: 10.1016/j.ijhydene.2010.01.143.

[187] Li, C.; Hirabayashi, D.; Suzuki, K. Development of New Nickel Based Catalyst for Biomass Tar Steam Reforming Producing H$_2$-Rich Syngas. *Fuel Process. Technol.* 2009, *90*, 790–796. DOI: 10.1016/j.fuproc.2009.02.007.

[188] Furusawa, T.; Saito, K.; Kori, Y.; Miura, Y.; Sato, M.; Suzuki, N. Steam Reforming of Naphthalene/Benzene with Various Types of Pt- and Ni-Based Catalysts for Hydrogen Production. *Fuel.* 2013, *103*, 111–121. DOI: 10.1016/j.fuel.2011.09.026.

[189] Li, D.; Koike, M.; Chen, J.; Nakagawa, Y.; Tomishige, K. Preparation of Ni–Cu/mg/al Catalysts from Hydrotalcite-Like Compounds for Hydrogen Production by Steam Reforming of Biomass Tar. *Ind. Eng. Chem. Res.* 2014, *39*(21), 10959–10970. DOI: 10.1016/j.ijhydene.2014.05.062.

[190] Czernik, S.; French, R. Distributed Production of Hydrogen by Auto-Thermal Reforming of Fast Pyrolysis Bio-Oil. *Ind. Eng. Chem. Res.* 2014, *39*, 744–750. DOI: 10.1016/j.ijhydene.2013.10.134.

[191] Czernik, S.; Evans, R.; French, R. Hydrogen from Biomass-Production by Steam Reforming of Biomass Pyrolysis Oil. *Catal. Today.* 2007, *129*(3–4), 265–268. DOI: 10.1016/j.cattod.2006.08.071.

[192] Balzarotti, R.; Italiano, C.; Pino, L.; Cristiani, C.; Vita, A. Ni/CeO$_2$-Thin Ceramic Layer Depositions on Ceramic Monoliths for Syngas Production by Oxy Steam Reforming of Biogas. *Fuel Process. Technol.* 2016, *149*, 40–48. DOI: 10.1016/j.fuproc.2016.04.002.

[193] Tsodikov, M. V.; Fedotov, A. S.; Antonov, D. O.; Uvarov, V. I.; Bychkov, V. Y.; Luck, F. C. Hydrogen and Syngas Production by Dry Reforming of Fermentation Products on Porous Ceramic Membrane-Catalytic Converters. *Ind. Eng. Chem. Res.* 2016, *41*, 2424–2431. DOI: 10.1016/j.ijhydene.2015.11.113.

[194] Gao, N.; Han, Y.; Quan, C.; Wu, C. Promoting Hydrogen-Rich Syngas Production from Catalytic Reforming of Biomass Pyrolysis Oil on Nanosized Nickel Ceramic Catalysts. *Appl. Therm. Eng.* 2017, *125*, 297–305. DOI: 10.1016/j.applthermaleng.2017.07.028.

[195] Zinoviev, S.; Müller-Langer, F.; Das, P.; Bertero, N.; Fornasiero, P.; Kaltschmitt, M.; Centi, G.; Miertus, S. Next-Generation Biofuels: Survey of Emerging Technologies and Sustainability Issues. *ChemSuschem.* 2010, *3*(10), 1106–11133. DOI: 10.1002/cssc.201000052.

[196] Chen, X.; Jin, J.; Sha, G.; Li, C.; Zhang, B.; Su, D.; Williams, C. T.; Liang, C. Silicon–Nickel Intermetallic Compounds Supported on Silica as a Highly Efficient Catalyst for CO Methanation. *Catal. Sci. Technol.* 2014, *4*(1), 53–61. DOI: 10.1039/C3CY00743J.

[197] Tucci, E. R.; Thomson, W. J. Monolith Catalyst Favored for Methanation. *Hydroc. Proc.* 1979, *58*, 123–126.

[198] Mokrani, T.; Scurrell, M. Gas Conversion to Liquid Fuels and Chemicals: The Methanol Route Catalysis and Processes Development. *Catal. Rev.* 2009, *51*(1), 1–145. DOI: 10.1080/01614940802477524.

[199] Milina, M.; Mitchell, S.; Crivelli, P.; Cooke, D.; Pérez-Ramírez, J. Mesopore Quality Determines the Lifetime of Hierarchically Structured Zeolite Catalysts. *Nat. Commun.* 2014, *5*(1), 3922. DOI: 10.1038/ncomms4922.

[200] Yang, X.; Chen, L.; Li, Y.; Rooke, J. C.; Sanchez, C.; Su, B. Hierarchically Porous Materials: Synthesis Strategies and Structure Design. *Chem. Soc. Rev.* 2017, *46*(2), 481–558. DOI: 10.1039/C6CS00829A.

[201] Dautzenberg, F. M. New Catalyst Synthesis and Multifunctional Reactor Concepts for Emerging Technologies in the Process Industry. *Catal. Rev.* 2004, *46*, 335–368. DOI: 10.1081/CR-200036729.

[202] Ivanova, S.; Louis, B.; Madani, B.; Tessonnier, J.; Ledoux, M.; Pham-Huu, C. ZSM-5 Coatings on β-SiC Monoliths: Possible New Structured Catalyst for the Methanol-To-Olefins Process. *J. Phys. Chem. C.* 2007, *111*(11), 4368–4374. DOI: 10.1021/jp067535k.

[203] Jiao, Y.; Jiang, C.; Yang, Z.; Zhang, J. Controllable Synthesis of ZSM-5 Coatings on SiC Foam Support for MTP Application. *Micropor. Mesopor. Mater.* 2012, *162*, 152–158. DOI: 10.1016/j.micromeso.2012.05.034.

[204] Guo, W.; Wu, W.; Luo, M.; Xiao, W. Modeling of Diffusion and Reaction in Monolithic Catalysts for the Methanol-To-Propylene Process. *Fuel Process. Technol.* 2013, *108*, 133–138. DOI: 10.1016/j.fuproc.2012.06.005.

[205] Choi, M.; Cho, H.; Srivastava, R.; Venkatesan, C.; Choi, D. H.; Ryoo, R. Amphiphilic Organosilane-Directed Synthesis of Crystalline Zeolite with Tunable Mesoporosity. *Nat. Mater.* 2006, *5*(9), 718–723. DOI: 10.1038/nmat1705.

[206] Zhao, J.; Hua, Z.; Liu, Y.; Guo, L.; Cui, W.; Bu, W.; Cui, X.; Ruan, M.; Chen, H.; Shi, J. Direct Fabrication of Mesoporous Zeolite with a Hollow Capsular Structure. *Chem. Commun.* 2009. 48, 7578–7580. DOI: 10.1039/B913920F.

[207] Milina, M.; Mitchell, D. S.; Cooke, D. D.; Crivelli, D. P.; Pérez-Ramírez, P. J. Impact of Pore Connectivity on the Design of Long-Lived Zeolite Catalysts. *Angew. Chem. Int. Ed.* 2014, *54*(5), 1591–1594. DOI: 10.1002/anie.201410016.

[208] Wang, N.; Qian, W.; Shen, K.; Su, C.; Wei, F. Bayberry-Like ZnO/MFI Zeolite as High-Performance Methanol-To-Aromatics Catalyst. *Chem. Commun.* 2016, *52*(10), 2011–2014. DOI: 10.1039/C5CC08471G.

[209] Ding, J.; Chen, P.; Zhao, G.; Liu, Y.; Lu, Y. High-Performance Thin-Felt SS-Fiber@HZSM-5 Catalysts Synthesized via Seed-Assisted Vapor Phase Transport for Methanol-To-Propylene Reaction: Effects of Crystal Size, Mesoporosity and Aluminum Uniformity. *J. Catal.* 2018, *360*, 40–50. DOI: 10.1016/j.jcat.2018.01.025.

[210] Duvenhage, D. J.; Shingles, T. Synthol Reactor Technology Development. *Catal. Today.* 2002, *71*(3–4), 301–305. DOI: 10.1016/S0920-5861(01)00456-4.

[211] Krishna, R.; Sie, S. Design and Scale-Up of the Fischer–Tropsch Bubble Column Slurry Reactor. *Fuel Process. Technol.* 2000, *64*(1–3), 73–105. DOI: 10.1016/S0378-3820(99)00128-9.

[212] Deugd, R. M.; Kapteijin, F.; Moulijin, J. A. Using Monolithic Catalysts for Highly Selective Fischer-Tropsch Synthesis. *Catal. Today.* 2003, *79-80*, 495–501. DOI: 10.1016/S0920-5861(03)00073-7.

[213] Pangarkar, K.; Schildhauer, T. J.; van Ommen, J. R. V.; Nijenhuis, J.; Kapteijn, F.; Moulijn, J. A. Structured Packings for Multiphase Catalytic Reactors. *Ind. Eng. Chem. Res.* 2008, *47*(10), 3720–3751. DOI: 10.1021/ie800067r.

[214] Steynberg, A. P.; Dry, M. E.; Davis, B. H.; Breman, B. B. *Fischer-Tropsch Technology*; Elsevier: Amsterdam. Netherlands, 2004. DOI: 10.1016/S0167-2991(04)80459-2.

[215] Giani, L.; Groppi, G.; Tronconi, E. Mass-Transfer Characterization of Metallic Foams as Supports for Structured Catalysts. *Ind. Eng. Chem. Res.* 2005, *44*(14), 4993–5002. DOI: 10.1021/ie0490886.

[216] Scala, C. V.; Wehrli, M.; Gaiser, G. Heat Transfer Measurements and Simulation of KATAPAK-M® Catalyst Supports. *Chem. Eng. Sci.* 1999, *54*(10), 1375–1381. DOI: 10.1016/S0009-2509(99)00077-9.

[217] Sheng, M.; Yang, H.; Cahela, D. R.; Yantz, W. R., Jr; Gonzalez, C. F.; Tatarchuk, B. J. High Conductivity Catalyst Structures for Applications in Exothermic Reactions. *Appl. Catal. A.* 2012, *445-446*, 143–152. DOI: 10.1016/j.apcata.2012.08.012.

[218] Cheng, X.; Yang, H.; Tatarchuk, B. J. Microfibrous Entrapped Hybrid Iron Based Catalysts for Fischer-Tropsch Synthesis. *Catal. Today.* 2016, *273*, 62–71. DOI: 10.1016/j.cattod.2016.02.048.

[219] Torres Galvis, H. M.; Bitter, J. H.; Khare, C. B.; Ruitenbeek, M.; Dugulan, A. I.; de Jong, K. P. Supported Iron Nanoparticles as Catalysts for Sustainable Production of Lower Olefins. *Science.* 2012, *335*(6070), 835–838. DOI: 10.1126/science.1215614.

[220] Han, L.; Wang, C.; Zhao, G.; Liu, Y.; Lu, Y. Microstructured Al-Fiber@meso-Al $_2$ O $_3$ @fe-Mn-K Fischer-Tropsch Catalyst for Lower Olefins. *AIChE. J.* 2016, *62*(3), 742–752. DOI: 10.1002/aic.15061.

[221] Han, L.; Wang, C.; Ding, J.; Zhao, G.; Liu, Y.; Lu, Y. Microfibrous-Structured Al-Fiber @ns-Al $_2$ O $_3$ Core–Shell Composite Functionalized by Fe–Mn–K via Surface Impregnation Combustion: As-Burnt Catalysts for Synthesis of Light Olefins from Syngas. *R.S.C. Adv.* 2016, *6*(12), 9743–9753. DOI: 10.1039/C5RA25212A.

[222] Ersson, A. G.; Järås, S. G. Catalytic Fuel Combustion in Honeycomb Monolith Reactors. In *Structured Catalysts and Reactors*; Cybulski, A. Moulijn, J. A., Eds.; Marcel Dekker: New York, 2006; pp. 215–241. DOI:10.1201/9781420028003.ch7.

[223] Saracco, G.; Cerri, I.; Specchia, V.; Accornero, R. Catalytic Pre-Mixed Fibre Burners. *Chem. Eng. Sci.* 1999, *54*, 3599–3608. DOI: 10.1016/S0009-2509(98)00463-1.

[224] Lyubovsky, M.; Karim, H.; Menacherry, P.; Boorse, S.; LaPierre, R.; Pfefferle, W. C.; Roychoudhury, S. Complete and Partial Catalytic Oxidation of Methane Over Substrates with Enhanced Transport Properties. *Catal. Today.* 2003, *83*(1–4), 183–197. DOI: 10.1016/S0920-5861(03)00231-1.

[225] Zhao, G.; Pan, X.; Zhang, Z.; Liu, Y.; Lu, Y. A. Thin-Felt Pd-MgO-Al$_2$O$_3$/Al-Fiber Catalyst for Catalytic Combustion of Methane with Resistance to Water-Vapor Poisoning. *J. Catal.* 2020, *384*, 122–135. DOI: 10.1016/j.jcat.2020.01.013.

[226] Gélin, P.; Primet, M. Complete Oxidation of Methane at Low Temperature Over Noble Metal Based Catalysts: A Review. *Appl. Catal. B.* 2002, *39*, 1–37. DOI: 10.1016/S0926-3373(02)00076-0.

[227] Tao, L.; Zhao, G.; Chen, P.; Zhang, Z.; Liu, Y.; Lu, Y. High-Performance Co-MnO X Composite Oxide Catalyst Structured Onto Al-Fiber Felt for High-Throughput O 3 Decomposition. *ChemCatchem.* 2019, *11*(3), 1131–1142. DOI: 10.1002/cctc.201801401.

[228] Tao, L.; Zhang, Z.; Chen, P.; Zhao, G.; Liu, Y.; Lu, Y. Thin-Felt Al Fiber Structured Pd-Co-MnO$_x$/Al$_2$O$_3$ Catalyst with High Moisture Resistance for High Throughput O$_3$ Decomposition. *Appl. Surf. Sci.* 2019, *481*, 802–810. DOI: 10.1016/j.apsusc.2019.03.134.

[229] Beirle, S.; Boersma, K. F.; Platt, U.; Lawrence, M. G.; Wagner, T. Megacity Emissions and Lifetimes of Nitrogen Oxides Probed from Space. *Science.* 2011, *333*(6050), 1737–1739. DOI: 10.1126/science.1207824.

[230] Felix, J. D.; Elliott, E. M.; Shaw, S. L. Nitrogen Isotopic Composition of Coal-Fired Power Plant NO $_x$: Influence of Emission Controls and Implications for Global Emission Inventories. *Environ. Sci. Technol.* 2012, *46*(6), 3528–3535. DOI: 10.1021/es203355v.

[231] Mou, X.; Zhang, B.; Li, Y.; Yao, L.; Wei, X.; Su, D. S.; Shen, W. Rod-Shaped Fe 2 O 3 as an Efficient Catalyst for the Selective Reduction of Nitrogen Oxide by Ammonia. *Angew. Chem. Int. Ed.* 2012, *51*(12), 2989–2993. DOI: 10.1002/anie.201107113.

[232] Wang, W.; McCool, G.; Kapur, N.; Yuan, G.; Shan, B.; Nguyen, M.; Graham, U. M.; Davis, B. H.; Jacobs, G.; Cho, K. Mixed-Phase Oxide Catalyst Based on Mn-Mullite (Sm, Gd)Mn 2 O 5 for NO Oxidation in Diesel Exhaust. *Science.* 2012, *337*(6096), 832–835. DOI: 10.1126/science.1225091.

[233] Kompio, P. G.; Brückner, A.; Hipler, F.; Auer, G.; Löffler, E.; Grünert, W. A New View on the Relations Between Tungsten and Vanadium in V$_2$O$_5$WO$_3$/TiO$_2$ Catalysts for the Selective Reduction of NO with NH$_3$. *J. Catal.* 2012, *286*, 237–247. DOI: 10.1016/j.jcat.2011.11.008.

[234] Thirupathi, B.; Smirniotis, P. G. Nickel-Doped Mn/TiO$_2$ as an Efficient Catalyst for the Low-Temperature SCR of NO with NH$_3$: Catalytic Evaluation and Characterizations. *J. Catal.* 2012, *288*, 74–83. DOI: 10.1016/j.jcat.2012.01.003.

[235] Zhang, L.; Zhang, D.; Zhang, J.; Cai, S.; Fang, C.; Huang, L.; Li, H.; Gao, R.; Shi, L. Design of Meso-TiO2@MnO$_x$–CeO$_x$/CNTs with a Core–Shell Structure as DeNox Catalysts: Promotion of Activity, Stability and SO2-Tolerance. *Nanoscale.* 2013, *5*(20), 9821–9829. DOI: 10.1039/C3NR03150K.

[236] Wan, Y.; Zhao, W.; Tang, Y.; Li, L.; Wang, H.; Cui, Y.; Gu, J.; Li, Y.; Shi, J. Ni-Mn Bi-Metal Oxide Catalysts for the Low Temperature SCR Removal of NO with NH$_3$. *Appl. Catal. B.* 2014, *148-149*, 148-149, 114–122. DOI: 10.1016/j.apcatb.2013.10.049.

[237] Pereda-Ayo, B.; De La Torre, U.; Romero-Sáez, M.; Aranzabal, A.; Gonzálezmarcos, J. A.; González-Velasco, J. R. Influence of the Washcoat Characteristics on NH$_3$-SCR Behavior of Cu-Zeolite Monoliths. *Catal. Today.* 2013, *216*, 82–89. DOI: 10.1016/j.cattod.2013.06.012.

[238] Sun, H.; Zhang, Y.; Quan, X.; Chen, S.; Qu, Z.; Zhou, Y. Wire-Mesh Honeycomb Catalyst for Selective Catalytic Reduction of NO_x Under Lean-Burn Conditions. *Catal. Today.* 2008, *139*(1–2), 130–134. DOI: 10.1016/j.cattod.2008.08.021.

[239] Han, L.; Gao, M.; Hasegawa, J.-Y.; Li, S.; Shen, Y.; Li, H.; Shi, L.; Zhang, D. SO_2-Tolerant Selective Catalytic Reduction of NO_x Over Meso-$TiO_2@Fe_2O_3@Al_2O_3$ Metal-Based Monolith Catalysts. *Environ. Sci. Technol.* 2019, *53*(11), 6462–6473. DOI: 10.1021/acs.est.9b00435.

[240] Yang, K. S.; Jiang, Z.; Chung, J. S. Electrophoretically Al-Coated Wire Mesh and Its Application for Catalytic Oxidation of 1,2-Dichlorobenzene. *Surf. Coat. Technol.* 2003, *168*, 103–110. DOI: 10.1016/S0257-8972(02)00569-8.

[241] Li, J.; Yang, J.; Wang, M.; Lu, Y.; He, M. A Microreactor Based on Sinter-Locked Microfibrous Media with Open Porous Structure for Nitration of Benzene. *Chin. J. Catal.* 2007, *28*, 931–933. DOI: 10.1016/S1872-2067(07)60077-1.

[242] Yang, J. L.; Li, J. F.; Lu, Y. Nitration of Benzene in a Continuous-Flow Microreactor Integrated with Microfiber-Structured Nafion/SiO_2 Solid Acid Catalyst. *Acta Phys.-Chim. Sin.* 2009, *25*, 2045–2049. DOI: 10.3866/PKU.WHXB20090926.

[243] Lai, I.; Liu, Y.; Yu, C.; Lee, M.; Huang, H. Production of High-Purity Ethyl Acetate Using Reactive Distillation: Experimental and Start-Up Procedure. *Chem. Eng. Process.* 2008, *47*(9–10), 1831–1843. DOI: 10.1016/j.cep.2007.10.008.

[244] Semagina, N.; Grasemann, M.; Xanthopoulos, N.; Renken, A.; Lioubov, K. M. Structured Catalyst of Pd/ZnO on Sintered Metal Fibers for 2-Methyl-3-Butyn-2-Ol Selective Hydrogenation. *J. Catal.* 2007, *251*(1), 213–222. DOI: 10.1016/j.jcat.2007.06.028.

[245] Górak, A.; Hoffmann, A. Catalytic Distillation in Structured Packings: Methyl Acetate Synthesis. *AIChE. J.* 2001, *47*(5), 1067–1076. DOI: 10.1002/aic.690470513.

[246] Klöker, M.; Kenig, E. Y.; Górak, A.; Markusse, A. P.; Kwant, G.; Moritz, P. Investigation of Different Column Configurations for the Ethyl Acetate Synthesis via Reactive Distillation. *Chem. Eng. Process.* 2004, *43*(6), 791–801. DOI: 10.1016/S0255-2701(03)00084-9.

[247] Gao, X.; Wang, F.; Zhang, R.; Li, H.; Li, X. Liquid Flow Behavior of a Seepage Catalytic Packing Internal for Catalytic Distillation Column. *Ind. Eng. Chem. Res.* 2014, *53*(32), 12793–12801. DOI: 10.1021/ie500665q.

[248] Deng, T.; Ding, J.; Zhao, G.; Liu, Y.; Lu, Y. Catalytic Distillation for Esterification of Acetic Acid with Ethanol: Promising SS-Fiber@HZSM-5 Catalytic Packings and Experimental Optimization via Response Surface Methodology. *J. Chem. Technol. Biotechnol.* 2018, *93*(3), 827–841. DOI: 10.1002/jctb.5436.

[249] Zou, X.; Zhang, Y. Noble Metal-Free Hydrogen Evolution Catalysts for Water Splitting. *Chem. Soc. Rev.* 2015, *44*(15), 5148–5180. DOI: 10.1039/C4CS00448E.

[250] Zhu, C.; Shen, G.; Chen, W.; Dong, X.; Li, G.; Song, Y.; Wei, W.; Sun, Y. Copper Hollow Fiber Electrode for Efficient CO_2 Electroreduction. *J. Power Sources.* 2021, *495*, 229814. DOI: 10.1016/j.jpowsour.2021.229814.

[251] Li, S.; Chen, W.; Dong, X.; Zhu, C.; Chen, A.; Song, Y.; Li, G.; Wei, W.; Sun, Y. Hierarchical Micro/Nanostructured Silver Hollow Fiber Boosts Electroreduction of Carbon Dioxide. *Nat. Commun.* 2022, *13*(1), 3080. DOI: 10.1038/s41467-022-30733-6.

[252] Yu, D.; Qian, Q.; Wei, L.; Jiang, W.; Goh, K.; Wei, J.; Zhang, J.; Chen, Y. Emergence of Fiber Supercapacitors. *Chem. Soc. Rev.* 2015, *44*(3), 647–662. DOI: 10.1039/C4CS00286E.

[253] Wang, Q.; Wang, X.; Xu, J.; Ouyang, X.; Hou, X.; Chen, D.; Wang, R.; Shen, G. Flexible Coaxial-Type Fiber Supercapacitor Based on $NiCo_2O_4$ Nanosheets Electrodes. *Nano. Energy.* 2014, *8*, 44–51. DOI: 10.1016/j.nanoen.2014.05.014.

[254] Liu, B.; Tan, D.; Wang, X.; Chen, D.; Shen, G. F. Planar-Integrated, All-Solid-State Fiber Supercapacitors with an Enhanced Distributed-Capacitance Effect. *Small*. 2013, *9*(11), 1998–2004. DOI: 10.1002/smll.201202586.

[255] Jiang, F.; Fang, Y.; Liu, Y.; Chen, L.; Xue, Q.; Lu, Y.; Lu, J.; He, M. Paper-Like 3-Dimensional Carbon Nanotubes (CNTs)–Microfiber Hybrid: A Promising Macroscopic Structure of CNTs. *J. Mater. Chem*. 2009, *19*(22), 3632–3637. DOI: 10.1039/B819083F.

[256] Li, Y.; Fang, Y.; Liu, H.; Wu, X.; Lu, Y. Free-Standing 3D Polyaniline–Cnt/ni-fiber Hybrid Electrodes for High-Performance Supercapacitors. *Nanoscale*. 2012, *4*(9), 2867–2869. DOI: 10.1039/C2NR30252G.